TECHNICAL REPORT

TEMPERATURE AND DENSITY MEASUREMENTS IN THE BASE REGION OF A CLUSTERED ROCKET MODEL USING AN ELECTRON BEAM TECHNIQUE

By: J. Llinas and W.C. Rustay

CAL No. HM-2107-Y-1

Prepared for:

Headquarters
National Aeronautics and Space Administration
Washington, D.C.

Contract No. NSR 33-009-030
July 1966

CORNELL AERONAUTICAL LABORATORY, INC.
OF CORNELL UNIVERSITY, BUFFALO, N. Y. 14221

CORNELL AERONAUTICAL LABORATORY, INC.
BUFFALO, NEW YORK 14221

TEMPERATURE AND DENSITY MEASUREMENTS IN THE BASE REGION OF A CLUSTERED ROCKET MODEL USING AN ELECTRON BEAM TECHNIQUE

CAL REPORT NO. HM-2107-Y-2
CONTRACT NO. NSR 33-009-030
JULY 1966

PREPARED FOR:
HEADQUARTERS
NATIONAL AERONAUTICS AND SPACE ADMINISTRATION
WASHINGTON, D.C.

BY: J. Llinas
J. Llinas

BY: W. C. Rustay
W.C. Rustay

APPROVED: K.C. Hendershot
K.C. Hendershot, Head
Propulsion Section

APPROVED: L. Bogdan
L. Bogdan, Head
Instrumentation Section

APPROVED: J.F. Martin
J.F. Martin, Head
Applied Hypersonic Research Dept.

ABSTRACT

34045

The application of electron beam technology to the measurement of density and temperature in the complex-structured base region flow field of clustered-rocket engine configurations is discussed. A description is given of the apparatus designed to perform these measurements while installed within an altitude simulation tank operating at pressure altitudes of approximately 200,000 feet.

Using short-duration testing techniques and shock-heated nitrogen as the model working fluid, base region density, temperature, pressure, heat-transfer and recovery temperature data were obtained for a 0.1 scale model of a four-engine Saturn booster stage. The feasibility of determining gas stream densities in the base region flow consisting of multi-specie rocket combustion gases with this technique is also discussed.

A summary of the test results and recommendations for future studies are included.

FOREWORD

The research reported herein was conducted for NASA Headquarters under Contract No. NSR-33-009-030. The effort was under the technical cognizance of Mr. Fred DeMeritte of NASA Headquarters.

This report deals primarily with the application of the electron beam technique to the measurement of rotational temperatures of recirculated gas in the base region of a typical clustered-engine rocket model. Related studies previously completed at CAL under NASA contract NAS8-20027 have involved the use of an electron beam for the measurement of base region gas densities, as well as the acquisition of considerable stage design information (heat transfer and pressure) through the use of hot flow models of this same configuration.

The authors wish to acknowledge the contributions of their colleagues in the CAL Applied Hypersonic Research Department, namely L. Bogdan for his contributions toward solving many of the instrumentation difficulties encountered, K. Hendershot for his assistance in the technical direction of the program and S. Liszewski who carried out the majority of the experiments.

TABLE OF CONTENTS

TABLE OF CONTENTS (Cont.)

I. INTRODUCTION

An important consideration in the design of clustered-rocket engine configurations is the need for an understanding of the detailed nature of the base region flows. By adapting techniques employed in the operation of its hypersonic shock tunnels, the Cornell Aeronautical Laboratory has successfully developed an experimental method for studying base flow phenomena using short duration testing technology.[1] While surface pressure and heat transfer data taken at the model base have been valuable for purposes of vehicle design, a knowledge of base flow parameters in the three-dimensional space of the base-nozzle region is critical to the broader understanding of base heating phenomena and the development of rational scaling criteria.

The small scale of the test models, the short duration of steady flow test time, the low density environment, and most importantly, the complex, high-shear, steep-gradient nature of the flow all rule against the practicality of physical probes. For this type of a test environment, the use of electron beam techniques is uniquely applicable. The electron beam probe, an important diagnostic tool for low-density, high-velocity flow, has experienced extensive development in recent years[2-5] and affords a probing capability without interference to the flow under study. Simply described, a collimated beam of energetic electrons ($\approx$20 kv) is injected into the test medium and induces a characteristic emission of light energy by the gas molecules through the mechanism of collisional excitation. Theoretical investigations of the details of this phenomenon have shown that by using appropriate optical sensing apparatus, this emission may be employed for quantitative measurement of number density and temperature with a high degree of spatial and temporal resolution. Because of electron scattering and collisional de-excitation (quenching), electron beam applications are generally confined to low density flow regimes (number densities corresponding to pressures less than approximately 1 mm Hg. at room temperature). These considerations are of small consequence to base flow studies since the reverse flow phenomena occur at flow densities compatible with the useful range of this technique.

Density and temperature measurements were made in the base region of a four-engine cluster model installed in the CAL 13-ft. diameter altitude simulation chamber using the electron beam technique. Shock-heated nitrogen, as supplied from a shock tube, was employed as the model working fluid. The nominal model combustor pressure and temperature were 200 psia and 2500° R respectively.

The apparatus developed to perform the density and temperature measurements is described. The application is unconventional in the respect that the physical size of the test chamber dictated that the major components of the equipment had to be located and operated within the low pressure environment ($\approx 100\ \mu$ Hg) of the altitude simulation chamber.

II. TEST EQUIPMENT

A. MODEL CONFIGURATION AND TEST FACILITY

A 0.1 scale four-engine cluster model once considered as an S-IV (second stage) configuration for the Saturn I booster was used for this test program. The model system consists of a constant-area shock tube, plenum chamber and porting manifold, four rocket nozzles and a circular instrumented heat shield as shown schematically in Figure 1. Model exhaust nozzles are scaled Pratt and Whitney RL10-A3 rocket engines normally fueled by liquid hydrogen and oxygen and are canted 4° radially outboard. The nozzles have a throat diameter of 0.6 inches and an area ratio $\epsilon = 40$. Figure 2 defines the model base region geometry. Provision for insertion of the rotational temperature measuring apparatus (R.T.A.) behind the heat shield was made by designing extended nozzle adapters. These adapters (shown in Figure 3a) allow space for the required axial movement of the R.T.A. relative to the beam to maintain focusing (the fixed objective lens in the R.T.A. has a 2-inch focal length).

The shock tube has an inside diameter of 2.75 inches and driver and driven tube lengths of 15 feet and 23 feet, respectively. Fast-response thin-film calorimeters were placed a known distance apart on the driven tube inside wall as a means of detecting the passage of the incident shock wave and deducing the incident shock Mach number. The outputs of these gages were fed into a Berkeley counter which measured the time interval between the arrival of the shock at each of the two gage stations.

The model heat shield is shown in Figure 3b. Provisions for heat transfer and pressure measuring instrumentation were made along the two vertical radii between engines. Along the other two horizontal radii are: (1) the fibre optic units previously employed on an electron beam density measuring program (Ref. 6) so that density measurements could be taken along with the temperature measurements and (2) a glass-covered slot through which the R.T.A. objective lens could focus on the beam.

The basic design requirements for the R. T. A. support bracket, shown in Figure 4, were:

(1) to provide radial mobility to position the objective lens at positions corresponding to the fibre optic locations so that spatial correlation of the temperature and density data may be made,

(2) to suspend the R. T. A. from the electron beam gun support pedestal in order to isolate the unit from shocks during model firing and to maintain the beam/lens orientation.

Figure 5 shows a schematic of the overall installation of the test equipment in the high altitude chamber. With this support scheme for the R. T. A., once the lens has been focused on the beam (at a given radial location with respect to the heat shield), simply moving the gun support pedestal on the guide rails allows an axial temperature survey (i. e., distance above the heat shield) to be made, as the beam/lens orientation remains fixed. Vernier dimensional adjustment capability was incorporated in the R. T. A. support bracket and allowed corrections to be made for slight dimensional and/or optical misalignments.

The density and temperature instrumentation, the electron beam generating apparatus, and the model were installed within an altitude simulation chamber which measures 15 feet in length and 13 feet in diameter (see Figure 6). Using mechanical pumps, an absolute chamber pressure of approximately 10 microns Hg is attainable (corresponding to a simulated pressure altitude of 260, 000 feet).

B. INSTRUMENTATION

1. Electron Beam Measurements

a) Technical Background

When high energy electrons transit a gas, inelastic collisions between beam electrons and gas molecules result in the excitation

of a characteristic emission spectrum. The intensity and the spectral details of the emission are related to the nature, number density, and temperature of the gas as well as the energy and number density of the electrons. Thus, under appropriate test conditions, this electroluminescence excited by a known and controlled stream of electrons may be used to measure gas number density and temperature.

It is required that the particular emission used for diagnostic purposes result from a direct excitation-emission sequence and that the excited state involved in the transition be reached by direct excitation from the ground state of the neutral molecule. In the case of nitrogen, which has been studied extensively by Muntz[2, 3] in the application of the electron beam probe to number density and temperature measurements in gas flows, the most prominent system excited is the first negative system N^+_2 (-1) with spectral emission generally located in the 0.38 to 0.43 micron band. The mean lifetime of the excited state is only about 6×10^{-8} sec. so that the extent to which radiating molecules are carried away from the beam position (that is, the initial point of excitation) by the flow is negligibly small for all but extreme flow velocities. As a result, the spatial resolution is limited only by the beam diameter and length of beam selected for observation.*

In addition to the inelastic collisions, elastic collisions between molecules and beam electrons can occur; these elastic collisions contribute primarily to scattering of the electron beam which causes a spreading of the light beam as a result of excitation of molecules not in the path of the incident beam. Scattering increases with number density and causes a loss of spatial resolution in density measurements since it is necessary to observe the total emission. A measure of control over scattering is possible by increasing the beam accelerating voltage since electron-neutral collision cross sections decrease with increasing electron energy.

---

* For rarefied gases and short test times where statistics of photon counting become important, spatial accuracy may need to be compromised in the interests of improving measurement accuracy.

However, a reduction in emission intensity (for a given beam current) also occurs due to the concurrent reduction in the number of inelastic collisions. Muntz has pointed out that the improvements resulting from the use of beam energies exceeding 50 kev to counteract beam spreading are small, especially in view of the rapidly increasing cost and complexity of operating equipment above that voltage level.

The measurement of gas number density is conceptually simple. Emission intensity is measured from the full width and some arbitrary length of the beam together with a coincident measurement of beam current. Since emission intensity is a direct function of beam current, accurate measurement of current is of fundamental importance and corrections for any variation during the test interval are necessary. In addition, the sensing optics must accommodate the full beam width; this consideration is especially important if accurate density measurements are to be obtained in the presence of appreciable beam spreading. The length of beam observed will generally be determined by the need to achieve satisfactory signal-to-noise ratios in the optical sensors at low densities.

For nitrogen densities equivalent to room temperature pressures of less than about 500 microns Hg, emission intensity is directly proportional to number density for given beam conditions. With increasing density, collisional de-excitation (quenching) becomes important and the linear relation between density and emission intensity is lost as is, ultimately, the sensitivity of emission intensity to changes in density. While it is possible to make density measurements at levels for which quenching occurs, the density of the base flows was deliberately constrained within the linear portion of the density probe operating characteristic for this test program.

The beam-excited emission of the first negative system of nitrogen exhibits a vibrational and rotational fine structure whose intensity distributions have been shown by Muntz[2] to be related quantitatively to the vibrational and rotational temperature of the gas molecules prior to their excitation. This initial study involved individual spectral lines and line intensities. Because of the slow optical speed of spectrographs and the low intensity of the emission, this technique was limited to the diagnosis of

essentially steady-state flows. In a later study Muntz[7] adapted this technique to short duration hypersonic flows by sensing intensity ratios of portions of the spectral band (rather than ratios of individual lines) where the spectral isolation was achieved with narrow bandpass optical interference filters. Muntz demonstrated that the ratios of the integrated intensities in judiciously selected portions of the emission spectrum were uniquely related to rotational temperature.* In essence, a two color pyrometer, called the Rotational Temperature Apparatus was developed by Muntz to observe the intensity distribution in the rotational fine structure.[7] Results of Muntz's theoretical calculations leading to the optimization of the interference filter's center wavelengths and passbands are given in References 5 and 7.

b) Beam Generating Apparatus

The electron beam was projected across the horizontal diameter of the model base; beam position in a direction normal to the plane of the base was variable to facilitate mapping of the flow field. To assure no disturbance of the flow field by the electron beam apparatus, the exit plane of the drift tube and the beam collector cup were located at points just off the edge of the base plate resulting in a beam length of approximately twelve inches. Density measurements were made using the last six inches of beam length.

The electron beam generating apparatus, exclusive of such peripheral equipment as vacuum pumps, power supplies, and vacuum gages, consists of three physically and functionally distinct components: the electron gun chamber (and mounting mechanism), the dynamic pressure stage, and the drift tube. Because of the large diameter of the tank and with useful lengths of electron beams measurable in inches, the entire electron beam apparatus was installed within the 13-foot diameter altitude chamber. Certain of the design features were governed by this factor. It will be helpful in understanding the subsequent description of the equipment to refer to the left-hand

*Since rotational and translational degrees of freedom are usually equilibrated in most nozzle flows, rotational temperature will be equal to static temperature.

portion of Figure 7 which is a simplified schematic of the three major components mentioned above, and to Figure 6 which shows the apparatus installed in the altitude chamber.

A type 7NP4 electrostatic focus electron gun,* used exclusively for all these tests, was installed within a glass envelope formed by the fusion of a 4 inch by 2 inch reducer to a straight length of 2 inch Pyrex piping. Representative of a hybrid structure, the 7NP4 electron gun lacks an integral anode which was formed in this case by an electrically grounded aquadag coating deposited on the inner surface of the glass envelope at its forward end. Vacuum sealing of the gun envelope is achieved at the vertical end plates with gasketed flange joints and the entire assembly is mounted on a mechanically adjustable platform. Fore and aft ends of the platform are independently adjustable in the vertical and horizontal planes imparting four degrees of freedom to permit a purely mechanical means of beam alignment. Four shafts, coupled to the platform positioning apparatus, project through the altitude chamber wall (via vacuum-type bulkhead fittings) to permit beam alignment even after the altitude chamber has been evacuated.

A flexible metal bellows couples the forward end of the gun envelope to the dynamic pressure chamber. At the opposite end, five RG-8/U cables are routed through O-ring vacuum seals in the end plate to supply proper potentials to the electron gun. With the anode at ground potential, the entire gun structure is essentially at full accelerating potential above ground. To permit operation within the vacuum environment of the altitude tank, the outer cover and braid of the high voltage cables were removed and the cable with its dielectric and inner conductor passed directly into the gun envelope without any discontinuity; the intent was to avoid corona problems. Satisfactory seals were achieved with O-rings bearing directly on the cable dielectric. Similar seals were employed in bringing the cables into the altitude tank.

*Superior Electronics Corp. Type SE-7N

Pressure buffering between the high vacuum required for the electron gun (10^{-5} to 10^{-6} mm Hg for reasonable life expectancy of the cathode and for high voltage operation) and the test environment ($\approx$0.5 mm Hg during the test event) was obtained by differential pumping. Made of stainless steel, the dynamic chamber contains two copper aperture plates placed perpendicular to the beam axis. The apertures, measuring 0.06 inches in diameter by 0.2 inches in length are coaxially aligned and help to collimate the electron beam. The electron gun side of the first aperture plate was pumped by a cold-trapped oil diffusion pump while the volume between the aperture plates was evacuated by a second cold-trapped diffusion pump. Both diffusion pumps operated satisfactory in the vacuum environment of the altitude tank (the cold traps were vented to the atmosphere).

A fast-operating, pneumatically-actuated ball valve was located beyond the second aperture plate. This valve permitted the electron gun to be operated independent of ambient pressure levels and protected the electron gun from high post-test pressures in the altitude tank by rapid closure subsequent to the test event. The ball valve assembly was modified by installing teflon seats to electrically insulate the ball and stem from ground. Thus, with the valve in the closed position, the ball functioned as a beam current detector to aid in "threading" the electron beam through the system apertures. As described elsewhere, microswitches operated by the ball valve were utilized to provide electrical triggers for data acquisition purposes.

A 0.5 inch diameter by 7.5 inch long drift tube, attached to the dynamic pressure chamber, allowed injection of the electron beam into the model flow field with minimal flow disturbance. Replaceable drift tube exit apertures typically measured 0.06 inch in diameter by 0.06 inches in length. The beam terminated in a collector cup which provided a means for monitoring the magnitude of the beam current. Brass cups coated with aquadag were used initially; however, more consistent results were obtained using cups machined from graphite.

Special problems arose since the apparatus was subject to a variable external pressure. Because alignment of the electron beam through the system orifices was made initially at atmospheric pressure, a

complete loss of the beam (at the drift tube exit orifice) sometimes occurred as the altitude chamber was evacuated. This effect was the result of relative movement of the gun envelope and the dynamic pressure chamber caused by the removal of the unbalanced force acting on these components at atmospheric pressure. Linear displacement potentiometers were installed to measure these movements and to permit realignment to the original position after tank evacuation by means of the remote gun platform adjustment controls.

A second problem of relative motion was associated with the model and the beam apparatus. Since the model was attached to the tank end wall and the beam apparatus mounted from the tank floor, chamber evacuation caused a relative displacement of 0.1 inch to occur. With this displacement determined to be reproducible, the beam apparatus was simply offset by this amount when adjusting the beam-to-model heat shield separation distance.

With the apparatus described, internal vacua of about 1×10^{-6} mm Hg were realized and accelerating potentials to 45 kev could be sustained without excessive electrical breakdown. As the altitude chamber was evacuated, however, electrical breakdown occurred to the extent that reduced potentials had to be employed. Tests were conducted at 30 kv since higher accelerating potentials resulted in intermittent high voltage breakdowns which led to extraneous sweeps on the data oscilloscopes causing difficulty in record interpretation. The exact cause for the occurrence of the electrical difficulties at low tank pressures has not been determined.

c) Rotational Temperature Apparatus

The function of the temperature measuring instrumentation is to sample the electroluminescence from a segment of the beam, divide this energy into two separate beams, and measure the ratio of the energies transmitted by a narrow passband optical filter placed in each beam. A schematic of the apparatus, which is closely patterned after Muntz's R.T.A. design, is shown in Figure 8. The particular geometry was dictated by the physical constraints imposed by adapting the unit to the test model.

Light from the beam is collimated by the objective lens (F/2), reflected by a first-surface folding mirror and focused upon an aperture measuring 0.06 inches by 0.12 inches (the long dimension is aligned parallel to the beam axis). The light is then recollimated and is incident upon a 45-55 beam splitter. Collimation is required since the characteristics of narrow passband optical interference filters are sensitive to the angle of incidence of the light.[8] Two light beams are generated as the result of the beam splitter action each of which transits a narrow band interference filter and a condensing lens to impinge upon a photomultiplier. As suggested by Muntz (Ref. 9), the interference filters used exhibited peak transmission at 4262 Å and 4282 Å with a half width of approximately 15 Å. The photomultipliers were low-dark current, high gain, 14-stage E.M.I. type 9502 B operating at approximately 1400 volts.

To permit standardizing the relative gain of each optical channel each time a temperature measurement was made, a ribbon-type tungsten lamp was incorporated in the apparatus. Energy from the lamp passed through a high-speed, electrically-actuated shutter and was collimated by a lens. After passing through a Wratten #38 filter (to restrict the lamp spectral energy to the same region as that of the beam fluorescence), the lamp energy was partially reflected into the main optic axis of the apparatus by a splitter plate of plane, clear glass.

A cylindrical air-tight container housed the two photomultipliers. This housing was vented to atmospheric pressure when the R.T.A. was in the vacuum tank to facilitate operating at the high voltage required. A photograph of the R.T.A. assembly is shown in Figure 9.

d) Density Sensors

Five optical channels for collecting density data were installed along the radius of the model heat shield directly below the last six inches of electron beam length as shown in Figure 3b. Each optical channel consisted of a window of Corning #5-58 filter glass (set flush in the base plate surface) and a recessed F/14 objective lens. The filter glass provided

discrimination against stray light by maximizing channel transmission in the spectral range of the beam fluorescence. The objective lens was adjustable so that the beam could be imaged on the aperature slit for a range of beam positions normal to the base (0.25 to 4 inches). For this particular system, the slit dimensions imaged in the plane of the beam (at a one inch height above the heat shield) measured 0.125 inch along the beam and 0.44 across the beam.

The aperture slit was attached to the input end of a two-foot length of fiber-optic light guide characterized by a numerical aperture of 0.5 and an aperture of 0.125 inch. These light guides were brought outside the altitude tank through vacuum seals and terminated in individual light-tight containers housing 931-A photomultipliers selected for maximum gain. Time resolved data from each channel were recorded photographically on oscilloscopes.

2. Heat Transfer

Heat transfer rates were determined by a technique that relies on sensing the transient surface temperature of the model heat shield. The sensing element is a thin film platinum strip (0.1 μ thick x 5 mm long x 0.5 mm wide) fused on a flat pyrex substrate (0.375 inch dia. x 0.0625 inch thick). Since the heat capacity of the film strip is negligible, the film temperature is equal to the instantaneous surface temperature and is related to the heat transfer rate to the model by the linear heat conduction theory discussed in detail in Ref. 10. These gages are limited to ambient temperatures of about 750°R as a result of soldered electrical connections used in their construction.

For the tests made to determine recovery temperature a special heat-transfer gage, capable of operation at sustained ambient temperatures up to 1460°R, was employed and is shown in Figure 10a. Contained within the gage case (0.75 inch dia. x 2.5 inch long) is an electrical heater to provide the elevated temperature environment. Other than the smaller gage substrate dimensions the gage construction differs from that of the standard gage only in the manner of electrical lead attachment. For the heated gage platinum

wires are fused into the pyrex substrate and the platinum film is fired directly between these leads whose terminals are flush with the substrate surface. The high temperature limit for these gages results from substrate softening considerations.

The outputs of both types of gages are fed through an analog network (described in Ref. 10) which converts the signal from one representing temperature to one directly proportional to the instantaneous heat transfer rate. This conversion is applicable over the range of gage temperatures near 540°R where the physical properties of the substrate remain sensibly constant at the values used in the calibrate and analog circuits. At higher ambient temperatures the data must be corrected by the procedure outlined in Ref. 10.

3. Pressure

Standard precision laboratory test gages were used to monitor the shock tube loading pressures.

Two commercial Kistler piezoelectric pressure transducers were used to measure the plenum chamber pressure and were located at two identical relative positions in the chamber (the second transducer is not shown in Figure 1). These transducers were mounted and calibrated in removable holders and sensed the plenum pressure through a long slender orifice intended to isolate the transducer from the relatively hot gas in the chamber.

Figure 10b shows the tray used to mount the transducers used for making heat-shield pressure measurements. The basic dimensions of the transducer assembly are 0.5 inch diameter by 0.125 thick. The sensing element consists of a small lead zirconium titanate crystal which exhibits a piezoelectric effect, connected to an 0.003 inch thick aluminum diaphragm. Sensitivities on the order of 1500 mv/psi are realized along with high frequency response necessary for the short test durations. The transducers are acceleration compensated internally by employing a second diaphragm/crystal assembly not exposed to the pressure input whose output is wired in opposition to the primary diaphragm signal. Further acceleration compensation is

provided through transducer mounting methods wherein a seismic mass is attached to the back of the transducer and the entire assembly spring-mounted from the forward surface of the heat shield. Tubular rubber connectors couple the assembly to the pressure orifice in the heat shield tray as shown in Figure 10b.

An Alphatron and liquid nitrogen cold-trapped McLeod gage were used to measure the pre-run altitude chamber pressure.

III. TEST PROCEDURE

A. CALIBRATION

1. Temperature

Following assembly and alignment of the R.T.A., a static calibration was performed separate from the model to determine the dependence of the intensity ratio on test gas temperature. To accomplish the calibration, a thick-walled, well-insulated, electrically heated brass oven was fabricated to provide a source of nitrogen at known levels of temperature and pressure. The oven attached to the electron beam generating apparatus to allow projection of the beam through the oven interior; a collector cup within the oven provided the means for monitoring beam current. The beam induced emission was viewed through an opening in the oven wall; a double window was utilized to minimize local convective cooling of the gas. Oven temperature was determined by two thermocouples in the oven wall; gas pressure was maintained at approximately the level expected during a test event (300 microns Hg). Equilibrium between oven wall and test gas temperatures was assured by preheating the gas before admission to the oven test chamber and by maintaining a low flow rate of nitrogen through the oven. However, the flow rate was sufficient to minimize errors in the data due to localized beam heating of the gas. Figure 11a shows the R.T.A., calibration oven, and electron beam apparatus in the calibration configuration.

The calibration procedure was as follows. Oven heaters were adjusted for a desired temperature; at the same time, the calibration lamp intensity was adjusted so that the light level incident on the photomultipliers was close to that experienced during observation of the beam-induced fluorescence. The nitrogen supply was adjusted to maintain the desired pressure. When oven pressure and temperature had stabilized, the lamp shutter was closed, the beam turned on and the outputs of the two channels of the R.T.A. recorded. The beam was then extinguished, the lamp shutter opened, and the photomultiplier outputs again recorded viewing the calibration lamp. Before changing the oven temperature, the measurement was repeated.

Prior to determining the dependence of the intensity ratio on temperature, supplementary data were first obtained which verified the ratio to be independent of beam current (between 40 and 120 μa), density (100 to 400 microns Hg at room temperature) and beam voltage (between 18 and 34 kv). Calibration of the intensity ratio as a function of temperature was then carried out starting at room temperature and increasing to about 550°K. At this temperature oven pressure could no longer be controlled due to failure of O-ring seals at the oven windows. An examination of the results obtained up to this time revealed an apparent insensitivity of the ratio to temperature above about 450°K. The source of this discrepancy was attributed to contamination of the oven atmosphere by fluorine gas evolved from the fluoro-elastomer O-ring seals at high temperatures. The likely presence of fluorine gas in the oven was confirmed by etching of the glass windows. Since the emission spectrum of fluorine is relatively strong in the region of the nitrogen band being observed, it was felt that its presence could cause the apparent loss of sensitivity of the ratio to temperature. To eliminate this possibility, the rubber O-rings were replaced with soft, pure aluminum sealing rings and the calibration repeated over the same 300-575°K range.

The final calibration of the R.T.A. intensity ratio versus gas temperature is shown in Figure 11b. The values of R are somewhat lower than anticipated for the filter specifications cited earlier from manufacturer's supplied data. Due to a lack of appropriate spectrographic apparatus, it was not possible to calibrate these filters as installed in the R.T.A. However, in view of the known sensitivity of interference filters to angle of incidence of illumination and the strong dependence of intensity ratio on filter characteristics, this result is not unreasonable.

2. Density

To verify the proportional relationship between emission intensity and molecule number density, a linearity check was conducted wherein the outputs of all the density channels were recorded for various gas pressures using room temperature dry air. This calibration was performed with all apparatus and components mounted in their normal run configuration. Data

were obtained for pressures between 50 and 520 microns Hg; the results are shown in Figure 12 where the ordinates are the photomultiplier outputs normalized to a beam current of 100 μa. Over the range of test densities encountered during the program (up to an equivalent room temperature pressure of approximately 350 microns Hg) the density channel outputs are seen to be quite linear. With increasing density, they tend to curve upwards (i.e. the system appears to become more sensitive). Since all channels exhibit this tendency, possibility of systematic error in the measurement of ambient gas density or beam current must be considered. The ambient density is thought to be quite accurately known since it was based on a vacuum tank pressure measurement using a cold-trapped McLeod gage. Errors in beam current measurement, however, could result from an effect suggested by Muntz. Under certain conditions the relation between indicated and actual beam current may be a function of the gas pressure around the collector cup. A current indication progressively smaller than the actual current at higher pressures would result in the behavior shown. It is also possible that at the higher pressures, sufficient beam scattering was being encountered to cause part of the beam to completely miss the collector cup. Such an effect would also produce calibrations of the sort shown in Figure 12.

3. Heat-Transfer Gages

The standard calibration procedure for the heat-transfer gages consists of measuring the gage resistance at nominal gage ambient temperatures of 530°R and 610°R (achieved by immersing the gages in a controlled hot water bath). The gage sensitivity $\Delta R/\Delta T$, which is a function of temperature, is thereby determined at an ambient temperature of 530°R. This information is then used to determine the value of a shunt resistor (dummy load resistor - DLR) that is "chopped" into the heat-transfer gage circuitry to generate the same voltage increment ΔV that would be produced if the gage increased in resistance, due to heating, by an amount ΔR. Proper DLR values are given by the following equation:

$$DLR = \frac{R_p^2}{K_{\Theta_T} \Delta T} \left(\frac{R_1 + R_g'}{R_1 + R_p} \right)^2 - R_p \qquad (1)$$

where: R_P = Precision resistor (normally 100Ω)

$K_{\Theta T} = \frac{\text{Change in gage resistance - } \Delta R}{\text{Change in gage temperature - } \Delta T}$ at the

= gage operating temperature, T

R_1 = Series resistor (normally 1,000Ω)

R_g' = Gage resistance at operating temperature, T

ΔT = Anticipated gage temperature change during test run.

For gages operating at elevated ambient temperatures (like the heated gage used for recovery temperature measurements), the gage resistance and substrate properties will vary significantly from their values at T = 530°R. In such a situation, appropriate corrections must be applied to the DLR equation as described in Reference 10. Taking these corrections into account, proper DLR values were defined and used to set the recording system sensitivity for the expected temperature rise during a test firing.

4. Pressure

The plenum chamber (Kistler) pressure transducers were calibrated (i.e., voltage output vs. applied pressure) after installation in the gage holders by using a dead-weight tester. The outputs are linear over pressure intervals considerably wider than those experienced during the test program.

The CAL-fabricated transducers were calibrated after installation in the heat shield tray by applying a known pressure step through a pneumatic calibrating device and recording the electrical output.

These calibrations, in conjunction with estimated values for the model pressure levels to be experienced during the test, also provide the basis for adjusting the gain of the data recording system to achieve maximum "readability" of the oscilloscope traces.

B. TEST PROGRAM

Since the primary emphasis of the program was directed toward making rotational temperature measurements, the extent of the base region which could be surveyed was limited by the fixed focusing limitations of the R.T.A. objective lens (focal length = 1.875 inches) although the fibre optic (density-sensing) units have the capability of focusing over a considerably larger interval. With a heat shield thickness of 0.5 inches, a small clearance between the R.T.A. and the heat shield (required for vibrational isolation of the R.T.A.), and the slight recess of the objective lens mounting plane from the R.T.A. surface (as well as the lens thickness), the total probing distance (height above heat shield) remaining is nominally one inch. The radial locations of the R.T.A. were selected to correspond to those of the fixed fibre optic units. Table I summarizes the run schedule and geometric positions at which measurements were made.

Table I

Electron Beam Temperature Program - Test Schedule

Run	RTA Location Radius inches	Beam Height above Heat Shield inches
1	1.625	1.0
2	2.6	↓
3	3.5	↓
4	4.5	↓
5	0.375	↓
6	0.375	0.75
7	1.625	↓
8	2.6	↓
9	3.5	↓
10	4.5	↓
11	4.5	0.50
12	3.5	↓
13	2.6	↓
14	1.625	↓
15	0.375	↓
16	0.375	0.25
17	1.625	↓
18	2.6	↓
19	3.5	↓
20	4.5	↓

Typical run data are shown in Figure 13 for a beam height above the heat shield of 1 inch and an RTA radial location of .375 inches from the center of the heat shield.

C. MODEL OPERATION

1. Shock-Tube

A constant area shock tube provided nitrogen working gas at a nominal total temperature of 2500°R and total pressure of 200 psia. The shock tube was operated in the "tailored interface" mode whereby the speed of sound and isentropic exponent ratios of the driver and the driven gases are controlled so that the reflected shock from the end of the driven tube does not, for the theoretical inviscid case, generate any reflected waves as the result of its interaction with the driver-driven gas contact surface (the interface). The isentropic exponent ratio for these tests was 1.0 as the individual isentropic exponents of all the working gases (H_2-N_2) were the same (1.4). The actual speed of sound ratio (driver/driven) used was 2.13 which results only from driver/driven gas molecular weight (the driver mixture was 84% H_2 and 16% N_2) differences since $\gamma_{driver} = \gamma_{driven}$ and $\tau_{driver} = \tau_{driven}$. A constant model supply pressure was maintained for approximately seven milliseconds although the pure nitrogen flow (and hence test time) was appreciably less because of interface mixing resulting from viscous effects. At an incident shock Mach number (M_i) of 3.2, pure nitrogen flow duration was about four milliseconds, more than a sufficient time interval for data acquisition. The pure nitrogen flow/test time interval was established from nozzle exit plane and heat shield convective heat-transfer rate measurements which exhibit a marked decrease as the relatively cool driver gas begins to pass through the nozzle (see Figure 14).

During the test event (corresponding to the period of steady nozzle flow), the altitude chamber ambient pressure remains constant until the disturbance created by the initiation of nozzle flow reflects from the chamber end wall and impinges upon the model. The time interval of constant ambient pressure for this particular vacuum chamber geometry has a maximum value of about 4 milliseconds which is compatible with the steady duration of nitrogen flow.

Shock tube operational procedures were as follows. A single, scribed, dead-soft copper diaphragm was installed at the driver-driven tube junction of the shock tube. Mylar diaphragms were placed in the four model nozzle throats to isolate the driven tube from the altitude chamber which was nominally at a pressure of 100 μ HgA for each test. After initially evacuating both the driver and driven tubes, the driven tube was loaded with nitrogen to absolute pressures on the order of 8 inches HgA. Anticipating rupture of the main diaphragm at the calibration pressure, hydrogen was loaded first into the driver tube to its correct partial pressure. The driver was then slowly "topped off" with nitrogen to the calibration pressure or until rupture of the diaphragm occurred. With single diaphragm operation of the shock tube, slight variations in M_i naturally occur as a result of nonrepeatibilities in diaphragm breaking strength, leading to variations in chamber pressure and temperature from design conditions of about ±7% and ±5%, respectively. Figure 15 shows the theoretical nonviscous relations between initial driven tube conditions and incident shock Mach number generated from the data of Ref. 11. The double-diaphragm technique, which ideally produces very repeatable test conditions, had been tried at these same operating conditions during a previous density-measuring program (Ref. 6), but poor diaphragm "petalling" characteristics were experienced, resulting in wider variations in reservoir conditions than given by the single diaphragm technique.

2. Electron Beam and Sensors

For all the tests, the electron beam was operated at an accelerating voltage of 25 to 30 kv, and a current level of approximately 100 μ a. After installation of model nozzle throat diaphragms and the driver-driven junction diaphragm, the vacuum chamber was evacuated and stabilized at the test altitude pressure. At this time, the ball valve was opened to inject the beam into the tank and R.T.A. data corresponding to the ambient pretest temperature were recorded.

From this point on, all data acquisition on the dual beam oscilloscopes was fully automatic through a sequence of triggers obtained from the shock tube wall heat-transfer gages and microswitches attached to the dynamic

stage ball valve stem. The first trigger, from the most upstream shock tube heat-transfer gage, caused all oscilloscopes to sweep and was timed to provide a few centimeters of trace corresponding to the initial tank conditions of temperature and density; the remainder of the trace was test event data. Immediately after the test event the ball valve closed and extinguished the beam with the microswitch closure signal causing all scopes to sweep again. For all the density channels and the beam current channel, this sweep represented the zero signal level. Since the R.T.A. calibrating lamp shutter opens coincidentally with ball valve closure, the oscilloscope recording R.T.A. data records the response of the two channels to the standard lamp at this time. Following this second sweep, a final appropriately timed pulse initiated lamp shutter closure and triggered a third sweep of the oscilloscope which records R.T.A. data to provide zero signal levels for these channels.

One dual beam oscilloscope was used for each density channel; the deflection of one trace was optimized (by adjusting oscilloscope sensitivity) for recording the signal corresponding to the initial tank density while the deflection of the other trace was optimized for recording test event data. Similarly, temperature data were recorded on two paralleled dual beam oscilloscopes. Gains of the two channels of one oscilloscope were optimized for recording test event temperature data while the gains of the second oscilloscope were optimized for recording the response of the R.T.A. to the calibrating lamp. The object of these procedures was to improve the readability of the records and thereby minimize the data reduction errors associated with small trace deflections. The timing sequence for data recording was chosen to minimize the time interval between the recording of data and zero signal levels, thus reducing the effects of any electrical drift in oscilloscopes or other equipment associated with data acquisition.

D. DATA REDUCTION PROCEDURES

1. Temperature

For each test there were R.T.A. data corresponding to the pre-run tank ambient temperature and to the actual test event temperature. Hence, for each run, values of intensity ratio corresponding to tank ambient temperature and run temperature were available.

Before considering the details of the data reduction procedure, it is desirable to first consider the following background material. Assume neutrality of all optic system elements except for the two interference filters and let constants C_1 and C_2 account for all the neutral lenses, reflectances, and path differences in the two channels. Let $T_{f1}(\lambda)$ and $T_{f2}(\lambda)$ represent the transmission characteristics of the two channels with T_{f1} (Max) $= T_{f2}$ (Max) $= 1$; call the light intensity incident on the apparatus inlet aperture $I(\lambda)$. For illumination by the standard lamp

$$\left(\frac{i_1}{i_2}\right)_{CAL} = \frac{C_1 S_1 \int_\lambda T_{f1}(\lambda) I_L(\lambda)\, d\lambda}{C_2 S_2 \int_\lambda T_{f2}(\lambda) I_L(\lambda)\, d\lambda} \tag{2}$$

where S_1 and S_2 are the photomultiplier sensitivities, i_1 and i_2 are the photocurrents of channels 1 and 2, and subscript L represents the lamp. For simplicity, let

$$A_1 = \int_\lambda T_{f1}(\lambda) I_L(\lambda)\, d\lambda$$

and

$$A_2 = \int_\lambda T_{f2}(\lambda) I_L(\lambda)\, d\lambda$$

Then,

$$\left[\frac{C_1 S_1}{C_2 S_2}\right] = \left(\frac{i_1}{i_2}\right)_{CAL} \frac{A_2}{A_1} \tag{3}$$

During observation of the beam excited fluorescence,

$$\left(\frac{i_1}{i_2}\right)_{EXP} = \left[\left(\frac{i_1}{i_2}\right)_{CAL} \frac{A_2}{A_1}\right] \frac{\int_\lambda T_{f1}(\lambda) I_B(\lambda)\, d\lambda}{\int_\lambda T_{f2}(\lambda) I_B(\lambda)\, d\lambda} \tag{4}$$

where subscript B refers to the beam.
Since the intensity ratio R is given by

$$R = \frac{\int_\lambda T_{f1}(\lambda) I_B(\lambda)\, d\lambda}{\int_\lambda T_{f2}(\lambda) I_B(\lambda)\, d\lambda} \tag{5}$$

it follows that

$$R = \left(\frac{i_1}{i_2}\right)_{EXP}\left(\frac{i_2}{i_1}\right)_{CAL}\frac{A_1}{A_2} \qquad (6)$$

Since the input signals to the oscilloscopes are voltages developed across 100 K-ohm resistors by photocurrent i_1 and i_2, the values needed to determine $\left(\frac{i_1}{i_2}\right)_{EXP}$ and $\left(\frac{i_2}{i_1}\right)_{CAL}$ can be found from the oscilloscope traces of the R.T.A. outputs when observing the beam excited fluorescence and standard lamp respectively. The value of A_1/A_2 can be calculated using the filter transmission characteristics and a measured value of lamp temperature. Using transmission data supplied by the manufacturer of the filters employed here and radiometry data from Reference 12, a value of 1.054 was calculated for A_1/A_2. Since the standard lamp current was always set at the same level, this value of A_1/A_2 should apply for every measurement.

The outputs from the two photomultipliers in the R.T.A. unit consist of the six traces as shown in Figure 13. These traces represent:

1. Prerun base line for channel 2.
2. Channel 2 output looking at calibration lamp.
3. Prerun base line for channel 1.
4. Channel 1 output looking at calibration lamp.
5. Channel 2 run output.
6. Channel 1 run output.

The ratio of precombustor firing levels on lines 5 and 6 represents the ambient prerun temperature with the run data represented by the ratio of the levels near the center of the oscilloscope picture.

For data acquisition during the test program, the outputs for the calibration lamp, prerun tank temperature and base flow field temperature were separately monitored on individual oscilloscopes, each set to allow maximum trace deflection and data reduction accuracy to be realized.

The data are reduced in the following manner:

$$R_{\substack{\text{Amb} \\ \text{Run}}_{or}} = \left(\frac{\Delta_{3-6 \; \substack{\text{Amb} \\ \text{Run}}_{or}}}{\Delta_{1-5 \; \substack{\text{Amb} \\ \text{Run}}_{or}}} \right) \cdot \left(\frac{\Delta_{3-4 \; CALIB}}{\Delta_{1-2 \; CALIB}} \right)^{-1} \tag{7}$$

with the value of gas temperature directly determined from the calibration curve of R vs temperature.

Data reduction revealed that, in a number of cases, the measured prerun value of R indicated an ambient temperature significantly higher than the temperature measured with a thermocouple mounted on the apparatus inside the tank. A limited experimental check subsequent to the completion of the program indicated such differences could result from small changes in the position of the R.T.A. with respect to the beam; this would cause a change in the optical path through the instrument resulting in a change in the filter transmission characteristics and hence a change in R for a given temperature. The difference between the prerun value of R and the value of R from the static calibration curve corresponding to the prerun ambient temperature as sensed by the thermocouple was sufficiently large that a correction to the value of R measured during the test event was deemed necessary if reasonable test event temperatures were to result.

This correction was made by shifting the calibration curve so that, at the measured (thermocouple) prerun ambient temperature, the curve passed through the measured prerun value of R ; the shape of the curve was unchanged. The shifted curve was then used to find the temperature corresponding to the test event value of R . Justification for this procedure is found in data presented by Muntz. He presents two curves for R vs temperatures resulting from calibrations of his R.T.A. (after which the present equipment was patterned); the difference between the two cases was a change in the size of the R.T.A. inlet aperture. Since this changes the optic path through the instrument with an attendant change in transmission characteristics, the two curves are different. However, over the range from 300°K to 500°K the difference simply amounts to a shift along the R axis; the variation of R with

temperature is the same. Moreover, the calibration data for this study, when plotted to the same scales used by Muntz with an additive factor to match the two values of R at 300°K fits his curve very closely. It was, therefore, felt that a translation of the R -axis could be performed so that the pretest value of R would correspond to the temperature measured with the thermocouple and the resulting shifted curve used with the measured run value of R to find the test event temperature. The test event temperature was then normalized to supply gas temperature (Tc) to account for run to run variations in model operation.

2. Density

Since the density calibration had shown the photomultiplier outputs to vary linearly with density, it was possible to reduce test event density data simply by scaling relative to the photomultiplier outputs for a known density; the known prerun tank density supplied the needed reference point. Since the total intensity of the beam-induced emission depends directly on beam current and since small changes in current level often occurred between the prerun and test event conditions, a correction to remove the dependence on beam current was necessary. In addition, a correction was necessary to account for the fact that the prerun atmosphere was air whereas the test gas was pure nitrogen. Considering the oscilloscope record of Figure 13, if a channel two trace deflection Δ_2 corresponds to a test event density ρ , a channel one prerun trace deflection Δ_1 corresponds to an ambient N_2 density ρ_a , S_1 and S_2 are the gains of channels one and two, and I_2 and I_1 , are the beam currents for the test event and prerun conditions, then

$$\frac{\rho}{\rho_a} = \frac{\left(\frac{\Delta_2}{\Delta_1}\right)}{\left(\frac{S_1}{S_2}\right)} \cdot \left(\frac{I_1}{I_2}\right) \tag{8}$$

where ρ_a is found from the measured initial temperature T_a (from the prerun R.T.A. data) and pressure P_a (from the McLeod gage reading) by

$$\rho_a = 0.78 \frac{P_a}{T_a R_{N_2}} \; ; \qquad R_{N_2} = \text{nitrogen gas constant} \tag{9}$$

The factor of 0.78 represents the nitrogen partial pressure in air.

For each run, the incident shock transit time between two points on the shock tube was measured, whence a determination of shock speed (M_i) was possible; the measured incident shock Mach number in conjunction with theoretical constant area shock tube relations[11] allowed the determination of the supply gas temperature (see Figure 15). This temperature and the measured value of plenum pressure permitted calculation of a combustion chamber density, ρ_c, from the ideal-gas equation of state. Normalization of test event density by ρ_c was performed to account for run to run variations in model operation.

3. Heat-Transfer

The thin-film heat-transfer gage is a resistance thermometer which reacts to the local surface temperature of the model. The theory of one-dimensional heat conduction to a semi-infinite slab is used to relate the surface temperature history to the heat-transfer rate. Assuming that the temperature sensed by the element is the surface temperature and that a first-order correction for element thickness will be adequate, the solution for the surface temperature as a function of time is

$$T(t) = \frac{1}{\sqrt{\pi C_2 \rho_2 K_2}} \int_0^t \frac{q(\lambda)\,d\lambda}{\sqrt{t-\lambda}} - q(t)\,\frac{\ell}{K_1}\left(\frac{C_1 \rho_1 K_1}{C_2 \rho_2 K_2} - 1\right) \qquad (10)$$

Here K is thermal conductivity; C, the specific heat; ρ, the density and ℓ, the film thickness; λ is a variable of integration and subscripts 1 and 2 refer to the metal film and pyrex substrate, respectively.

When the above equation is properly inverted to express the heat-transfer rate as a function of temperature and time, it can be programmed into a digital computer for solution. However, considerable effort is involved in converting the raw temperature-time data into a form suitable for insertion into the computer program. To overcome this restriction, an analog network, referred to as a "q-meter" has been developed to convert the temperature signal directly into a heat flux in real time for presentation on the oscilloscope. All heat-transfer data for this study were obtained directly through the use of q-meters.

a) Heat Shield Convective Heating

Using either the single- or double-diaphragm shock-tube operating technique, small variations in the reservoir conditions are experienced on a run-to-run basis. As a result, it was desired to normalize the heat-transfer data for both plenum pressure and temperature variations to the nominal plenum conditions (P_c = 200 psia and T_c = 2,500°R). It is shown in Ref. 13 that the turbulent flow heat-transfer coefficient for compressible flow over a flat plate can be described with reasonable precision with an equation of the Colburn type wherein the film coefficient is proportional to the 0.8 power of Reynolds number. Then, using the familiar convective heat-transfer equation, $q = h\ (T_R - T_w)$ where h = film coefficient, T_R = recovery temperature and T_w = wall (gage) temperature, one can write $q \propto (Re)^{0.8}\ (KT_c - T_w)$ where Re = Reynolds number and $K = T_R/T_c$. With velocity proportional to the square root of temperature and viscosity proportional to the 0.5 - 0.75 power of temperature (Ref. 14) we can write

$$Re = \frac{\rho V D}{\mu}$$

$$\propto \frac{P\sqrt{T}}{T(T^{.5-.75})}$$

$$\approx \propto \frac{P}{T}$$

so that with K known the normalization of the heat-transfer data can be carried out, using

$$\frac{q}{q_{NOM}} = \frac{\left(\frac{P_B}{T_B}\right)^{.8}}{\left(\frac{P_B}{T_B}\right)^{.8}_{NOM}} \left[\frac{KT_c - T_w}{K_{NOM}T_{c_{NOM}} - T_w}\right] \qquad (11)$$

Previous studies (Ref. 15) have shown that there is essentially a one-to-one correspondence between base pressure and combustor pressure. Further, if the base temperature is adequately described by the recovery temperature, we have

$$\frac{q}{q_{NOM}} = \frac{\left(\frac{P_c}{KT_c}\right)^{.8}}{\left(\frac{P_{c_{NOM}}}{K_{NOM}T_{c_{NOM}}}\right)^{.8}} \left[\frac{KT_c - T_w}{K_{NOM}T_{c_{NOM}} - T_w}\right] \qquad (12)$$

The value of K, which is a function of nozzle exit plane Reynolds number, is essentially constant for small variations in Reynolds number (i.e., P_c and T_c) so that it may be taken to be constant at the nominal plenum conditions.[16] This finally results in

$$\frac{q}{q_{NOM}} = \frac{\left(\frac{R}{T_c}\right)^{.8}}{\left(\frac{R}{T_c}\right)^{.8}_{NOM}} \left[\frac{KT_c - T_w}{KT_{c_{NOM}} - T_w}\right] \qquad (13)$$

A value of K of 0.53 was predicted from the results of Ref. 16 for the nozzle exit plane Reynolds number given by the nominal reservoir conditions for the present study. The actual recovery temperature determined from the experimental measurements indicated the actual value of K to be 0.47. However, because of the slight difference in the predicted and actual values and the relatively small effect of the temperature term (for the variations in T_c during the program), no further corrections to the normalized heat-transfer data were considered necessary.

b) Determination of Recovery Temperature

If it is assumed that the film coefficient is independent of wall temperature, it may be noted that, with $q = h\ (T_R - T_w)$, the recovery temperature can be determined experimentally if the wall (gage) is heated sufficiently to produce a condition where $q \rightarrow 0$ (i.e., $T_w = T_R$). In practice, the recovery temperature is generally considerably higher than a practical maximum gage temperature so that it becomes necessary to make an extrapolation of the data to obtain the indicated recovery temperature. Using the heated gage described previously, test firings were made at elevated gage temperatures, the data normalized using Eq. (13) and extrapolated to the indicated base region recovery temperature.

4. Pressure

All the pressure transducers employed measure the difference between the pressure to which they are initially exposed and the applied local pressure. The initial pressure for the plenum chamber transducers was the

driven tube pressure and for the heat shield transducers was the initial altitude tank pressure. These initial values are added to the measured ΔP to obtain absolute model pressures.

Because of the large model acceleration resulting from shock reflection in the shock tube, coupled with low pressure levels in the base region, little usable heat-shield pressure data were obtained with pressure transducers in spite of the acceleration compensation and isolation employed. Rather, heat-shield pressures were primarily deduced from the density and temperature data measured with the electron beam apparatus. For a given beam height above the heat shield, the local static pressure was calculated from the ideal gas law using the average measured density for the sequence of runs at this beam height and the measured temperature at the same radial location. These calculated pressures were then normalized to the average measured combustor pressure for the same sequence of runs. Extrapolation of the flow field pressures to the heat-shield surface then yielded base pressures.

IV. PRESENTATION AND DISCUSSION OF RESULTS

A. TEMPERATURE

Recirculated gas flow static temperature data (normalized to combustor temperature) are shown for each beam height as a function of base radius in Figs. 16 through 19. For all but the one inch beam height, a minimum temperature region is observed at a radius of 2.6 inches. This effect is not unexpected as this radius represents the plane of minimum base flow venting area between adjacent nozzles and hence a region of high flow velocity -- see Fig. 20. Figure 21 shows the approximate plume interaction loci calculated from the methods of Ref. 17 for the shock-heated nitrogen gas case. A large increase and subsequent drop in temperature may be noted at the two extreme outboard radial locations over this same height interval. The reasons for these changes are not clear at present. The possibility of a peripheral shock lying close to the base is felt to be rather remote as the ambient altitude pressure, 0.00285 psia, should be sufficiently lower than the pressure levels in the base region (total pressure approximately 0.015 psia) to assure a continuous expansion of the flow in traversing and exhausting from the base region. Further, no discontinuities were observed in the density data over this same region. For the one-inch beam height the decrease and subsequent increase in temperature occur at the 3.5 and 4.5 inch radial positions, respectively. Unless the base flow is skewed to the geometrical venting area plane, these data are in contradiction with geometrical considerations since the venting area between nozzles decreases (although only slightly) with increasing height from the heat shield. Further, the measured density data indicate higher flow velocities with increasing distance from the base plate. It should be noted that although most of the temperature data represent single test points, some replicated data were obtained and repeated very well; further, the trends in the data at all but the one-inch height are fairly consistent, two facts which add credibility to the data as a whole. A temperature map of the base region, generated by cross-plotting the data of Figures 16 through 19, is shown in Fig. 22. Uniform flow acceleration and deceleration, as judged

by the spacing of the isotherms, is again seen to occur in the 2-3 inch radial interval for heights up to about 0.8 inches. Figure 23 shows the heat shield temperature profile taken from the map data at $H = 0$ and exhibits the same qualitative trends as shown in Figs. 16 through 19. The temperature ratio at the heat-shield stagnation point ($R=H=0$) is seen to be approximately 0.47 ($= K$), or for a nominal combustor temperature of 2500°R, indicates a recovery temperature of about 1170°R.

B. DENSITY

Radial variations in density, presented in nondimensionalized form as the ratio of base region-to-combustor density, are shown in Figs. 24 through 27 for various heights above the heat shield. The points shown represent the arithmetically averaged experimental data with the bars indicating the data scatter. Since the beam height was held constant for five runs while the R.T.A. unit surveyed each of five radial positions, five repeat runs on the density channels were obtained at each beam height. It may be noted that the density increases with decreasing height and decreasing radius, except for the radii from 2.5 to 4.5 inches where, for the height interval from 0 to about .50 inches, the densities at each radius are nearly constant. This may be seen more clearly on the density map shown in Fig. 28 which was generated from cross-plots of the averaged data of Figs. 24 through 27. The recirculated flow in the height interval examined is seen to decelerate (increasing density) in the interior regions of the base ($0 < R <$ 2 inches) and accelerate uniformly as it passes out through the venting area between engines. A fairly high-shear region is seen to exist in the height interval $.5 < H < .7$ inches as the flow for $H <$ .5 inches accelerates slower than the flow for $H >$ .5 inches. The approximate density distribution along the heat shield surface, generated from the data shown on the map at $H = 0$, is shown in Fig. 29.

C. PRESSURE

Using the average density data, the measured temperature data and the ideal gas equation of state (N_2 at temperatures of $\approx$ 1200°R and pressures of 0.01 psia should behave as an ideal gas -- see Ref. 18), base region pressure levels were calculated and plotted versus radius for the test beam heights as shown in Figs. 30 through 33.

Except for the H = 1.0 data, the radial distributions show the same qualitative trends as temperature and density with the pressure increasing with decreasing height for the inboard radial positions as the flow stagnates. As a result of the monotonically decreasing radial density distributions and the high temperature region for the outboard radii, the pressure data exhibit an inflection and interval of near-constant pressure for $2.5 < R < 3.5$ inches. The pressure then uniformly decreases for the extreme outboard radial positions.

Cross-plotting these data resulted in the pressure map shown in Fig. 34. For this and the other maps the regions near the outer radii are the most difficult to construct as the cross-plotted data tend to become insensitive to variations in height and radius (as was noted with the density data) such that only incremental changes in a given parameter ratio, beyond the resolution of the data, would have allowed the completion of the maps in these regions. Note, for example, the fine increments needed to construct the pressure map even for $3 < R < 4$ inches. Using the pressure map data at H = 0 gave the heat shield pressure profile shown in Fig. 35. Shown also on Figure 35 are the heat-shield pressure data from Ref. 6, obtained (with difficulty) with CAL crystal-type pressure transducers. The data are within about 20% of each other, a not unreasonable agreement considering that they represent average experimental data from separate studies employing considerably different measuring techniques. Extrapolation of the pressure map data for R = 0 allowed the determination of the pressure distribution along the extension of the model axial centerline shown in Fig. 36 compared to reflection plane data of Ref. 6. In Ref. 6 it is noted that the heat shield/reflection plane combination induces a centered conical-shaped separated flow near the base so that the pressure measurements for small H are of questionable validity. As

anticipated, calculated centerline pressures obtained during this program do not agree very well with the data of Ref. 6 for $0 < H < 1$ inches, but appear to fair well into the data of Ref. 6 for $H > 2$ inches. This is consistent with the observations of Ref. 6 which indicates the separated flow region does not persist beyond the nozzle exit plane. Finally, the pressure distribution along a model nozzle centerline projected into a plane between engines is shown in Fig. 37 along with reflection plane data from Ref. 6 where an improvement in the agreement can be noted, probably as a result of decreasing effects of the separated flow region at this more outboard position.

D. CONVECTIVE HEAT TRANSFER

The radial heat shield heat-transfer rate distribution along a ray between engines, normalized for variations in combustor pressure and temperature to the nominal conditions of P_c = 200 psia and T_c = 2500°R, is shown in Fig. 38. The distribution is qualitatively very similar to those measured with combusted gas flow;[16] the large quantitative difference in nitrogen/combusted gas results can be explained upon examination of the heat-transfer equations (see succeeding discussion).

Since the results of more comprehensive programs utilizing electron beam techniques may be used in the future for the formulation of heat-transfer rate scaling laws, a brief comparison of the heated nitrogen/combustion gas results for this model was carried out using the present data and those of Ref. 16. Using the familiar convective heat-transfer rate equation and assuming that an equation of the Colburn type will adequately describe the film coefficient we have

$$\frac{q_{N_2}}{q_{COMB}} = \frac{h_{N_2}}{h_{COMB}} \frac{(T_R - T_W)_{N_2}}{(T_R - T_W)_{COMB}} \tag{14}$$

and

$$Nu = a\, Re^{.8} Pr^{.33} \tag{15}$$

or

$$h = \frac{K}{\ell} a\, Re^{.8} Pr^{.33} \tag{16}$$

Then assuming $a_{N_2} = a_{comb}$ and with $\ell_{N_2} = \ell_{comb}$, $Tw_{N_2} = Tw_{comb}$,

Eq. (14) becomes

$$\frac{q_{N_2}}{q_{COMB}} = \frac{\left[K Re^{.8} Pr^{.33} (T_R - T_w)\right]_{N_2}}{\left[K Re^{.8} Pr^{.33} (T_R - T_w)\right]_{COMB}} \tag{17}$$

where K, Re and Pr are all to be evaluated at the base region conditions. The Reynolds number

$$Re = \frac{\rho V \ell}{\mu}$$

can be written as

$$Re = \frac{\rho M \sqrt{\gamma RT}\, \ell}{RT \mu}$$

$$= \frac{\rho M \ell}{\mu} \sqrt{\frac{\gamma}{RT}} \tag{18}$$

For a heat-transfer gage near the heat-shield stagnation point (R = 1 inch) the following input data are obtained from Refs. 16, 18 and 19 and from the present study:

	NITROGEN DATA	COMBUSTION GAS DATA (H_2 -O_2, P_c = 350 psia, O/F = 5.5)
Gage Radius ~ in.	1	1
Pressure ~ psia	0.0145	0.04
Temperature ~ °R	1050	2220
Viscosity ~ poise	2.88×10^{-4}	4.2×10^{-4}
Gas constant ~ $\frac{\text{ft-lb}}{\text{lb-°R}}$	55.2	117
γ	1.4	1.3
Conductivity ~ $\frac{\text{cal}}{\text{cm-sec-°K}}$	10.68×10^{-5}	38×10^{-5}
$(\text{Prandtl No})^{0.33}$	0.882	0.9285

The temperature presented and used in determining the transport properties is the experimentally measured recovery temperature since the comparison is being made near the stagnation point. These data, along with

$$\frac{q_{N_2}}{q_{COMB}} = \frac{\left[K\left(\frac{\rho}{\mu}\sqrt{\frac{\gamma}{RT}}\right)^{.8}\rho_2^{.33}(T_R - T_W)\right]_{N_2}}{\left[K\left(\frac{\rho}{\mu}\sqrt{\frac{\gamma}{RT}}\right)^{.8}\rho_2^{.33}(T_R - T_W)\right]_{COMB}} \tag{19}$$

resulting from Eqs. (16), (18) along with assuming that $M_{N_2} = M_{cold}$, give

$$\frac{q_{N_2}}{q_{COMB}} = 0.085 \tag{20}$$

Reference 16 gives $q_{2comb} = 3.5$ BTU/ft^2-sec for R = 1 inch which implies $q_{N_2} = 0.30$ BTU/ft^2-sec from Eq. (20); the data of Fig. 38 show q_{N_2} as measured here to be 0.32 ± 0.04 BTU/ft^2-sec. This excellent agreement between the measured heating rate and that predicted from combustion gas results, unless coincidental, adds credence to the experimental data and assumptions used in the calculation. The base region flow, although in both cases having low Reynolds number ($\leq$ 1000) can apparently be described as turbulent as regards the heat-transfer rates. This type of Reynolds number-heat transfer rate correlation (i.e., low Reynolds numbers with apparent turbulent heating rates) has been observed on previous CAL studies[16,26] and by other researchers[20,21]. The data of Ref. 20, for example, show a large increase in stagnation point heating rates for relatively low turbulence levels while Ref. 21 states that the boundary layers of clustered engines (which are already turbulent) have to adjust to turbulence levels of 100% (turbulent velocity fluctuations equal in magnitude to the nominal free-steam velocity) while being recirculated into the base region as a result of the turbulence induced from the exhaust plume interactions.

E. RECOVERY TEMPERATURE

The results of the brief series of tests with the heated-heat transfer gage are shown in Fig. 39 where it may be seen that the indicated value of recovery temperature is approximately 1000°R which compares favorably with that indicated by the extrapolated R.T.A. measurements, 1170°R.

V. FEASIBILITY OF DENSITY MEASUREMENTS IN COMBUSTED GASES

A. TRAJECTORY/PROPELLANT CONSIDERATIONS

In addition to the electron beam measurements in nitrogen nozzle flows, a second objective of the present program was an evaluation of the possibilities of extending the electron beam probe to the measurement of densities in hot combusted gases. Although radiating systems can be excited by an electron beam in gases other than nitrogen (e.g., Ar, He, O_2, NO, CO - some of which may be present in rocket exhaust gases or in booster base regions), these systems have the disadvantage (excepting He) that the intensity of emission is significantly lower than that of N_2 for similar conditions.

At the present time, two propellant combinations of primary interest to NASA in large rocket engine technology are RP-1/liquid oxygen (LOX) and liquid hydrogen/LOX. These propellants have normally been simulated at CAL by ethylene (C_2H_4)/oxygen and hydrogen/oxygen, all in the gaseous phase. Of the emitting set of gases mentioned above, only CO is present as a natural combustion product from the C_2H_4-O_2 reaction (for performance reasons rocket engine propellant mixture ratios are normally fuel-rich so that molecular oxygen is not present in any quantity as a typical combustion product). The proportions of CO or other natural products of combustion in the recirculated exhaust flow in the base region (which of course must be known to determine total density) are potentially calculable only for altitudes sufficiently high that the degree of external air - entrainment in the base region is small so that no extraneous reactions take place. Definition of these proportions in itself requires the assumption that the recirculated flow composition is, for example, either frozen at the nozzle exit plane value or remains in chemical equilibrium in flowing through the base region. Concentration calculations in the latter case, however, generally require knowledge of the gas state, which can be established if the CO spectral constants are sufficiently well known. That is, the CO temperature could be measured with the R. T. A. in addition to a CO partial density measurement.

The combustion gas total density could then be determined by the following procedure. An assumed CO concentration, in conjunction with the measured CO partial density, will yield a calculated total density. For this calculated density and experimentally measured temperature, an equilibrium CO concentration can be found. This value can then be compared with the originally assumed concentration and an iteration performed until a consistent gas state is established.

In contrast to the high altitude situation, the lower booster stages which operate at the lower altitude portions of the trajectory normally employ scoops and deflectors to purposely introduce air into the base region for cooling purposes. With this operating mode, some of the other gas components of the set mentioned above will be present in the base in proportions, for example, existing naturally in air or, more generally, in unknown proportions. Clearly the deduction of base region total density from the measured emission of even a known mixture of emitting gases (the measurement itself would be a significant accomplishment since the gases emit in overlapping and separated spectral regions) could only be accomplished with extensive pre-test calibration experiments using base region gas mixtures anticipated throughout a given test program. The introduction of air into the base region (which may occur in the lower altitude case even without external airflow) may also lead to "base-burning" whereby the combustibles from the recirculated exhaust products react with the scooped or aspirated ambient air.

With hydrogen-fueled stages the measurement of base region densities relies on the successful seeding of the working gases with an emitting gas since the only natural combustion products are hydrogen and water vapor for the nominal fuel-rich mixture operating conditions. Although no hydrogen-fueled lower stages presently exist, the same low altitude problems mentioned above would exist for this case as well. Nitrogen seeding in the case of hydrocarbon fuels does not present a solution to any of the low altitude problems.

For the lower stages then, the proportions and even the type of various gas species present become virtually impossible to predict since the chemical reactions which occur, the amount of air scooped or aspirated in and the amount of recirculated exhaust products vary unpredictably along the trajectory and with the particular stage geometry. (The amount of re-circulated gases and hence total density in the base is also dependent on the trajectory (altitude) point and stage geometry for the upper stage as well). Further, the total densities in the base region for the lower stage cases (Fig. 40 shows some typical base pressure-altitude relations for various Saturn stages), in addition to the higher ambient densities, may very well be sufficiently high to cause either electron gun operational problems, excessive beam spreading or collision quenching to occur.

With these considerations in mind, it seems unlikely at this time that the electron beam base region gas density measuring technique could be successfully applied toward obtaining any low operating altitude stage information, independent of the propellants and/or seeding technique employed.

On the basis of these considerations, it appears that high altitude experiments offer the best, (and possibly only) approach to density measurements in combusted gases. For the unseeded hydrocarbon-fueled case even high altitude tests would pose experimental difficulties due to the considerably less intense CO flourescence, in addition to the problem of defining concentrations. Since CO exhaust-gas concentrations at the nozzle exit planes are normally on the order of 30-40% by volume, it is questionable whether sufficient (high signal-to-noise ratio) CO emission would exist to allow density measurements. The combustion chamber equilibrium concentrations of CO, which are considerably higher than nozzle exit plane concentrations, are shown in Fig. 41 as a function of mixture ratio for the RP-1/LOX case.

B. SEEDING OF COMBUSTED GASES

Seeding of the exhaust gases, employing a relatively inert, fluorescing gas as a tracer (the most promising of which is nitrogen), is a technique which seems to offer the most chance of success for either propellant

system. The seeding technique, however, is not free of problems and due consideration will have to be given to a number of factors, including the effects of:

1) Other gases which fluoresce when excited by the electron beam. Although species which are known to fluoresce may be formed in the rocket combustion chamber, (for example CN, NO (only as a result of the N_2 seed gas), CO, OH, CH and various ions of nitrogen, oxygen, hydrogen, carbon monoxide and nitric oxide[19,22]) the existence of these species in the base region (and in fact at the nozzle exit plane) is rather remote. Furthermore, except for CO these species are generally present only in small or trace quantities, even in the combustion chamber (see, for example, Fig. 42) and decay in concentration during the nozzle expansion process. Should the nitrogen tracer gas react to form compounds such as CN or NO and should these species persist in the flow, then an adjustment to the nominal seed gas concentration level would also need to be made.

The other species which form the primary constituents of the exhaust flow and which will definitely be present in the base region will also emit (except for water vapor) in the 3800 Å - 4300 Å wavelength interval (the interval used to make density measurements in N_2) when subjected to electrical discharges.[23] The intensity of the emission from these species, their effect on the density measurements and their dependence on specie concentrations and electron beam conditions, for example, are currently not well defined.

2) Background radiation and absorption from the rocket plumes and base region flow. Unless adjustments in the fiber-optic/electron beam orientation can be made, the fiber-optic units will observe the clustered-engine plume structure and base region flow as a background radiative source. Although the most intense bands in an ethylene flame appear to be a result of the presence of CH ($\approx$ 3900 Å which is, if at all, present only in trace quantities in the plume/base flow, emission of lower intensity does occur for $3800\,\text{Å} < \lambda < 4300\,\text{Å}$. The hydrogen flame also has a variety of emitting bands in the interval of interest, the intensity of which decrease with

decreasing chamber pressure and mixture ratio (O/F)[24]. Beam emission absorption by the base region gas between the beam location and fiber-optic unit, although anticipated to be small, will have to be equivalent to the absorption during the calibration process.

In an effort to delete both these sources of unwanted spectral signals, it may be possible to observe only certain narrow spectral bands through the use of narrow bandpass optical filters rather than the fairly broad bandpass filters presently employed in the fiber-optic units. Proportionately lower signal levels will result however and, in addition, it is likely that the density measurements may become gas temperature sensitive (recall that the temperature-measuring technique relies on the temperature-dependent changes in spectral signals in the fine structure for its success).

3) Base region total density levels which, as in the non-seeding case, must be high enough to compensate for the N_2 partial density and resultant lower level of light intensity (which is directly proportional to the partial to total pressure ratio of the emitting gas) and signal/noise ratio of the detecting system. The effects of beam spreading at these total density levels must fall within the allowable tolerances set on spatial resolution and detector size since the total intensity must be observed.

With the N_2 tracer method, consideration will also need to be given to the amount of tracer that may be tolerably introduced while attaining combustion (which presents no significant problems for H_2-O_2 reactions due to the wide H_2 flammability limits but requires consideration for C_2H_4-O_2 reactions) as well as the point at which this addition may be made. For example, injection of the tracer could be made subsequent to combustion to minimize interference with the combustion process. For this scheme the density range of the technique will be less than that of situations where pure N_2 flows are employed.

Despite this limitation the beam technique may still provide a valuable measurement capability for gas flows at densities below the quenching limit. It is not know, without experimental verification, what quantity of N_2 tracer will be required for meaningful measurements in a

given flow situation or over what range of base densities a given quantity of nitrogen will facilitate reliable measurement. However, the approximate minimum usable densities of N_2 have been determined for an improved hypothetical electron beam density probe (the many independently variable parameters in the electron beam apparatus render a precise calculation difficult).

At this time the prospects of conducting successful experiments with the complex hydrocarbon fuel systems appear remote even for the high-altitude case. Considerably more reconnaissance-type experiments and analytical effort would be required in the hydrocarbon case than in the hydrogen case in order to establish a firm foundation upon which to base comprehensive experiments using the electron beam apparatus. Other hydrocarbon fuel-related problem areas requiring investigation have not even been mentioned here (e.g., the effect of carbon deposition on density-sensing unit optics) in the interest of brevity but, in addition to the aforementioned problems, indicate the magnitude of research required before accurate interpretation of electron beam measurements can be made.

C. MINIMUM SEED GAS CONCENTRATION - TEST TIME

Based on experimentally measured results, a number (designated C) has been derived that is useful in evaluating threshold levels of density measurable with a given configuration of apparatus (Ref. 5). The number C represents the number of photons per second per microampere beam current per unit solid angle per molecule emitted by the gas for a specific excitation process. A value of $10^{-9\pm1}$ was found to apply to the emission from the first negative system of nitrogen. Note that the beam accelerating voltage is not included in the dimensions of C even though the intensity of the fluorescence is known to be a function of electron energy. Compared to the order of magnitude uncertainty in the value of C, the modest voltage effect has been ignored (Ref. 25).

An appropriate criterion to use in calculating minimum densities based on the value C is the fundamental limitation of the photomultiplier in

the measurement of fluorescent intensity. This inherent limitation is the error associated with the statistics of photon counting for the situation of very weak signals. Assume that on the average N photoelectrons per second are emitted from a photocathode. The exact number emitted in a time interval Δt is not $N\Delta t$, but differs from this value by an amount d. From probability theory, the average square deviation is given by Equation 21.

$$\bar{d}^2 = N\Delta t \tag{21}$$

The relative accuracy of the measured photocurrent (under ideal conditions) is given by ϵ.

$$\epsilon = \frac{\sqrt{\bar{d}^2}}{N\Delta t} = \frac{1}{\sqrt{N\Delta t}} = \frac{1}{N_C} \tag{22}$$

N_C = number of photoelectrons counted.

Thus for an accuracy of 1%, a total of 10^4 photoelectrons would need to be counted and a total of 10^5 photons would need to be incident on a photocathode having a 10% quantum efficiency. With the photon requirement established, the value of C may be used to compute the minimum density for some assumed set of test conditions.

To establish the reasonableness of the value of C, a calculation was made to test the agreement of the results of some CAL measurements with predicted results and a level of confidence has been established that realistic results are obtained with this parameter.

Computations were made for an improved hypothetical electron beam density probe to establish minimum density measurements as functions of observation (averaging) time and accuracy. The word "improved" is used in the sense that a more favorable optical system and a higher beam current have been assumed. The results of this analysis are shown in graphical form in Fig. 43 together with the applicable probe parameters.

Values assumed for the optical system represent essentially optimum values. To achieve a transmission of 50% would preclude the use of fiber-optic light guides. Quantum efficiencies as high as 20% may also be realized

with certain photocathodes. Perhaps the greatest leeway lies in the value of the beam current which was chosen based on CAL experience. With an improved beam focusing system, beam currents up to 1 ma could probably be achieved thus lowering minimum densities by a factor of five from those shown in Figure 43. In general, it is felt that the plotted data are representative of a near-optimum, practically-realizable system.

Using the data from Fig. 43, the minimum N_2 density required for a 10% allowable error and a test time of 1 msec is 20×10^{-8} g/cc. Assuming that the base region total/combustor density ratio is the same for the combustion and nitrogen flow cases (for similar geometry and equivalent plume expansion), the data from Fig. 28 indicate a minimum value of this ratio of about 0.5×10^{-4}. Then, since

$$\rho_c = \rho_{N_2} \left(\frac{\rho_T}{\rho_{N_2}} \right) \frac{1}{\left(\frac{\rho_T}{\rho_c} \right)} \tag{23}$$

we have, using the above inputs,

$$\rho_c = 1.443 \times 10^{-4} \left(\frac{\rho_T}{\rho_{N_2}} \right) \sim lb/in^3 \tag{24}$$

From the above, if the allowable error for a given test time is selected along with the region of the base flow field which is to be observed such that the value of (ρ_T/ρ_c) is known, it is possible to generate the required relation between the percent of nitrogen seed, (ρ_{N_2}/ρ_T), and required combustor density, ρ_c . Equation (23) is shown plotted in Fig. 44 for test times of 1, 2 and 5 msec where it can be seen that as the amount of seed and/or test time increases, the allowable values of ρ_c (which lie above the curves) increase, as would be expected. Alternately, assuming that other effects are of second order importance, the maximum value of ρ_c for any given percentage seed may be approximated by the region in the flow field where ρ_T is greater than the room-temperature density at P = 1 mm Hg, since this is the nominal upper density limit from beam-spreading/quenching considerations. This maximum value of ρ_T and those larger, however, occur along and within a particular geometric locus, respectively, so that the maximum value of ρ_c depends on the degree of beam penetration desired. That is, for a given value of ρ_c the density map indicates the locus along which $\rho_T \geq \rho_{T\,allow}$. For the flow region outside of this locus $\rho_T \leq \rho_{T\,allow}$

and probing of the flow may, in principle, be carried out while excessive beam spreading occurs within the region interior to this locus.

With time established as an important criteria in determining the accuracy of density measurements, it is desirable to briefly consider the model test times which are available. Two factors control the amount of available test time for short-duration rocket experiments. These are (1) the time for reflected expansion waves from the ends of propellant supply tubes to enter the combustion chamber and (2) the time for reflection of the shock wave generated upon rocket ignition to reflect from the endwall of the altitude chamber and upset the flow in the base region. The first effect is controllable by simply making the propellant load tubes as long as desired as long as model overheating does not take place.

The second effect depends on the model combustion pressure and test altitude pressure (shock strength), the model total flow rate and type of ambient gas used in the altitude chamber. For typical models, end wall reflection times lie in the range of 3-10 msec with the lower values corresponding to higher test altitudes. It is apparent that a careful balance must be maintained between the amount of seed gas employed, the desired measurement accuracy, and available test time when considering electron beam measurements in combusted gases.

D. OPERATING CONDITIONS

In addition to the measurement accuracy considerations discussed above, a separate, independent relation between ρ_c and ρ_{N_2}/ρ_T exists as a result of the chemical/thermodynamic occurrences within the combustion chamber. For the seeded hydrogen-fueled case, for example, the following reaction will exist in the combustor for an oxidizer/fuel ratio of 5.0 (a typical rocket engine value):

$$\left[\frac{5}{8}H_2 + \frac{5}{16}O_2\right] + \frac{3}{8}H_2 + xN_2 \longrightarrow \frac{3}{8}H_2 + \frac{5}{8}H_2O + xN_2 \qquad (25)$$

assuming that the only combustion products are those indicated. Upon selecting various values of x, the adiabatic flame temperature for constant-pressure combustion may be calculated. Since

$$\frac{x}{\frac{3}{8}+\frac{5}{8}+x} = \frac{x}{1+x} = \frac{\rho_{N_2}}{\rho_T} \quad , \tag{26}$$

and assuming that this ratio persists into the base region (which in fact must be assumed to interpret the data), values of x may be selected such that

$$0 \leq \frac{x}{1+x} \leq 1.0 \tag{27}$$

After calculating $T_c = T_c(x)$, combustor densities

$$\rho_c = \frac{P_c}{\frac{\mathcal{R}}{MW_c} T_c} \quad ; \qquad \begin{aligned} \mathcal{R} &= \text{universal gas constant} \\ MW_c &= \text{molecular wt. of comb. prod.} \end{aligned} \tag{28}$$

may be calculated by selecting P_c (T_c is a very weak function of P_c) and calculating MW_c for various values of x using

$$MW_c = \frac{\frac{3}{8}(2)+\frac{5}{8}(18)+x(28)}{1+x} = \frac{12+28x}{1+x} \tag{29}$$

The results of these calculations are shown as the upper left-hand curves of Fig. 44 for various values of P_c . The intersection points of these curves with the lines of minimum allowable ρ_c represent the optimum (minimum N_2 seed) operating conditions to achieve a given percentage error for a given test time. Along with the density map, these minimum values of ρ_c also define (via the maximum ρ_T level) the maximum probing region in the base for any given P_c .

This type of operating map can be constructed for a variety of allowable error-test time criteria and various mixture ratios and will represent realistic operating limits if the experimental equipment, etc. assumed in constructing Fig. 43 are realized and if other potential operating limitations may be ignored.

For the use of nitrogen as a tracer or seed gas, further consideration must be given to additional effects about which only limited information is currently available. One of these effects is that of collision quenching due to the various species present in the combustion products. Exactly how the quenching phenomena is amplified or attenuated due to the presence of these species is not known. Internal CAL research is presently being conducted to determine the effects of a series of gaseous diluents on electron beam measurements in nitrogen.

E. PRACTICAL SEED GAS INJECTION

The homogeneity of the injected seed gas is a very important factor. Clearly, local high or low concentrations of N_2 will lead to erroneous measurements and may upset the character of the base flow (local thermodynamic quenching, for example). This requirement demands, if the nitrogen is introduced into the oxidizer prior to combustion, extremely symmetric type combustor injection patterns and engine porting. Even with the geometrically symmetric models (which are in fact employed now) the uncertainties in microscopic combustion events may present a problem in actually achieving homogeneity.

If the seed gas is injected after combustion occurs, injection will have to be accomplished through the porting or nozzle walls or through small seed gas injectors inserted into the main flow streams, either of which will tend to upset the main flow conditions. This would be especially true with wall injection of the seed gas which upsets the boundary layer characteristics which are critical in determining the nature of the recirculated gases and resultant base flow. Depending on the amount of seed gas employed (which is desirably low) uniform injection may lead to practical problems associated with miniature injector geometries (e.g., calculation of discharge coefficients).

F. SUMMARY

Despite a host of potential problem areas requiring investigation before electron beam techniques may be employed for measuring gas densities in

recirculated flow fields it is felt that, particularly for the hydrogen-fueled high-altitude case, successful application of the technique is possible and offers advantages not associated with any other measuring technique. Detailed investigations of the flow field parameters offer the only means of determining an accurate base flow model from which to establish scaling laws and determine critical parameters and can essentially be carried out only with electron beam techniques.

VI. CONCLUSIONS AND RECOMMENDATIONS

Extension of the electron beam rotational temperature measurement principle to a practical system capable of providing a detailed survey of the base flow field of a scale model rocket vehicle has been successfully demonstrated. With the realistic model operating conditions employed, useful beam lengths on the order of 12 inches were realized. Consistency between the data acquired with the electron beam apparatus and with more conventional techniques has been demonstrated. Although measurements at a solid surface cannot be obtained directly with the electron beam technique, it appears that the data may be extrapolated with confidence to obtain the values at a surface or other plane in the flow field. Temperature, density and pressure maps of the base region flow may be readily generated and although restricted in these experiments to a rather small spatial region, such maps provide insight in to the nature of the flow field.

The ease with which heat shield recovery temperature may be determined with the electron beam - R.T.A. technique is a significant result of this study since the means used to date have required: (a) heated heat-transfer gages (the entire heat shield has also been heated), (b) a number of test firings, (c) the assumption that the film coefficient is independent of wall temperature and (d) at times, large extrapolations of the data. (The recommendations of the study of Ref. 26, for example, deal primarily with improvements to the experimental techniques for determining recovery temperature).

Based on operational experience with the electron beam R.T.A., two desirable improvements are recommended for future applications. One involves the incorporation of a focussing capability into the R.T.A. to allow a more extensive survey of the flow field than was possible during this investigation. The second improvement concerns the need for mechanical apparatus to facilitate accurate geometrical alignment of the R.T.A. relative to the fluorescent beam (as in any optical system, alignment is of critical importance to proper performance).

A number of technically useful future programs are suggested on the basis of the results obtained during this project. A natural extension of the present study would be a program to map the base flow temperature field in a detailed manner for a given test condition or variety of test conditions. Although consideration of the seeding technique for obtaining density measurements has brought to light a number of potential difficulties, the magnitude of these difficulties has not been defined and, in fact, their existence in some cases is largely speculative. Experiments should be conducted to investigate these problem areas, and in the case of a particular set of test conditions and seed gas, it is felt that a simple program would be sufficient to establish the practicality of proceeding with more comprehensive tests. The development of a successful seeding technique for combusted gas flows would allow direct examination of the flow fields of more practical interest and avert many of the problems associated with converting "cold" gas results to equivalent combustion flow results. Subsequent to the development of such a technique (nitrogen seeding of hydrogen-fueled high-altitude stage engines is suggested) programs may be formulated to provide an experimental basis for extending the scaling techniques of Ref. 16.

Another propulsion-system oriented problem felt to be amenable to investigation with electron beam techniques is that of rocket nozzle plume definition. The conditions (pressures, densities, etc.) in the peripheries and downstream fields of highly underexpanded plumes, typical of those existing in high-altitude flight, appear to be compatible with those necessary for making measurements with the beam technique.

VII. REFERENCES

1. Bird, K.D., Matthis, C.L., and Reece, J.W.: "The Application of Short-Duration Techniques to the Experimental Study of Base Heating. Part I: High Altitude Testing Technique and Experimental Results for a 4-Engine Rocket Configuration," CAL Report No. HM-1510-Y-1 (I), April 1962.

2. Muntz, E.P.: "Static Temperature Measurements in a Flowing Gas," Phys. Fluids 5, 80, 1962.

3. Softly, E.J., Muntz, E.P., and Zempel, R.E.: "Experimental Determination of Pressure, Temperature, and Density in Some Hypersonic Near Wakes," G.E. Report TIS R64SD35, May 1964.

4. Muntz, E.P. and Marsden, D.J.: "Electron Excitation Applied to the Experimental Investigation of Rarified Gas Flows," Rarified Gas Dynamics Vol II Academic Press, 1963.

5. Muntz, E.P., Abel, S.J., and Maguire, B.L.: "The Electron Beam Fluorescence Probe in Experimental Gas Dynamics," Supplement to IEEE Transactions on Aerospace Vol. AS-3, No. 2, June 1965.

6. Bogdan, L. and Muench, R.K.: "Density Measurements in the Reverse Flow Field of a Four-Engine Rocket Cluster Model Using an Electron Beam Technique," CAL Report HM-2045-Y-1, to be published.

7. Muntz, E.P. and Abel, S.J.: "The Direct Measurement of Static Temperatures in Shock Tunnel Flows," G.E. TIS R64SD25, 1964.

8. Blifford, I.H., Jr.: "Factors Affecting the Performance of Commercial Interference Filters," Applied Optics, Vol. 5, No. 1, January 1966.

9. Personal communications with E.P. Muntz, 24 July 1964.

10. Bogdan, L.: "Heat-Transfer Instrumentation," CAL Report WTH-021, March 1963.

11. Lewis, C.H. and Burgess, E.G.: "Nitrogen Normal Shock Properties," private communication.

12. Gray, D.E. ed.: "American Institute of Physics Handbook," McGraw-Hill Co., Inc., 1957.

13. McAdams, W.H.: "Heat-Transmission," McGraw-Hill Co., Inc., 1942.

14. Bartz, D.R.: "A Simple Equation for Rapid Estimation of Rocket Nozzle Convective Heat-Transfer Coefficients," Jet Propulsion, January 1957.

15. Goethert, B.H.: "Base Flow Characteristics of Missiles with Cluster-Rocket Exhausts," Aerospace Engineering, March 1961 (also IAS Paper 60-89, National Summer Meeting, 28 June-1 July 1960.)

16. Sergeant, R.J.: "Base Heating Scaling Criteria for a Four-Engine Rocket Cluster Operating at High Altitude," AIAA Paper 65-826, Presented at the AIAA Aerothermochemistry of Turbulent Flows Conference, San Diego, California, December 1965.

17. Latvala, E.: "Spreading of Rocket Exhaust Jets at High Altitude," AEDC TR-59-11, June 1959.

18. National Bureau of Standards Circular 564.

19. Gordon, S., and McBride, B.J.: "Theoretical Performance of Liquid Hydrogen with Liquid Oxygen as a Rocket Propellant," NASA Memo 5-21-59E, June 1959.

20. Kestin, J., et al: "The Influence of Turbulence on the Transfer of Heat to Cylinders Near the Stagnation Point," NACA Tech. Note 4018, October 1957.

21. Krause, F., et al: "Heat Transfer Below Reattaching Turbulent Flows," AIAA Paper 65-825, Presented at the AIAA Conference on Aerothermochemistry of Turbulent Flows, December 1965.

22. Huff, V.N., et al: "Theoretical Performance of JP-4 Fuel and Liquid Oxygen as a Rocket Propellant; II Equilibrium Composition," NACA Research Memo E56D23, September 1956.

23. Pearse, R.W.B., and Gaydon, A.G.: "The Identification of Molecular Spectra," John Wiley and Sons, 1941.

24. Burrows, M.C., and Povinelli, L.A.: "Emission Spectra from High-Pressure Hydrogen-Oxygen Combustion," NASA Tech. Note D-1305, July 1962.

25. Personal communications with E. P. Muntz, 2 August 1965.

26. Sergeant, R. J.: "The Application of Short-Duration Techniques to the Experimental Study of Base Heating; Part II: A Study of Reynolds Number and Temperature Effects on Base Heating for a Four-Engine Hot Rocket Configuration Operating at High-Altitude," CAL Report HM-1510-Y-1 (II), April 1965.

VIII. NOMENCLATURE

A = $\int_\lambda T_f(\lambda) I(\lambda) d\lambda$ (Eq. 2)

a = constant dependent on geometry (Eq. 15)

C = optical constants

D = characteristic length

h = film coefficient

I, i = current, light intensity (Eq. 2)

K = thermal conductivity

l = characteristic length

M = Mach number

MW = molecular weight

N = photoelectrons per second

Nu = Nusselt number

P = pressure

P_r = Prandtl number

q = heat-transfer rate

R = radius; electrical resistance; gas constant; R.T.A. measured intensity ratio (as noted)

R_e = Reynolds number

S = instrument sensitivity

T = temperature

t = time

V = velocity

X = mol fraction of nitrogen (Eq. 25)

γ = isentropic exponent

Δ = oscilloscope trace deflection

ϵ = accuracy (Eq. 22); area ratio

λ = wavelength or dummy variable (Eq. 10)

μ = viscosity

ρ = density

LIST OF FIGURES

LIST OF FIGURES (Cont.)

Figure

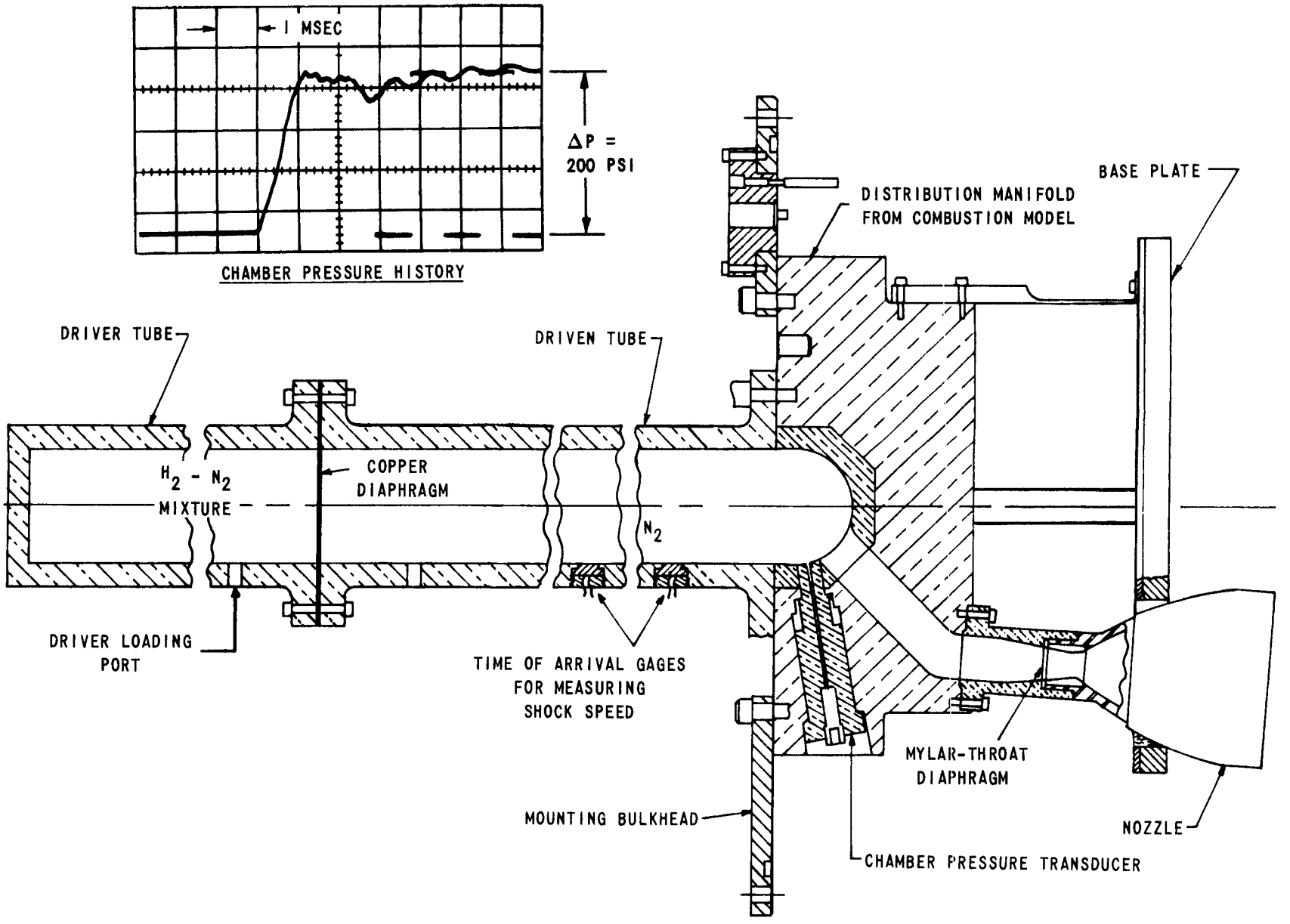

Figure 1 MULTI - ENGINE MODEL SHOCK TUBE CONFIGURATION

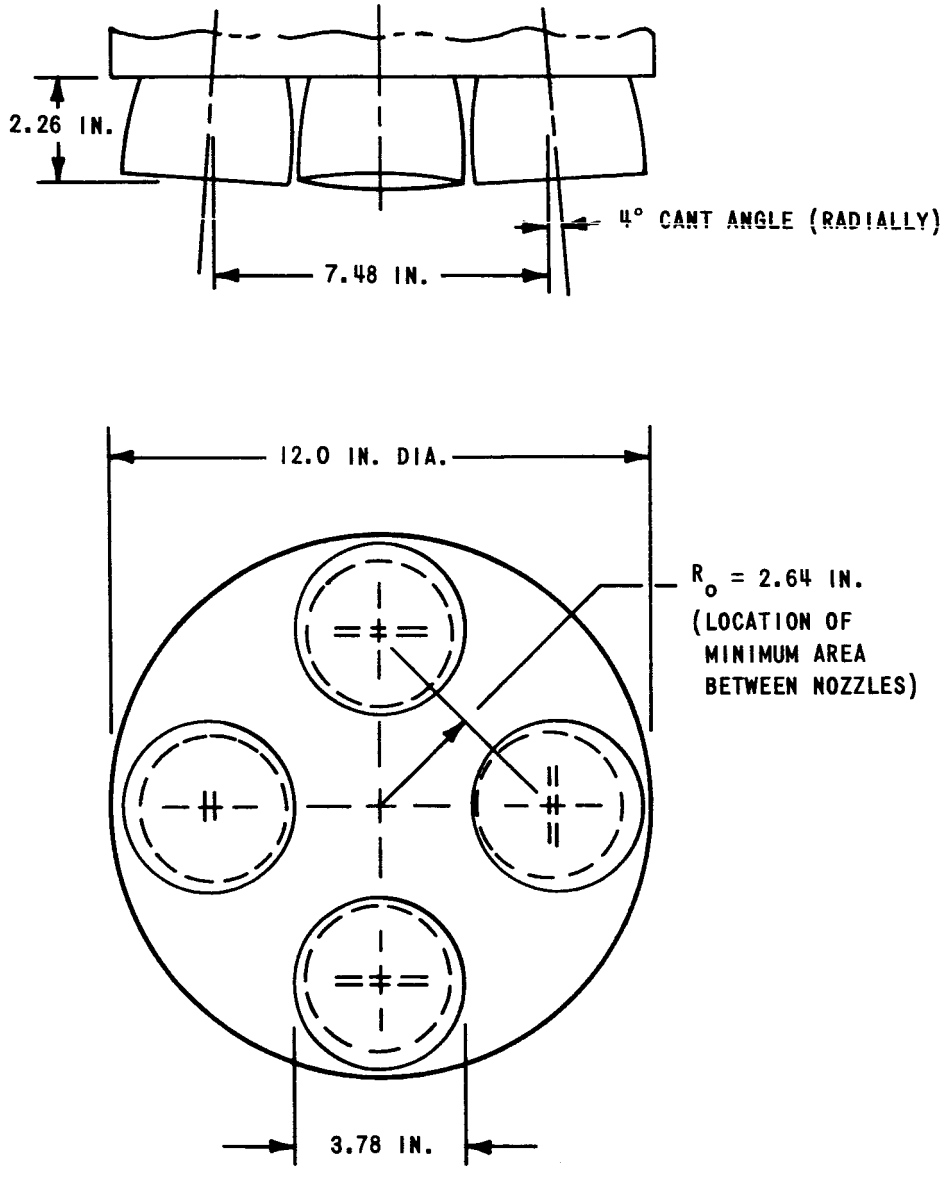

Figure 2 MODEL BASE CONFIGURATION

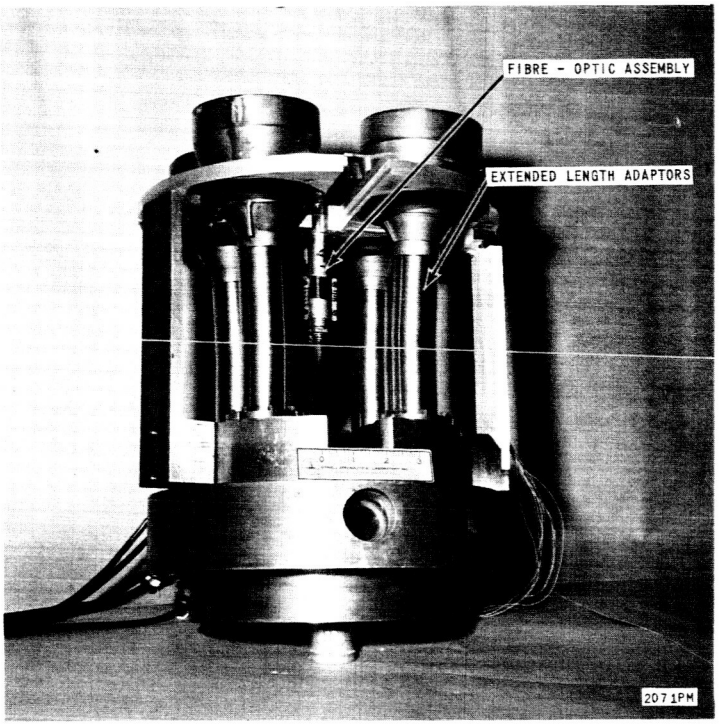

a. AFT VIEW

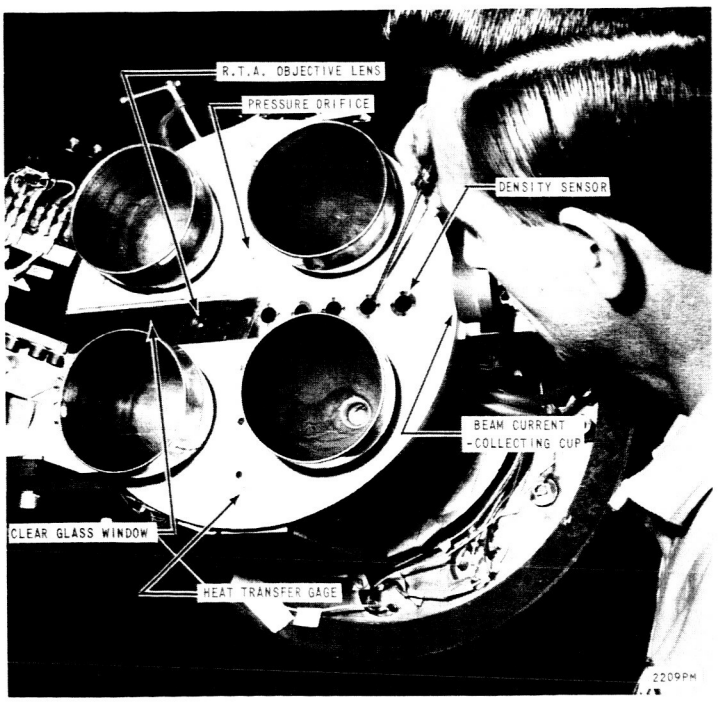

b. FORWARD VIEW

Figure 3 MODEL BASE REGION

Figure 4 MOUNTING BRACKET FOR R.T.A.
(ARROWS INDICATE MOTIONS POSSIBLE)

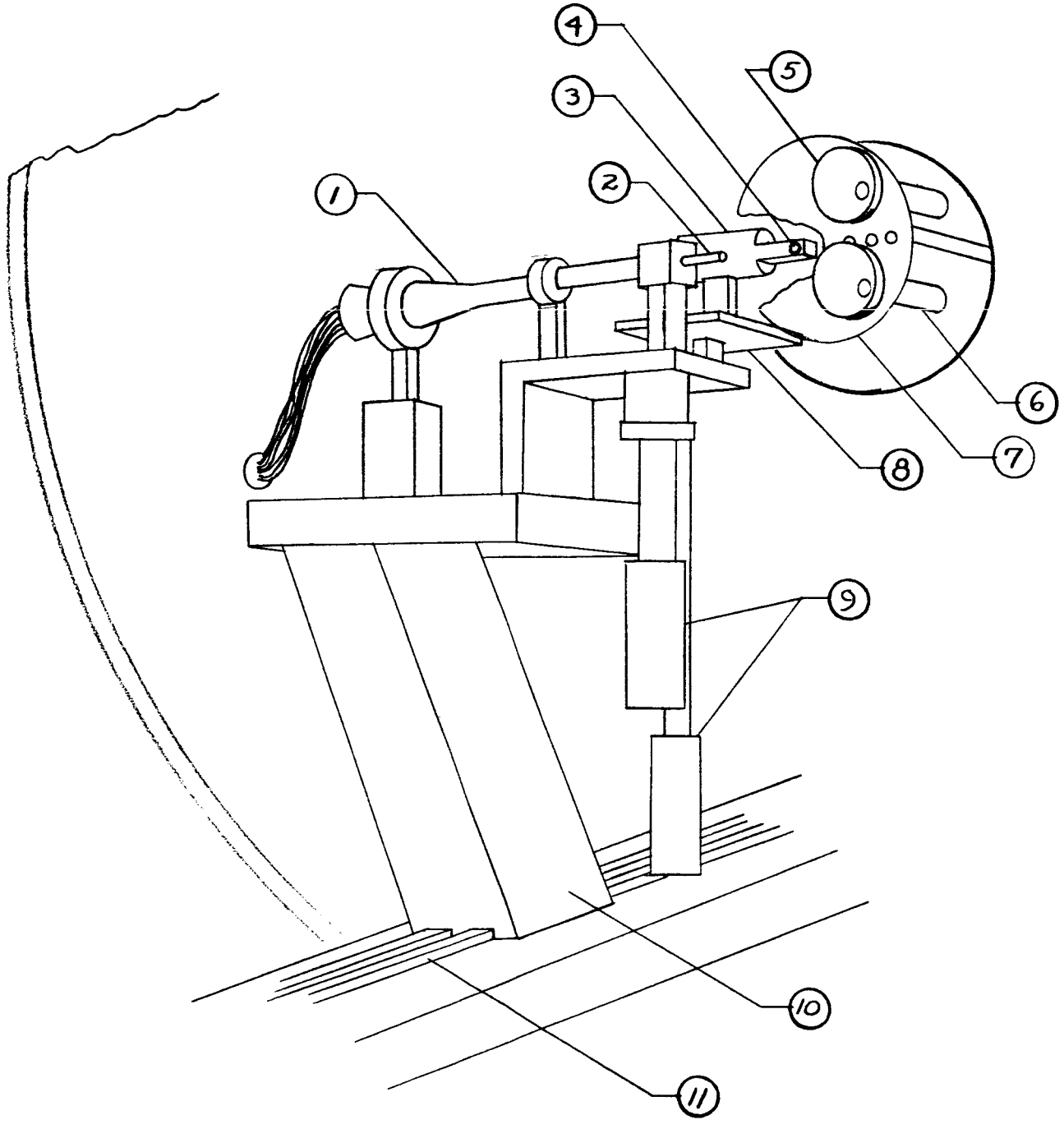

1. Electron Gun
2. Drift Tube
3. R. T. A.
4. Objective Lens
5. Nozzle
6. Adapter
7. Heat Shield
8. Support Bracket
9. Diffusion Pumps
10. Support Pedestal
11. Guide Rails

Figure 5 ELECTRON BEAM TEMPERATURE STUDY-INSTALLATION SCHEMATIC

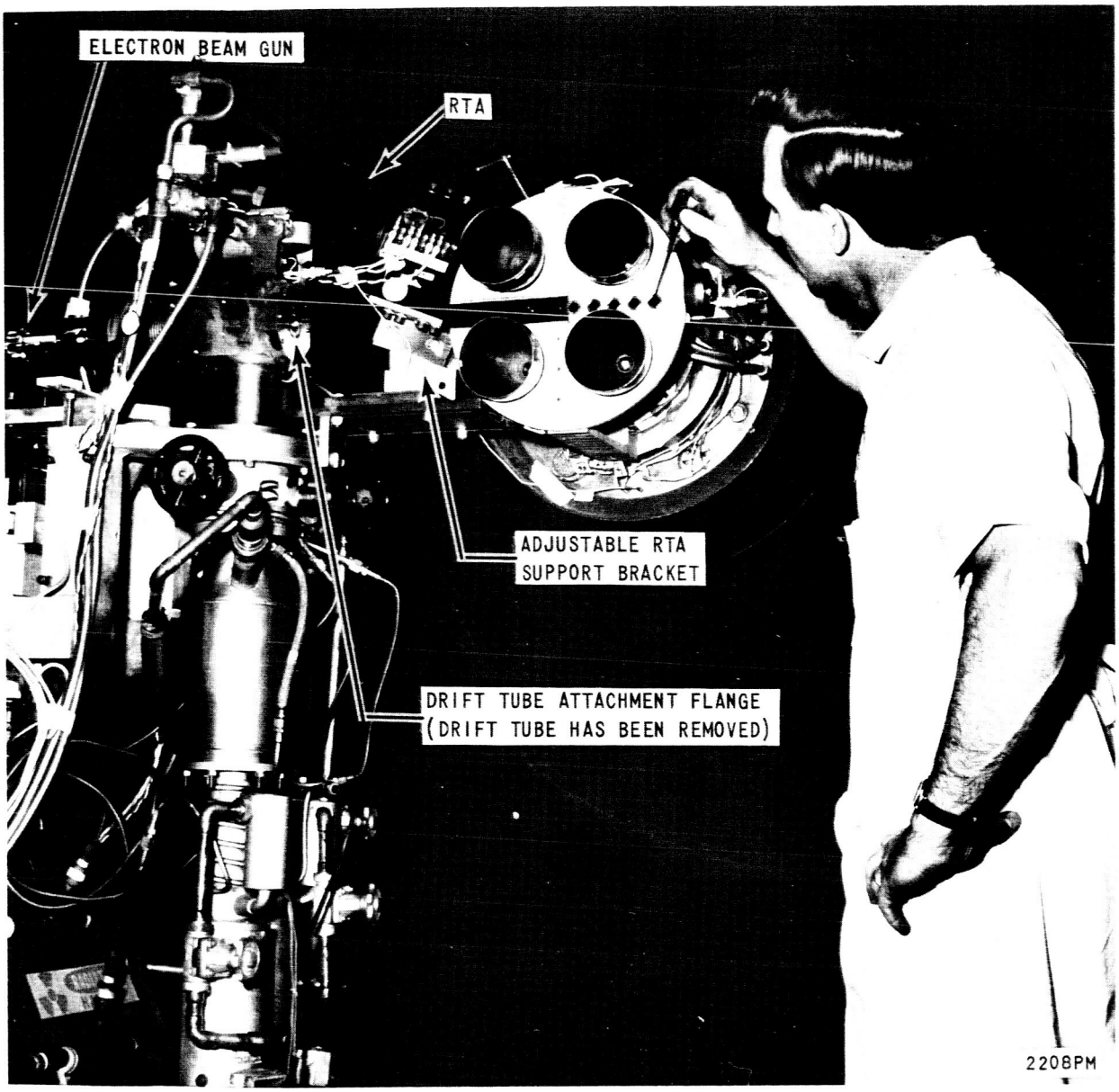

Figure 6 INSTALLATION - CLUSTER NOZZLE MODEL AND TEMPERATURE MEASUREMENT APPARATUS

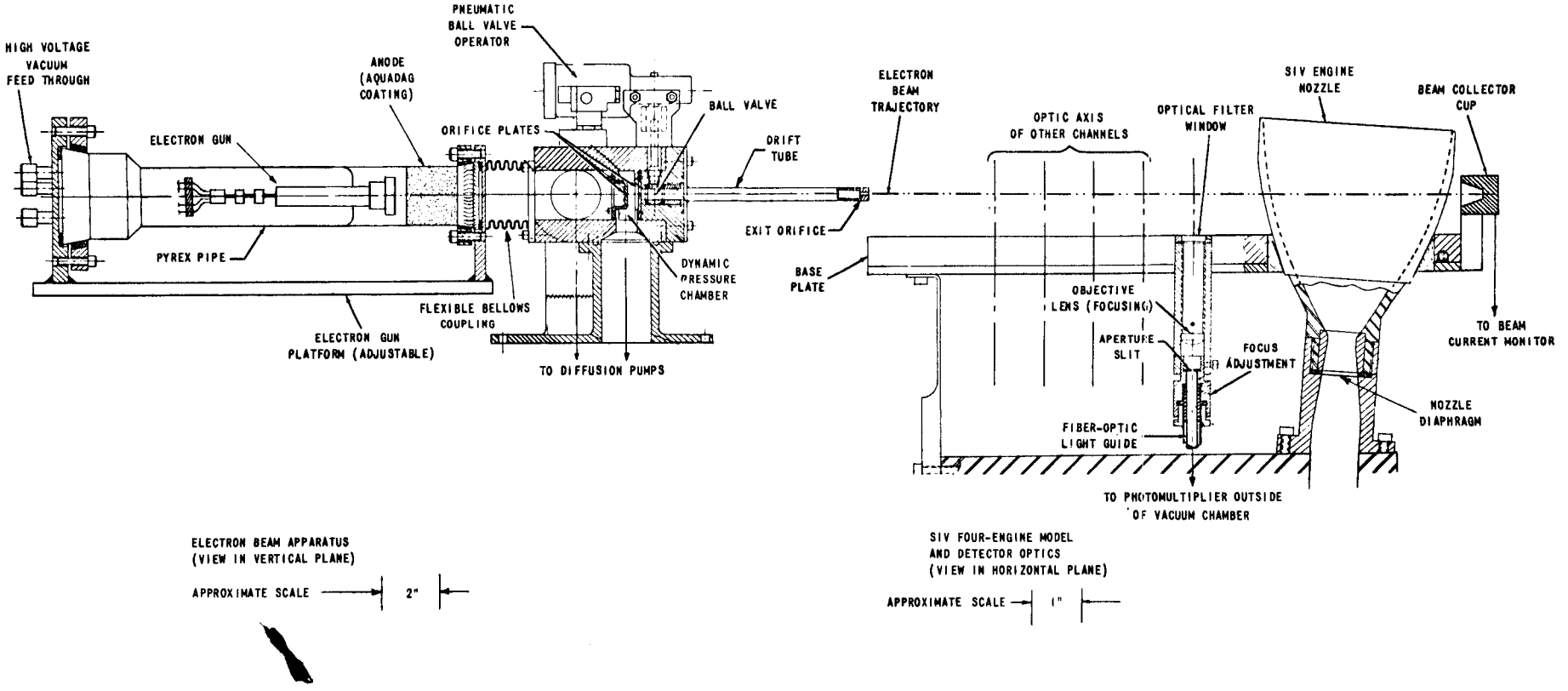

Figure 7 SCHEMATIC OF ELECTRON BEAM DENSITY PROBE SETUP

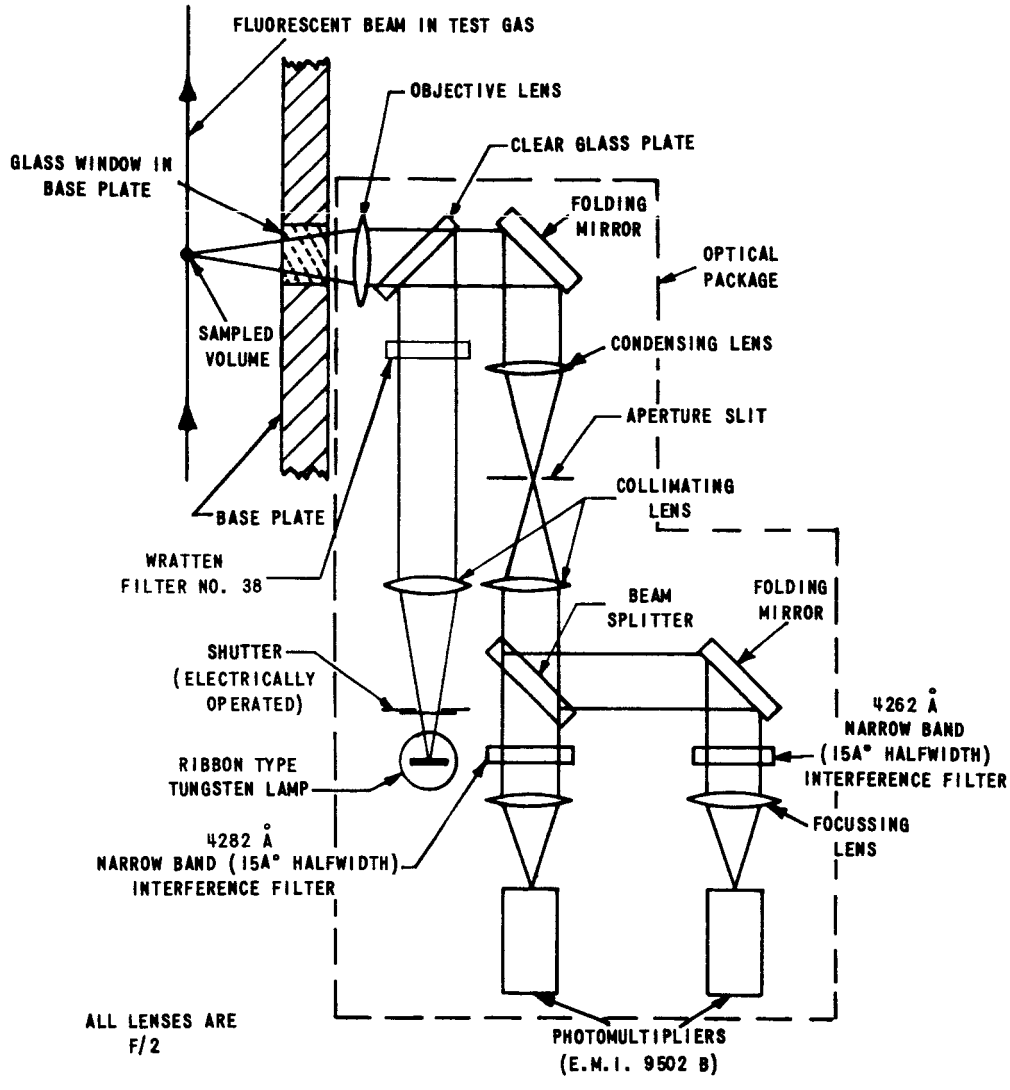

Figure 8 SCHEMATIC VIEW TEMPERATURE MEASURING APPARATUS

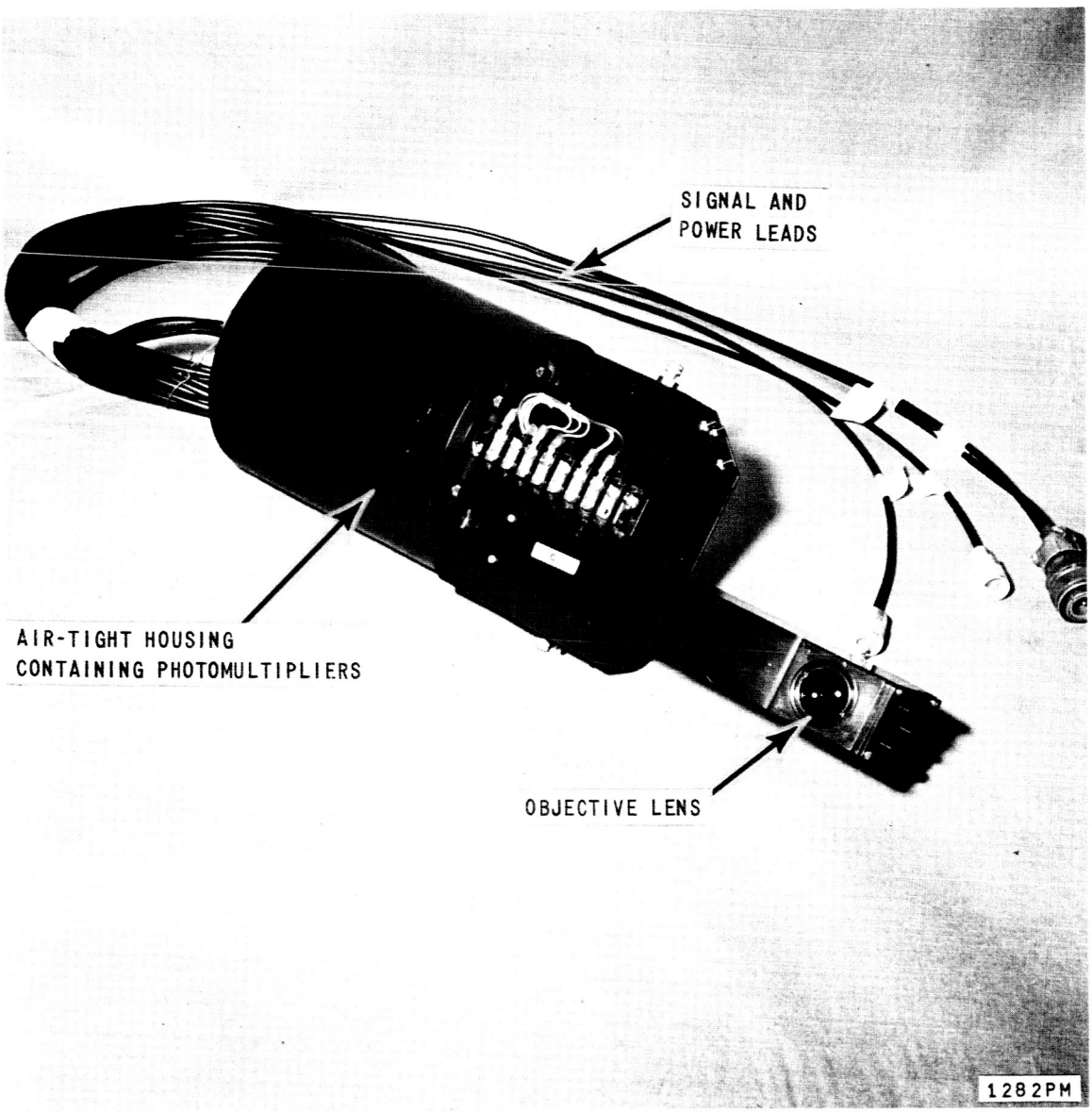

Figure 9 ASSEMBLED ROTATIONAL TEMPERATURE APPARATUS (RTA)

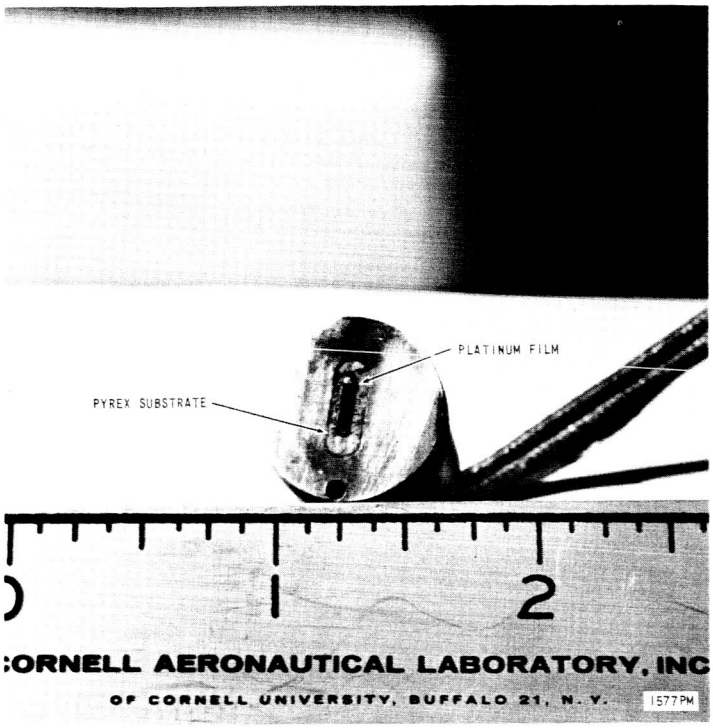

a. HEATED HEAT - TRANSFER GAUGE

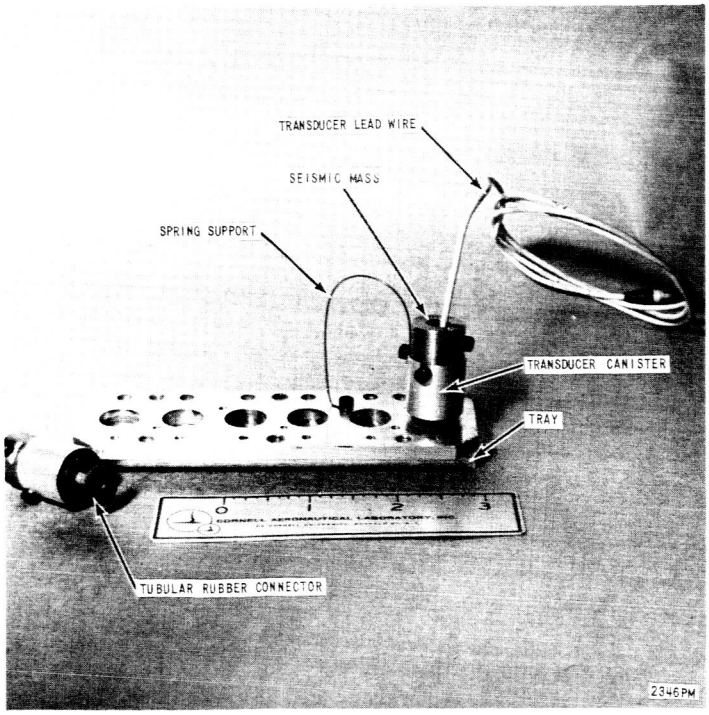

b. PRESSURE TRANSDUCER MOUNTING TRAY

Figure 10 MODEL INSTRUMENTATION

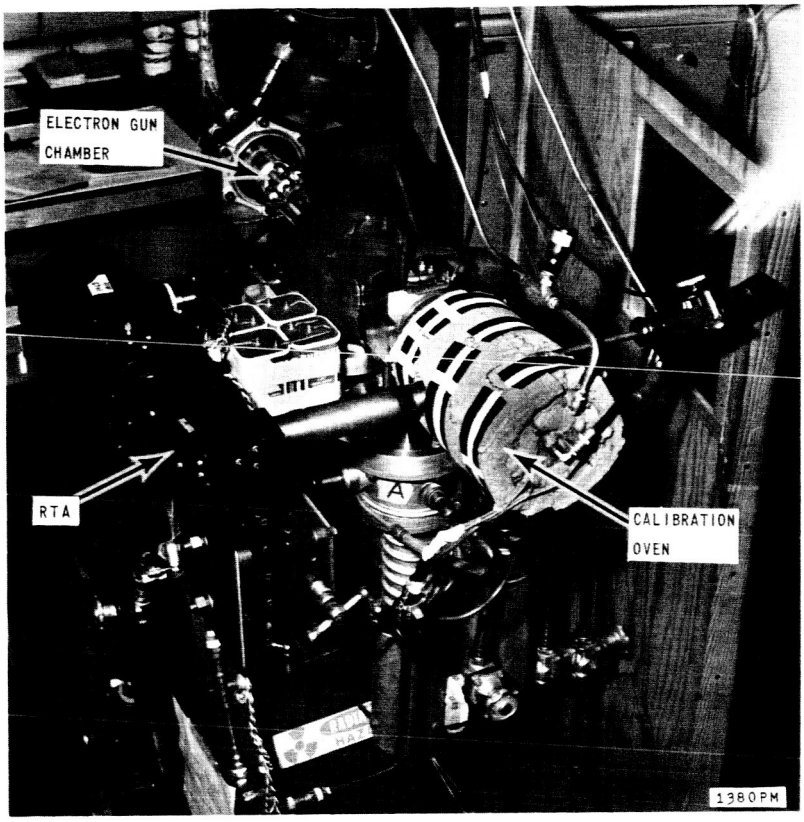

a. CALIBRATION ARRANGEMENT OF THE RTA

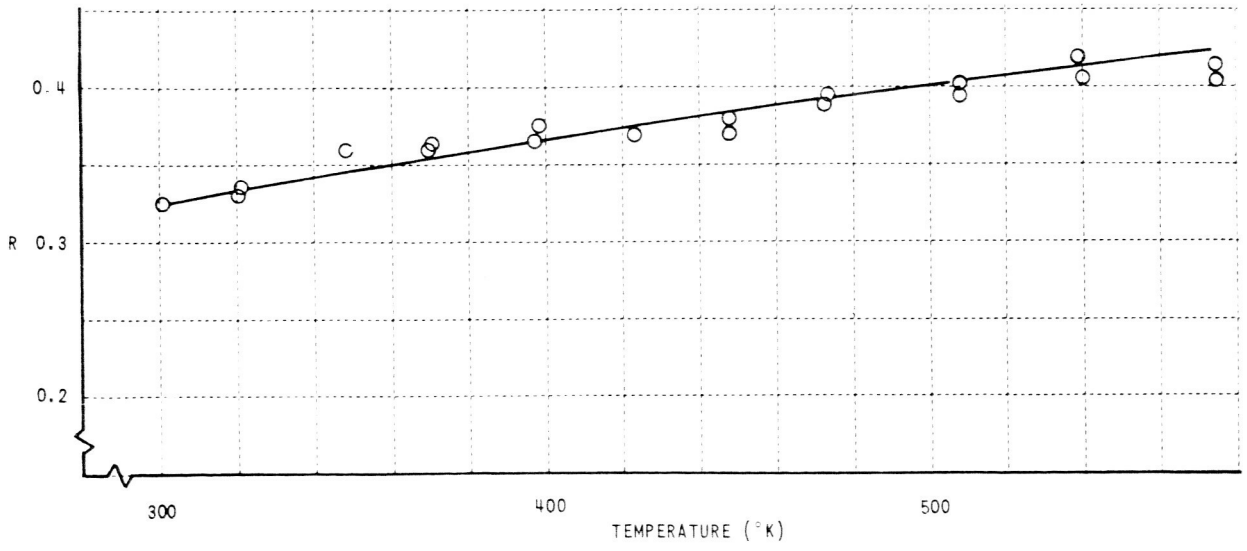

b. CALIBRATION CURVE FOR TEMPERATURE MEASURING APPARATUS

Figure 11 RTA CALIBRATION

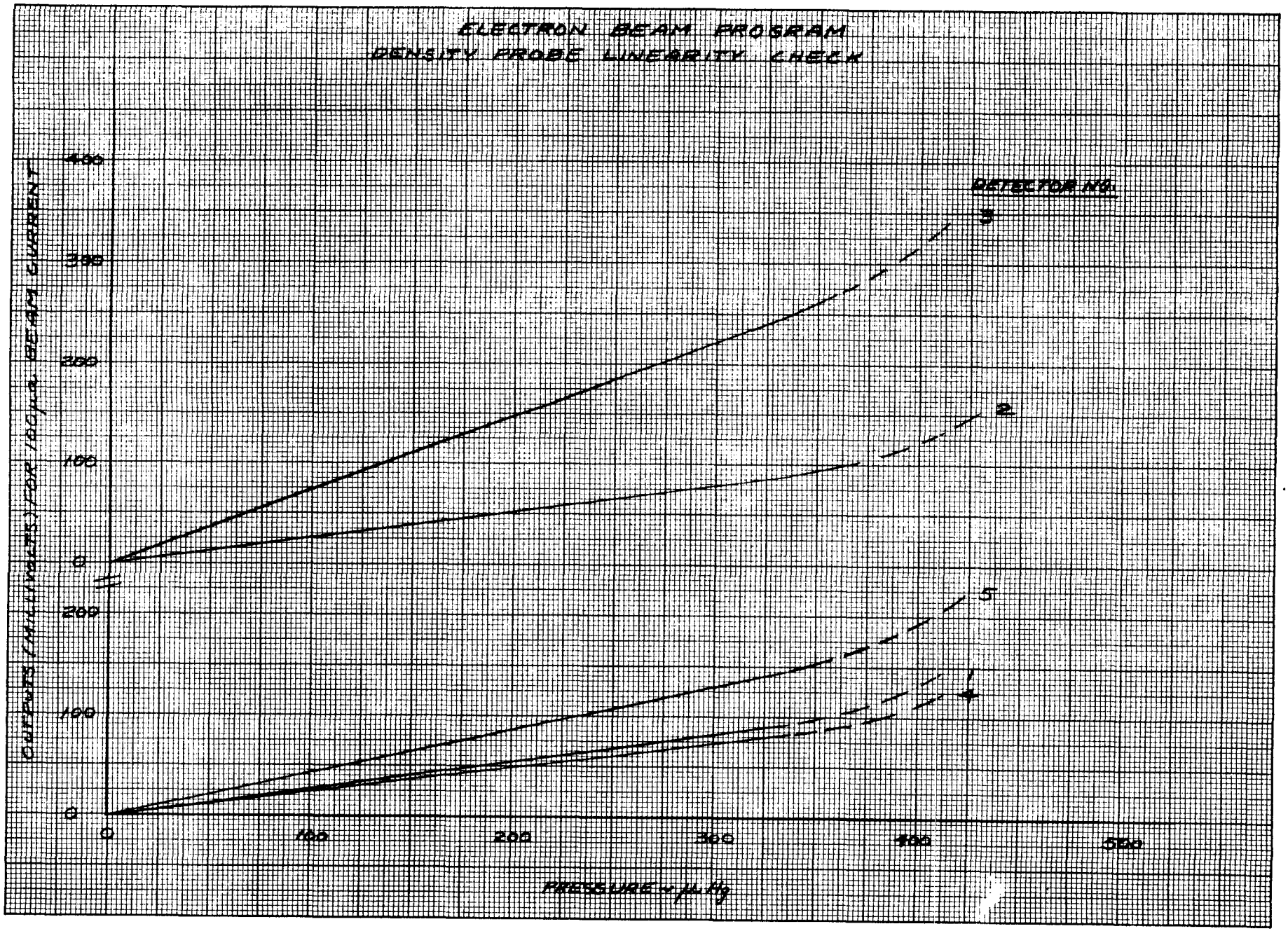

FIG. 12

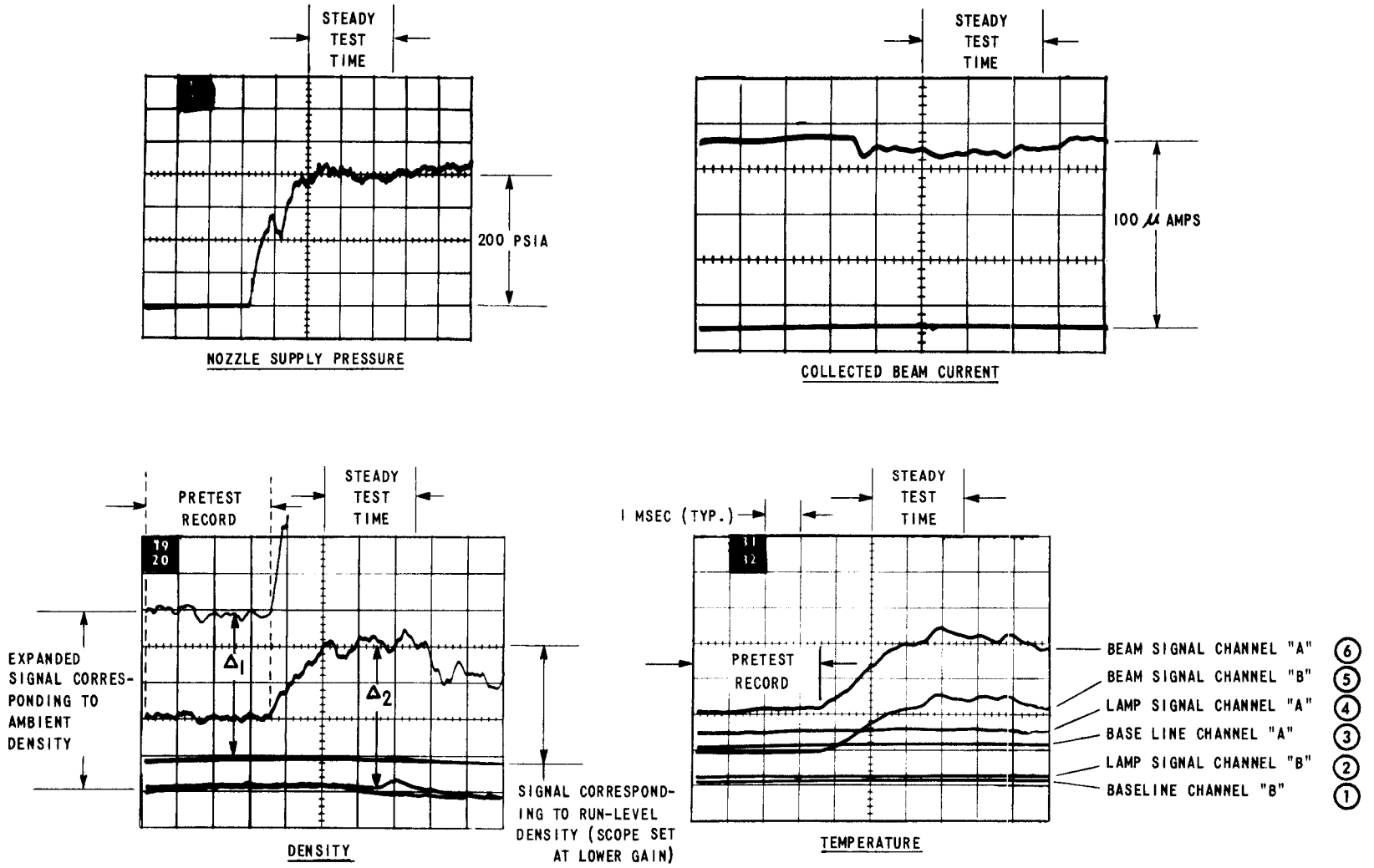

Figure 13 TYPICAL ELECTRON BEAM TEST RECORDS

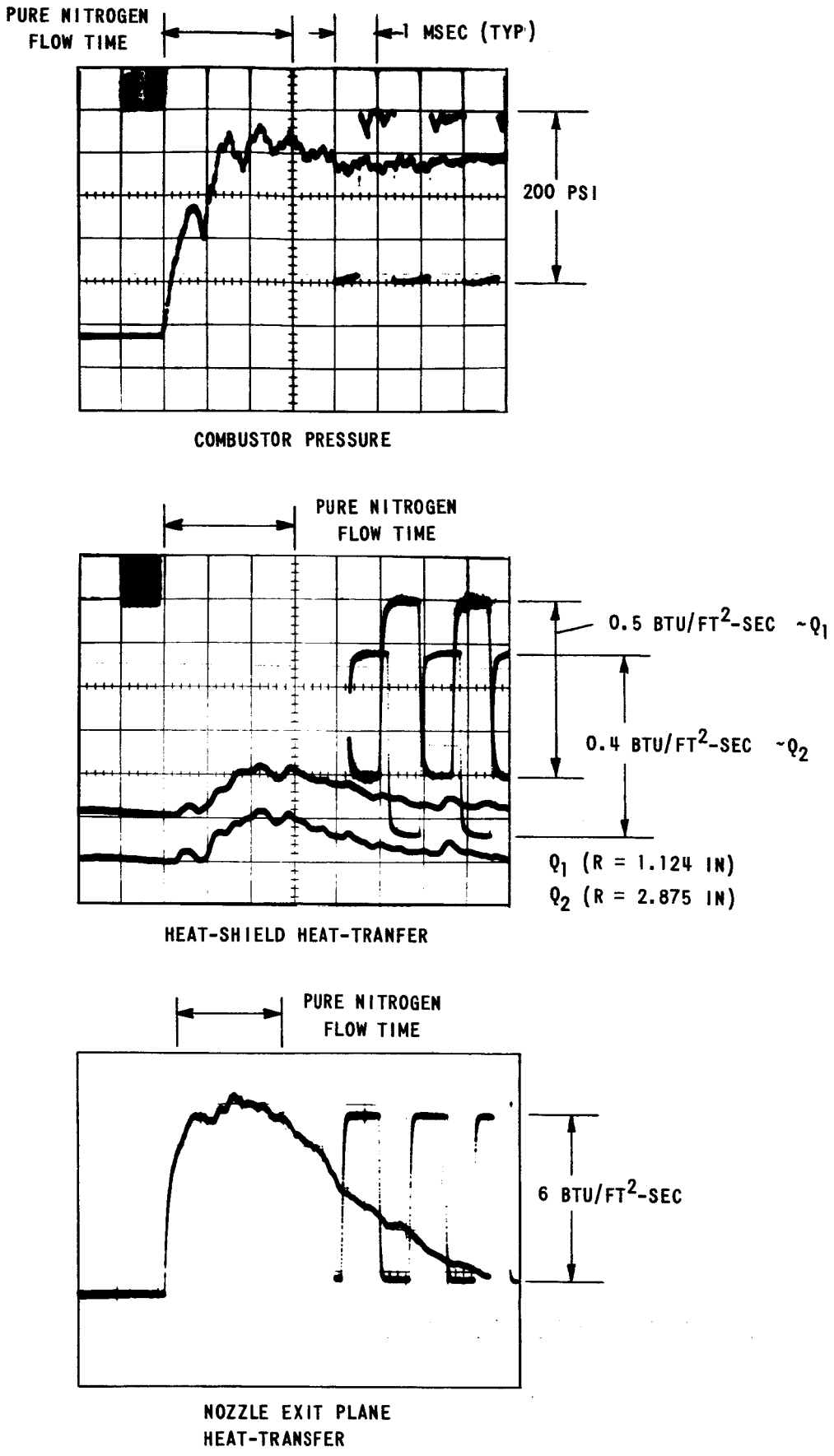

Figure 14 TYPICAL HEAT TRANSFER DATA

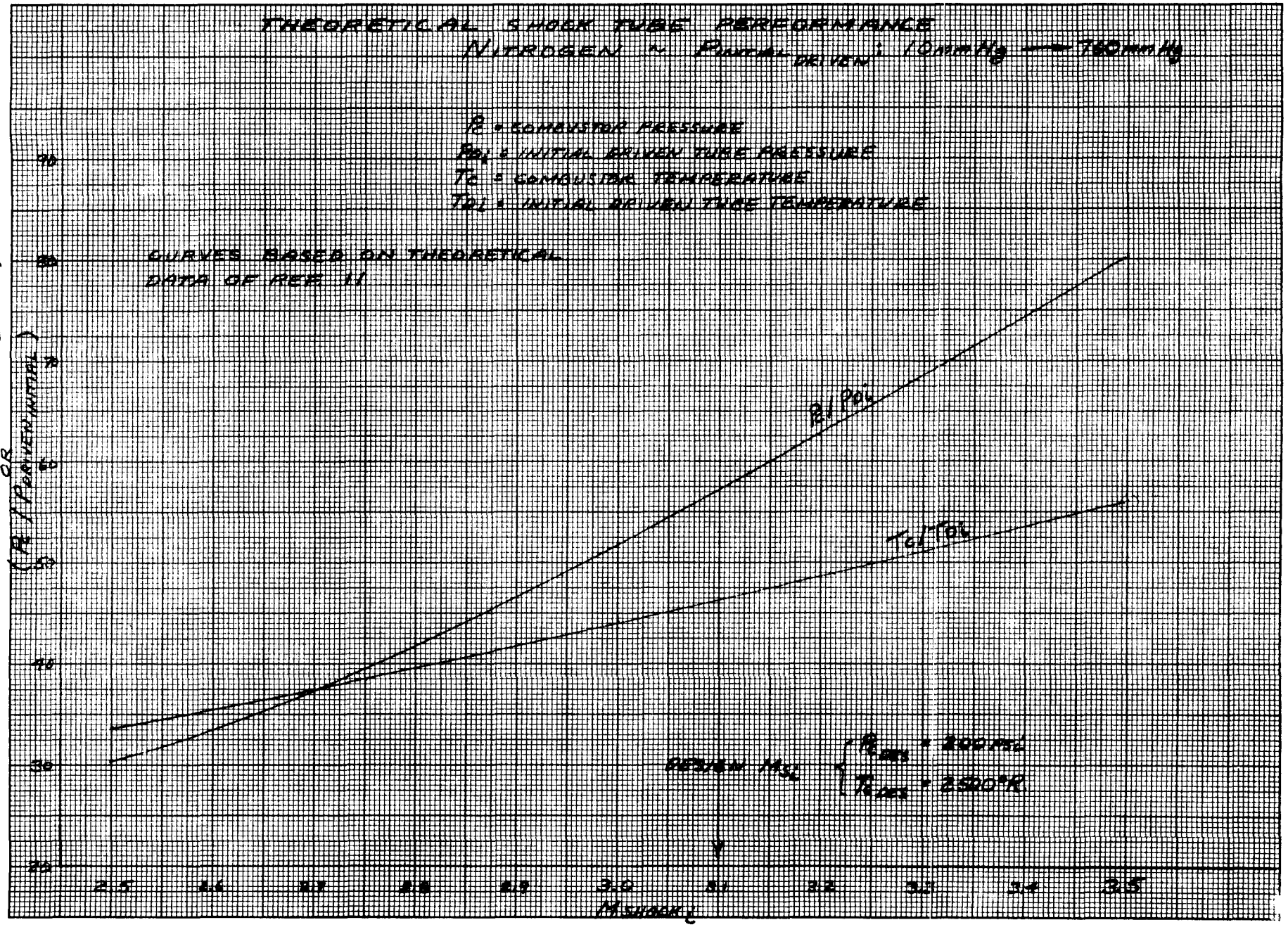

FIG. 15

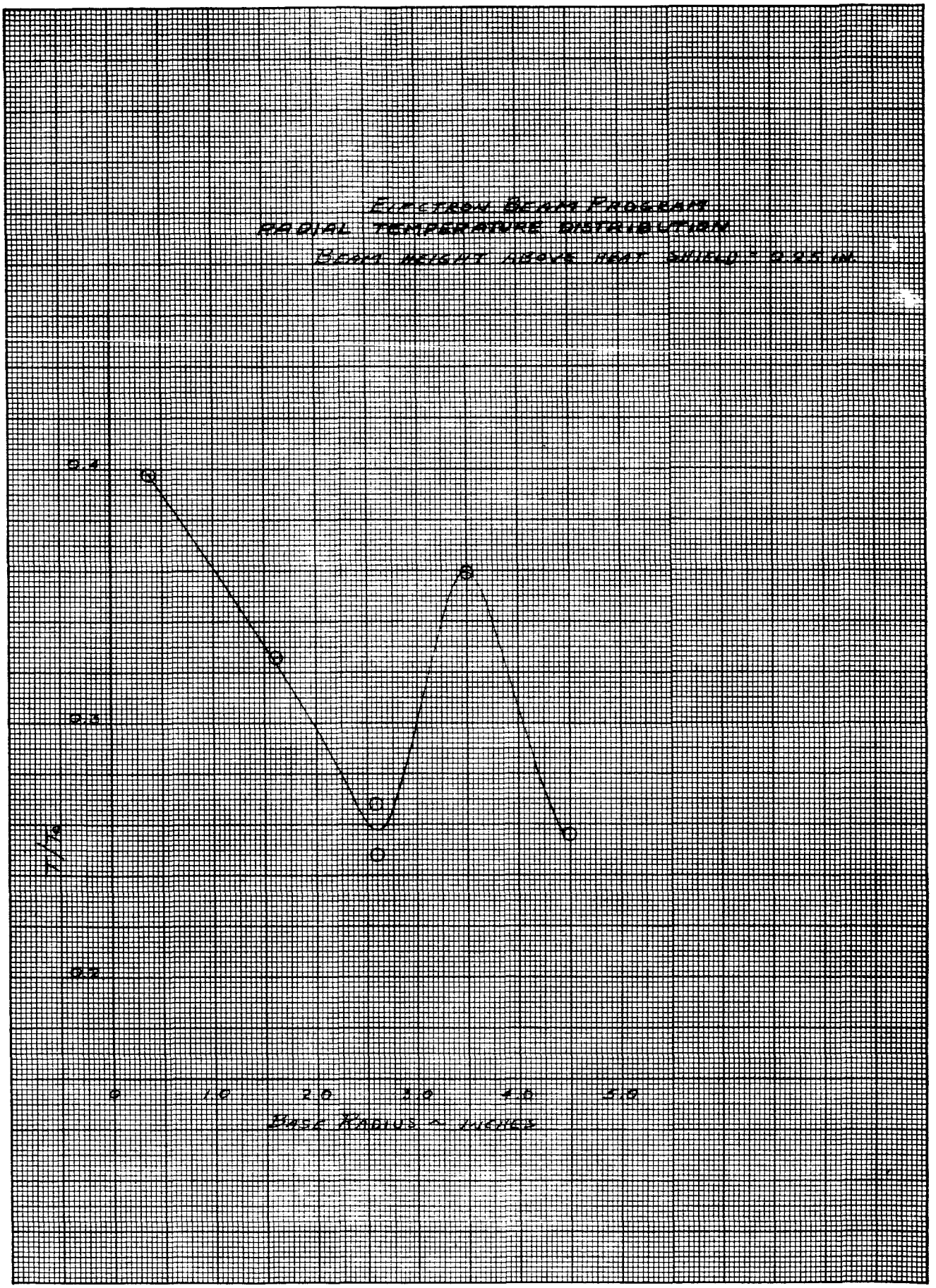
ELECTRON BEAM PROGRAM
RADIAL TEMPERATURE DISTRIBUTION
BEAM WEIGHT ABOVE HEAT SHIELD = 0.25 LB.
0.4
0.3
0.2
0
1.0
2.0
3.0
4.0
5.0
BASE RADIUS - INCHES

FIG. 16

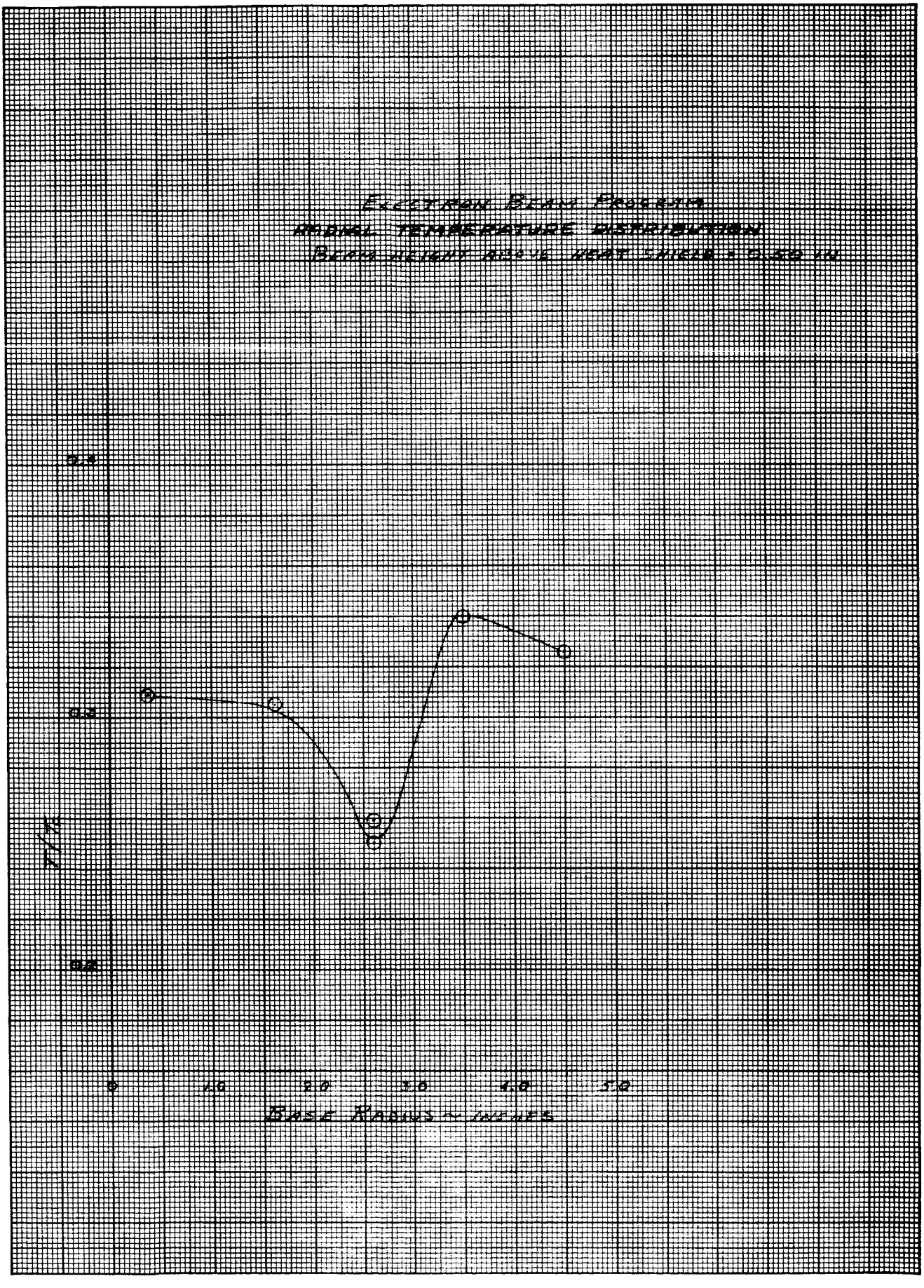

FIG. 17

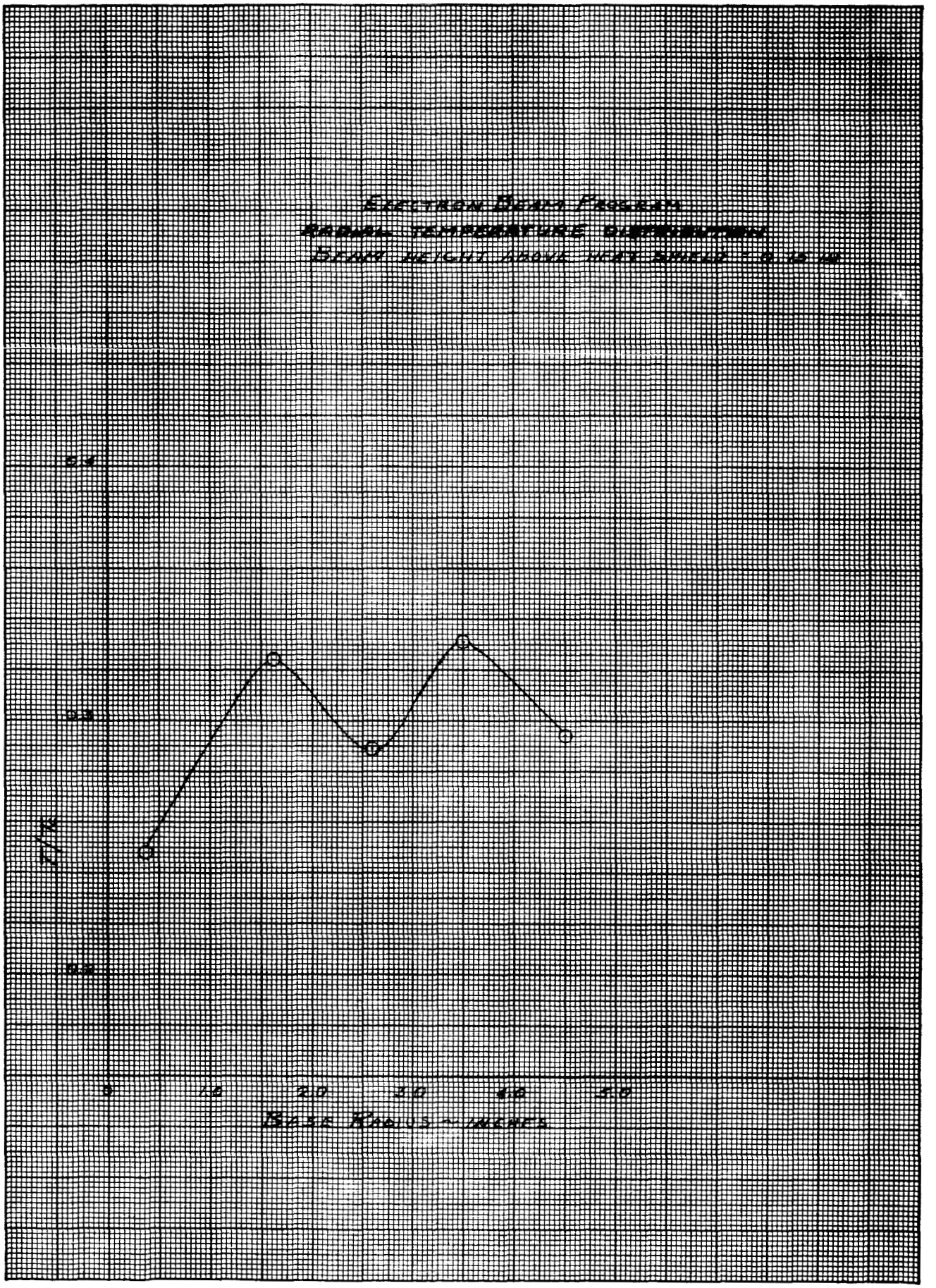

K&E 10 X 10 TO THE CENTIMETER 18 X 25 CM. 46 1513 MADE IN U.S.A. KEUFFEL & ESSER CO.

FIG. 18

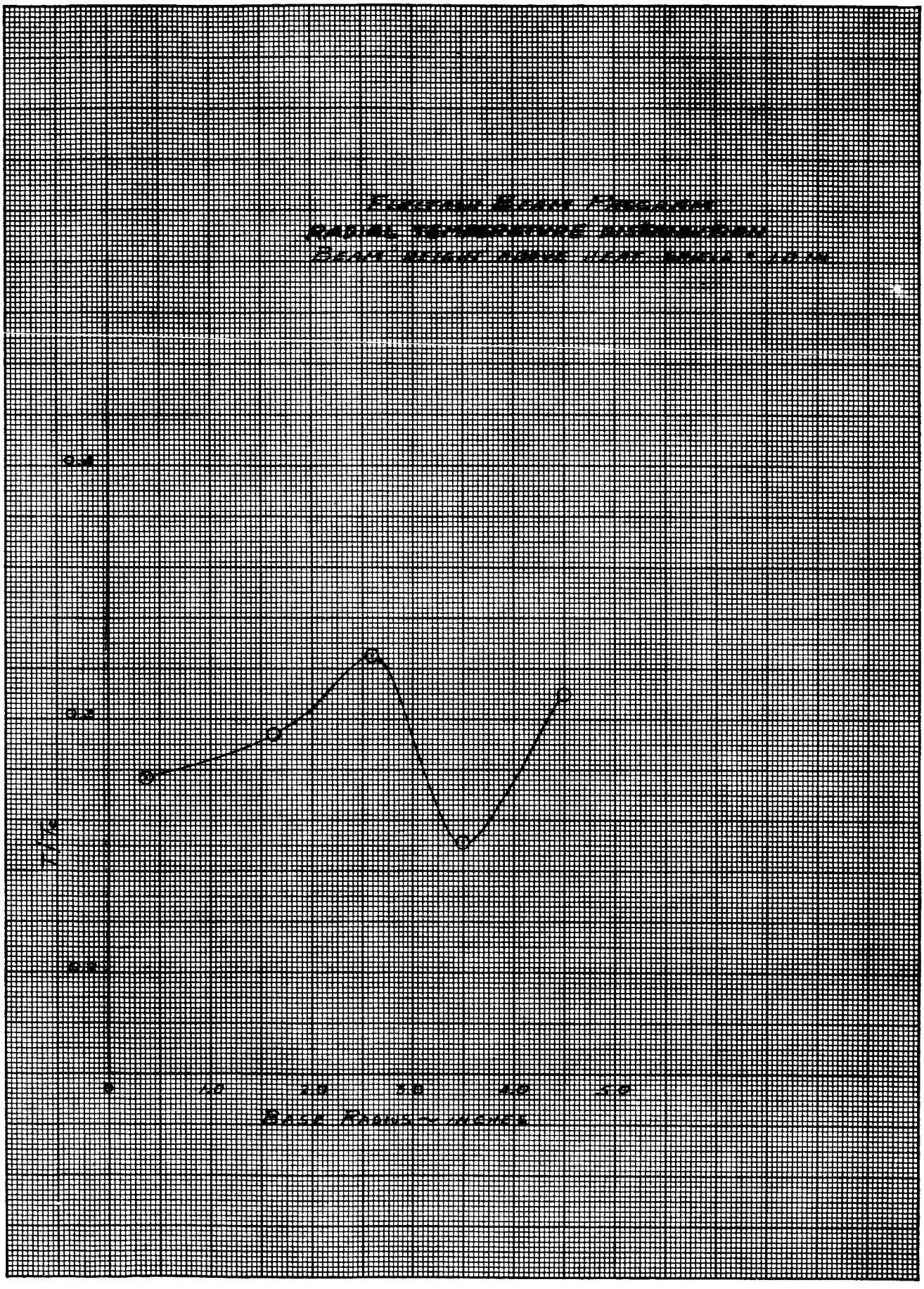

K&E 10 X 10 TO THE CENTIMETER 46 1513
25 X 25 CM.
MADE IN U.S.A.
KEUFFEL & ESSER CO.

FIG. 19

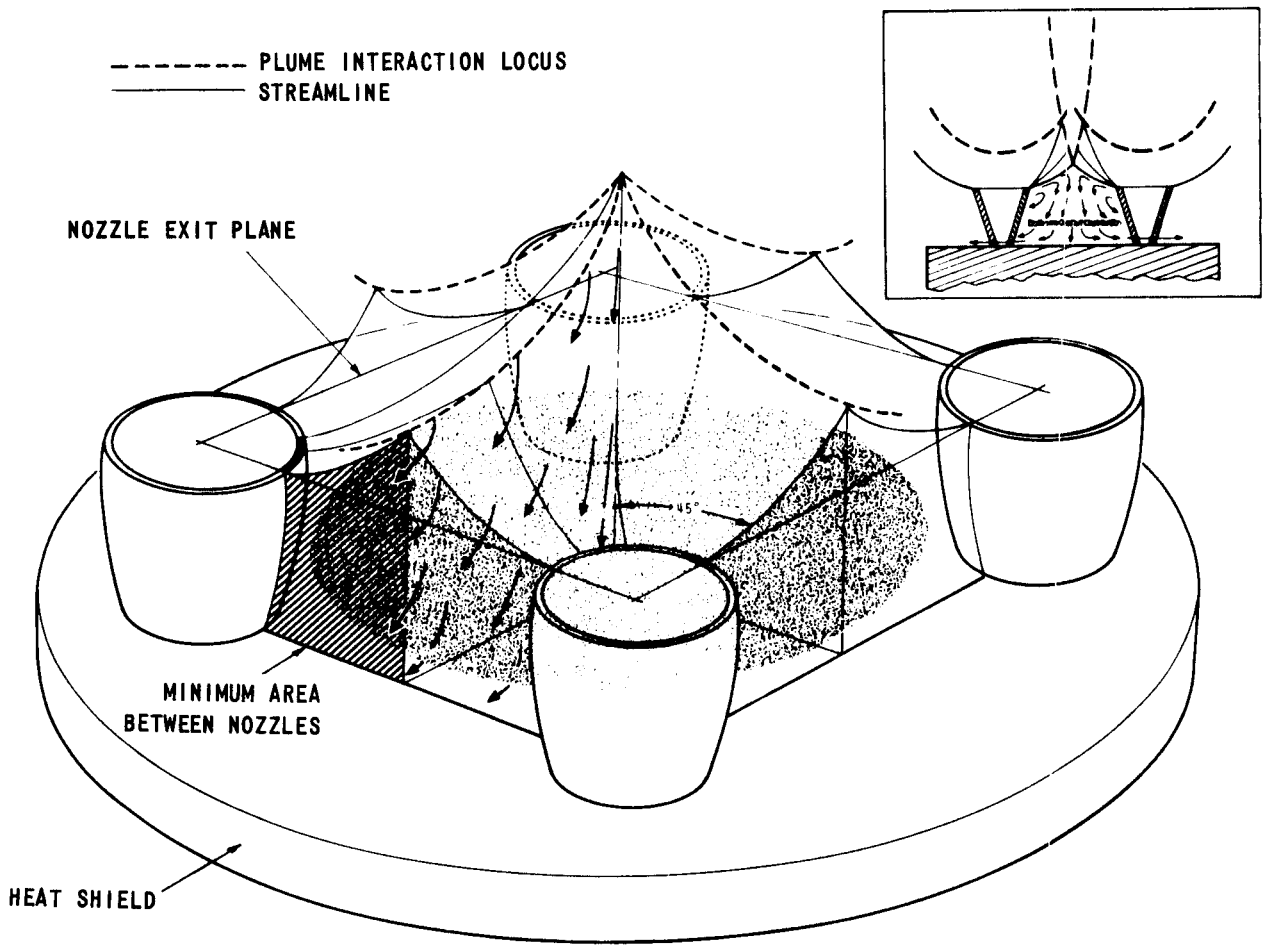

Figure 20 THREE-DIMENSIONAL FLOW SCHEMATIC - FOUR ENGINE CLUSTER

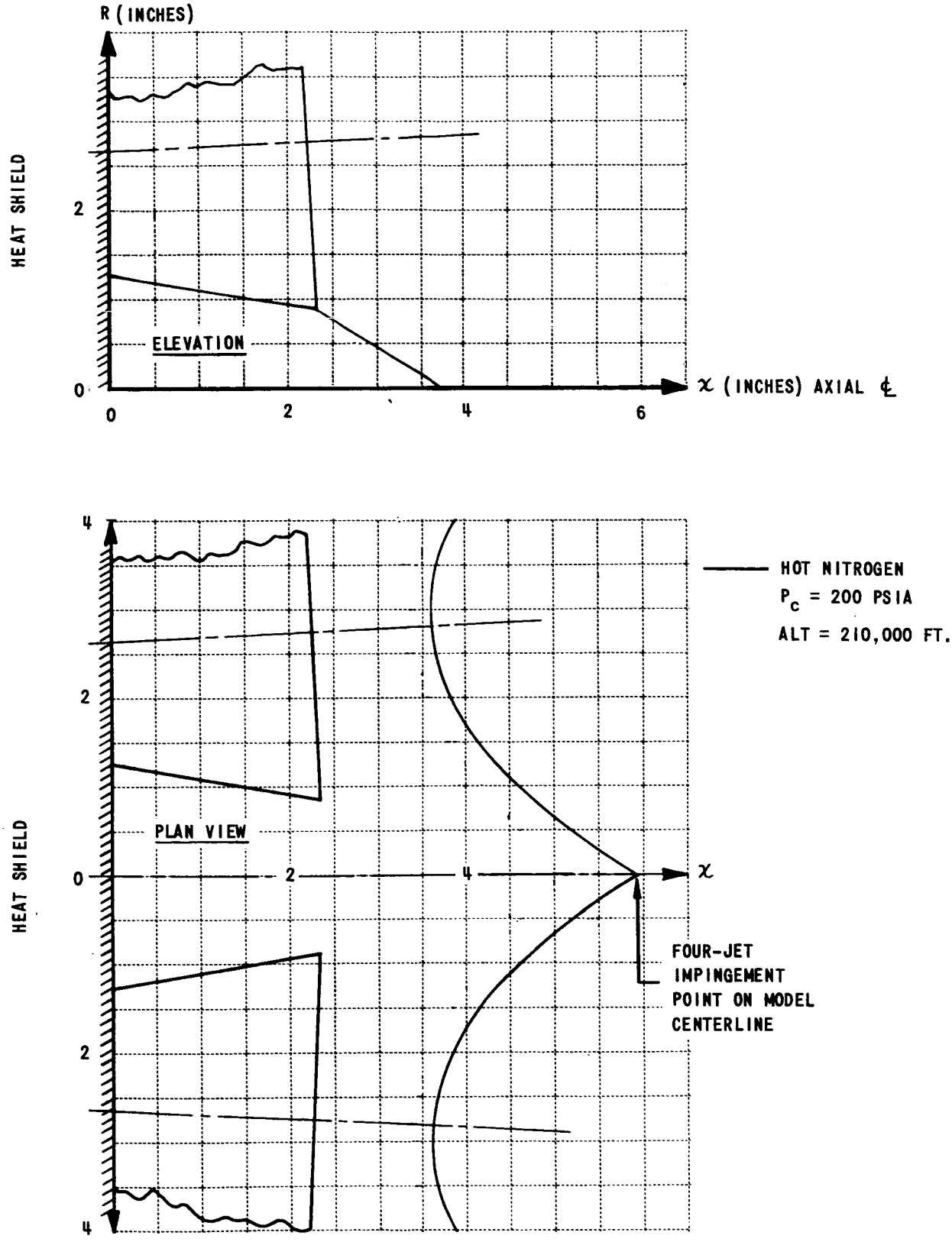

Figure 21 APPROXIMATE EXHAUST PLUME INTERACTION CHARACTERISTICS

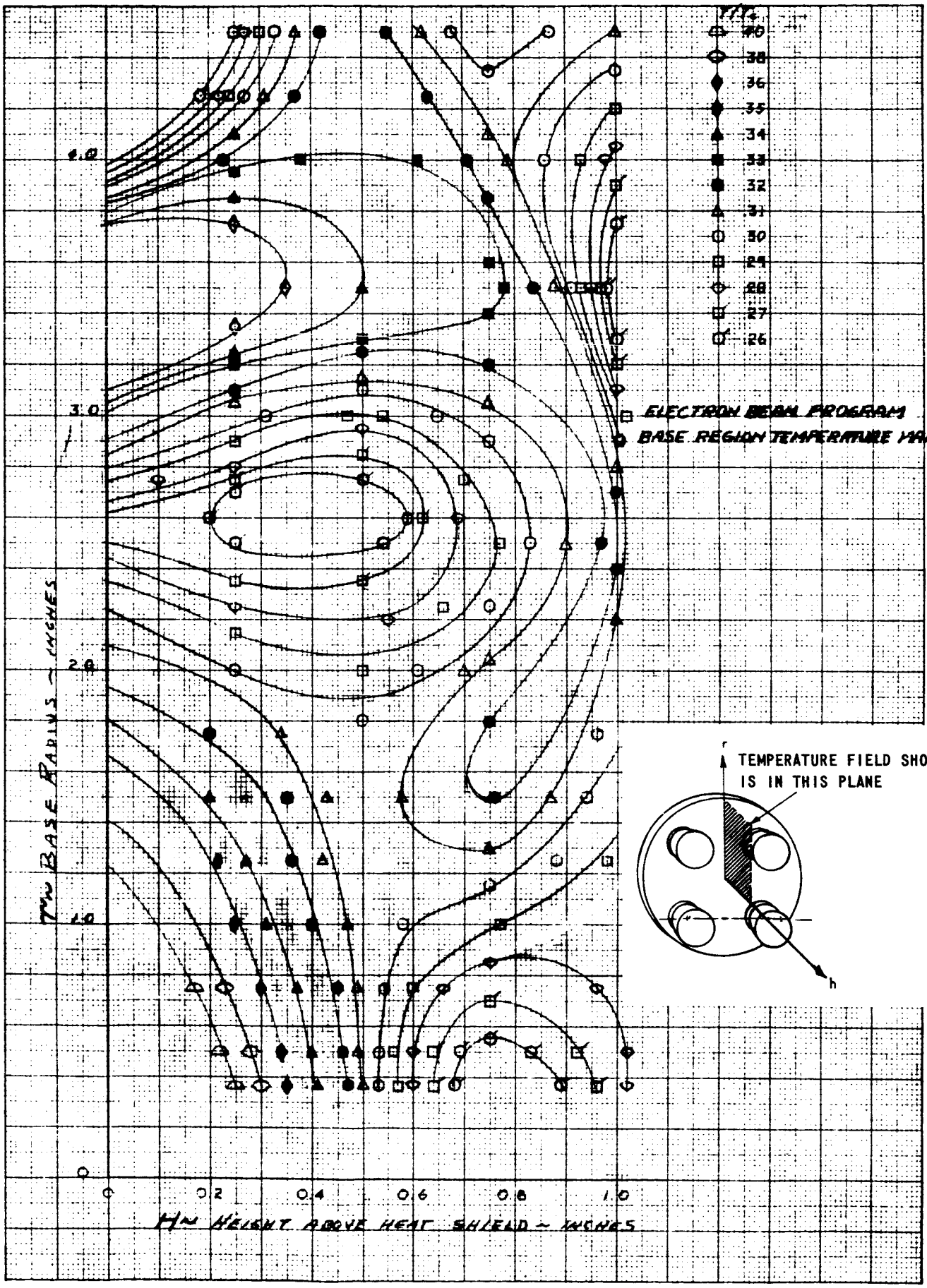
ELECTRON BEAM PROGRAM
BASE REGION TEMPERATURE MAP
TEMPERATURE FIELD SHOWN
IS IN THIS PLANE
r
h
r_w BASE RADIUS ~ INCHES
H_w HEIGHT ABOVE HEAT SHIELD ~ INCHES
1.0
2.0
3.0
0.2
0.4
0.6
0.8
1.0
40
38
36
35
34
33
32
31
30
29
28
27
26

FIG. 22

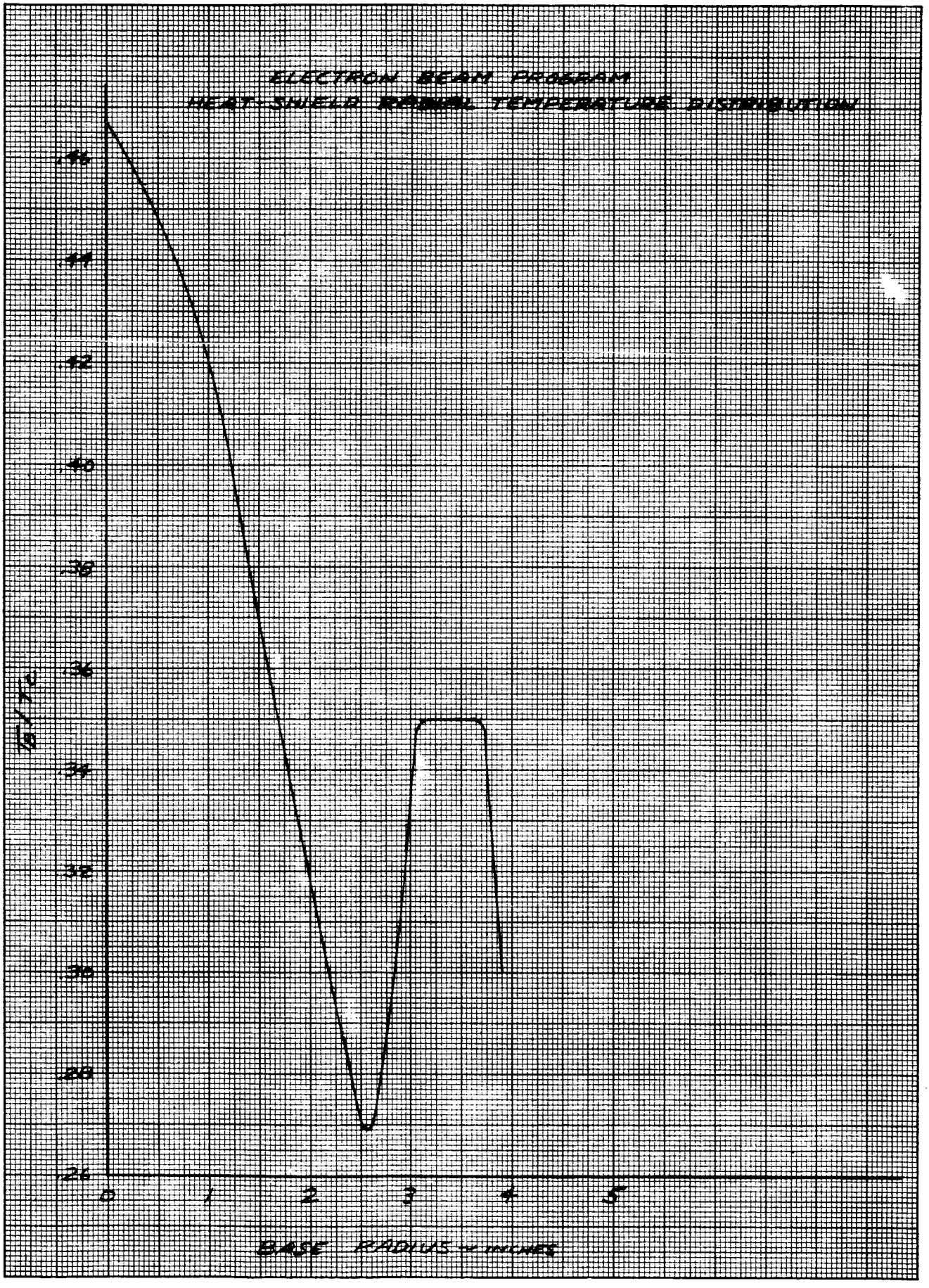
ELECTRON BEAM PROGRAM
HEAT-SHIELD RADIAL TEMPERATURE DISTRIBUTION
46
44
42
40
38
36
34
32
30
28
26
0
1
2
3
4
5
BASE RADIUS IN INCHES

FIG. 23

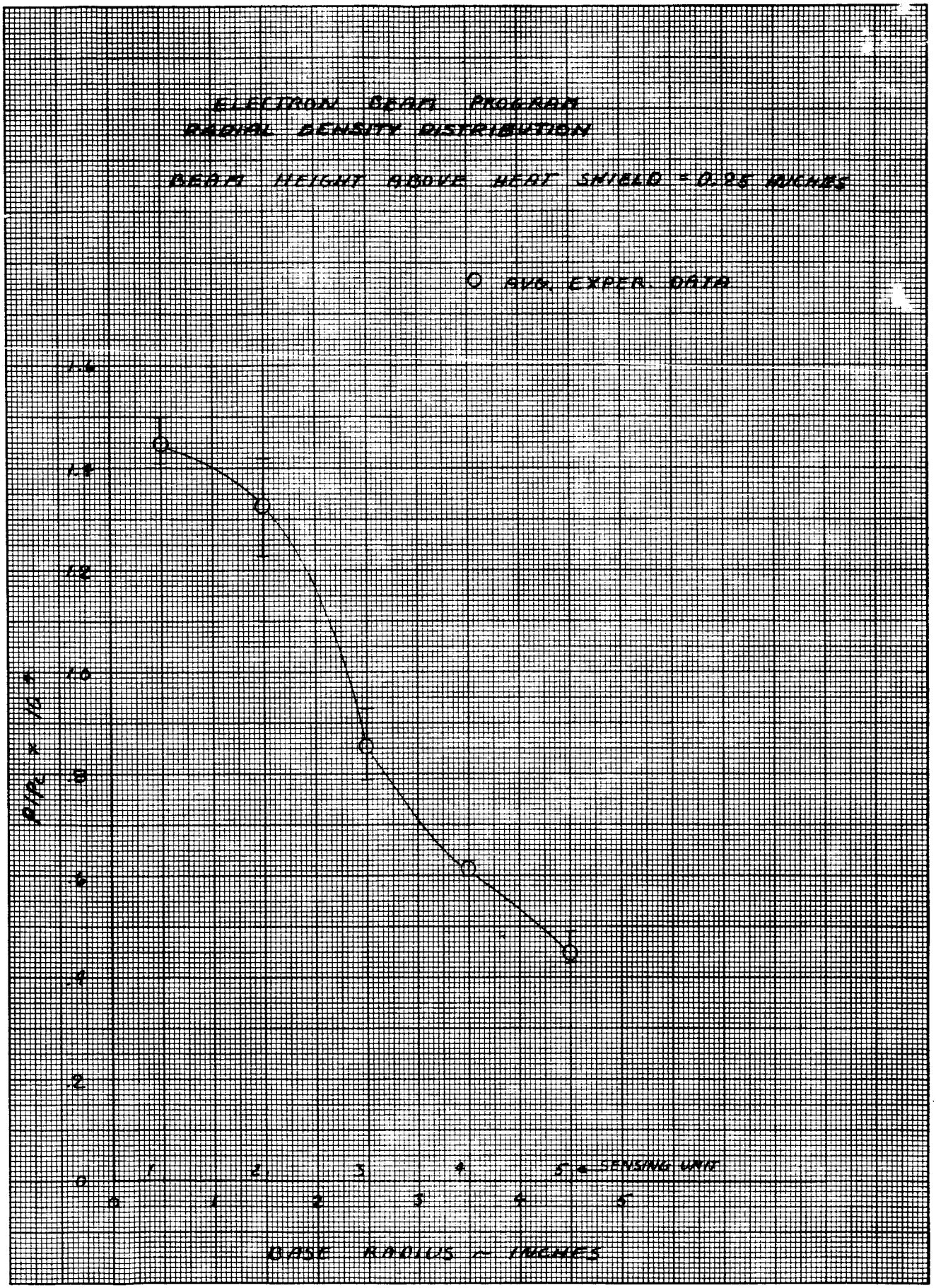
ELECTRON BEAM PROGRAM
RADIAL DENSITY DISTRIBUTION
BEAM HEIGHT ABOVE HEAT SHIELD = 0.25 INCHES
O AVG. EXPER. DATA
1.6
1.4
1.2
1.0
.8
.6
.4
.2
0
1
2
3
4
5
SENSING UNIT
BASE RADIUS — INCHES

FIG. 24

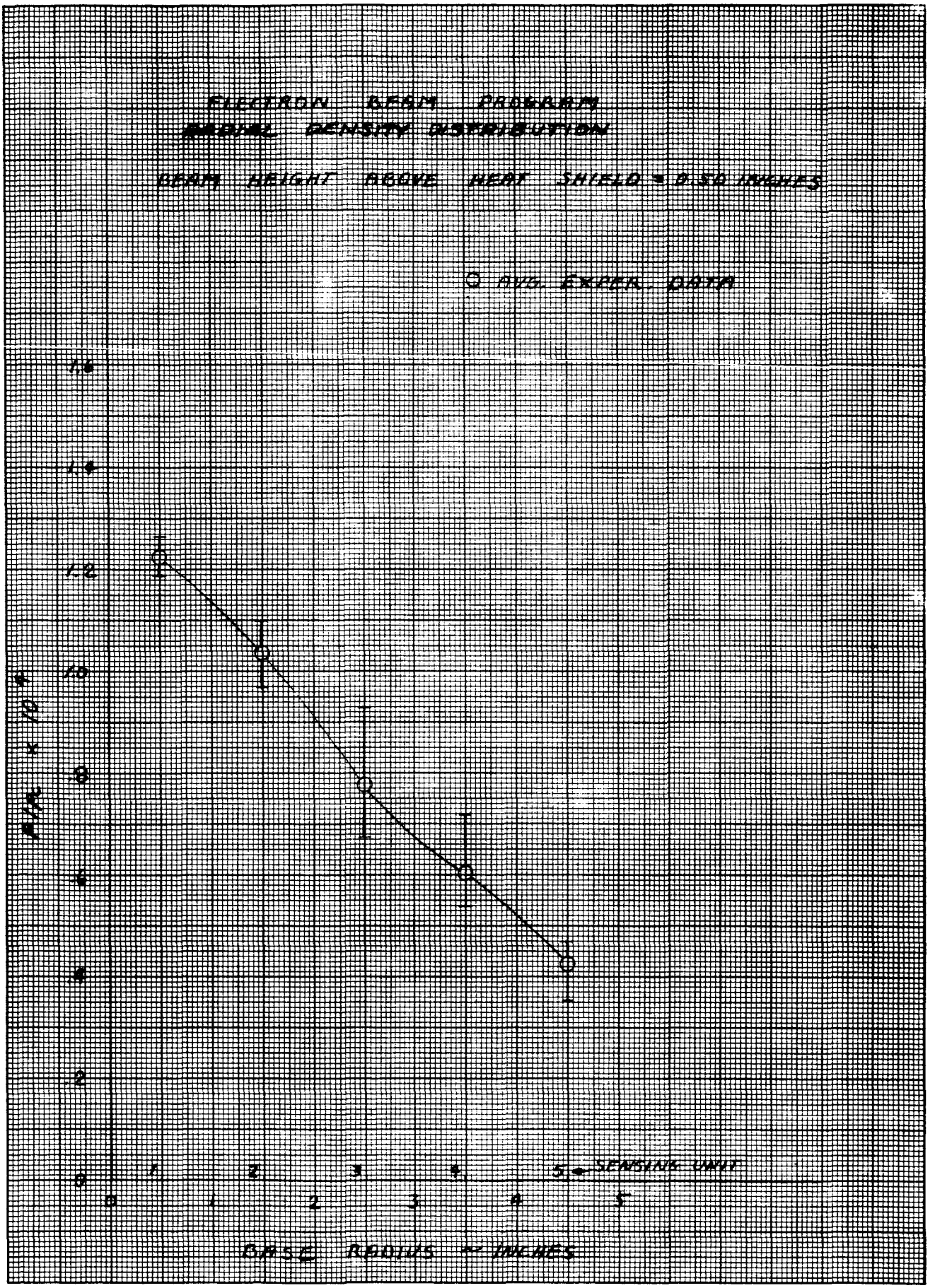
ELECTRON BEAM PROGRAM
RADIAL DENSITY DISTRIBUTION
BEAM HEIGHT ABOVE HEAT SHIELD = 0.50 INCHES
O AVG. EXPER. DATA
1.6
1.4
1.2
1.0
.8
.6
.4
.2
0
0
1
2
3
4
5
SENSING UNIT
0
1
2
3
4
5
CORE RADIUS — INCHES

FIG. 25

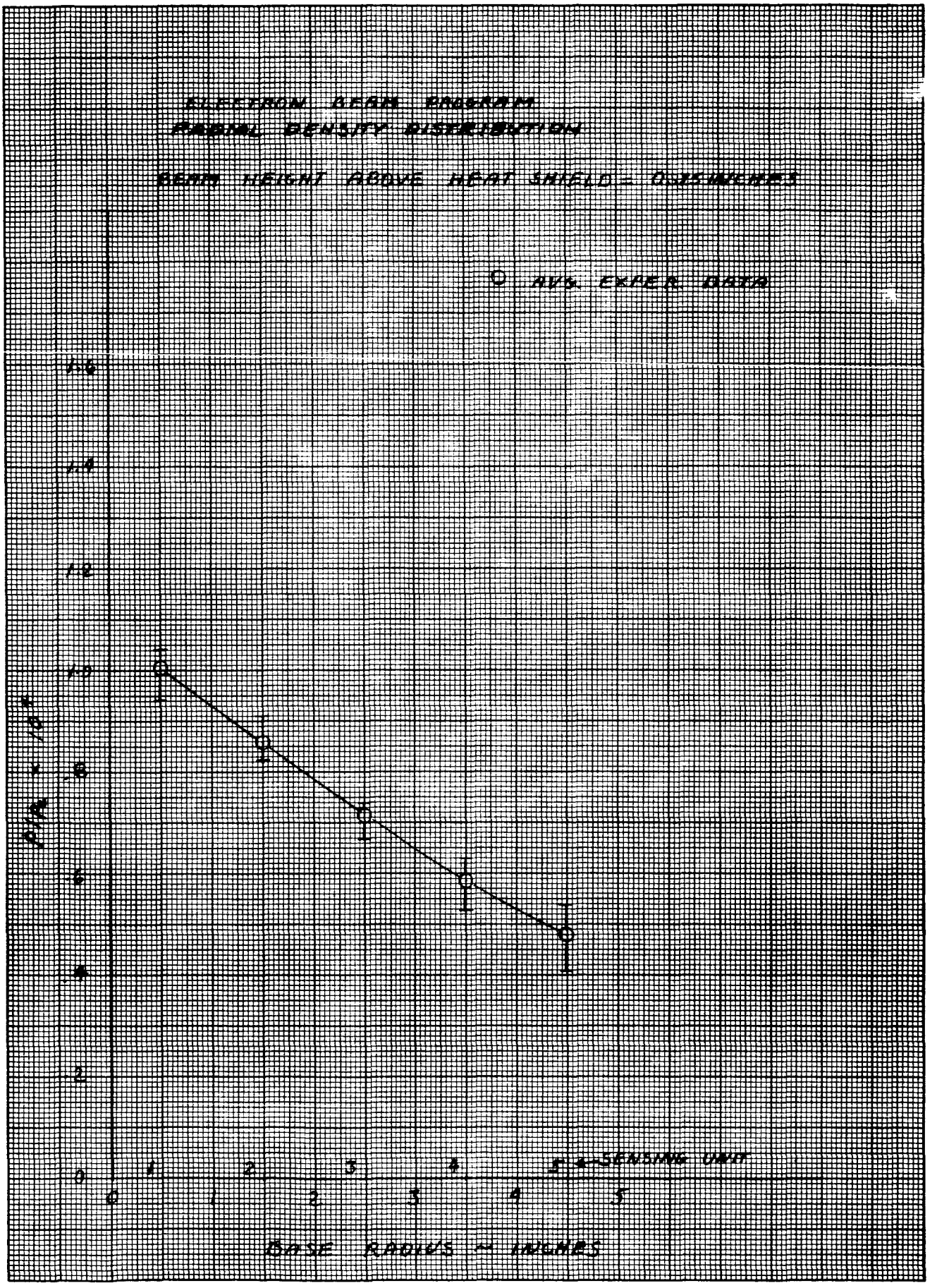
ELECTRON BEAM PROGRAM
RADIAL DENSITY DISTRIBUTION
BEAM HEIGHT ABOVE HEAT SHIELD = ONE INCHES
AVG. EXPER. DATA
1.6
1.4
1.2
1.0
.8
.6
.4
.2
0
0
1
2
3
4
5
SENSING UNIT
BASE RADIUS - INCHES

FIG. 26

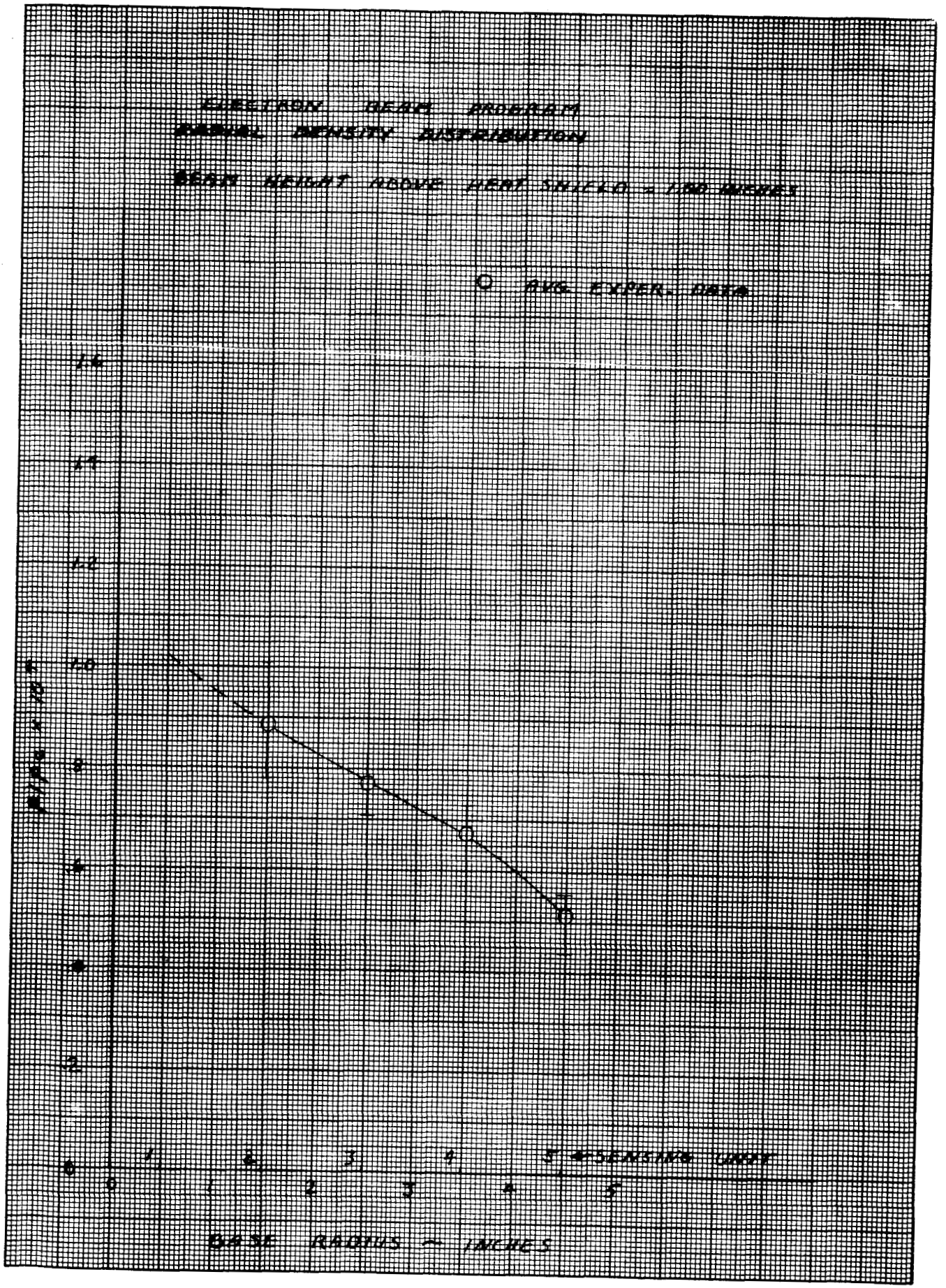
ELECTRON BEAM PROGRAM
RADIAL DENSITY DISTRIBUTION
BEAM HEIGHT ABOVE HEAT SHIELD = 1.190 INCHES
AVG. EXPER. DATA
1.6
1.4
1.2
1.0
.8
.6
.4
.2
0
0
1
2
3
4
5
RADIUS - INCHES

FIG. 27

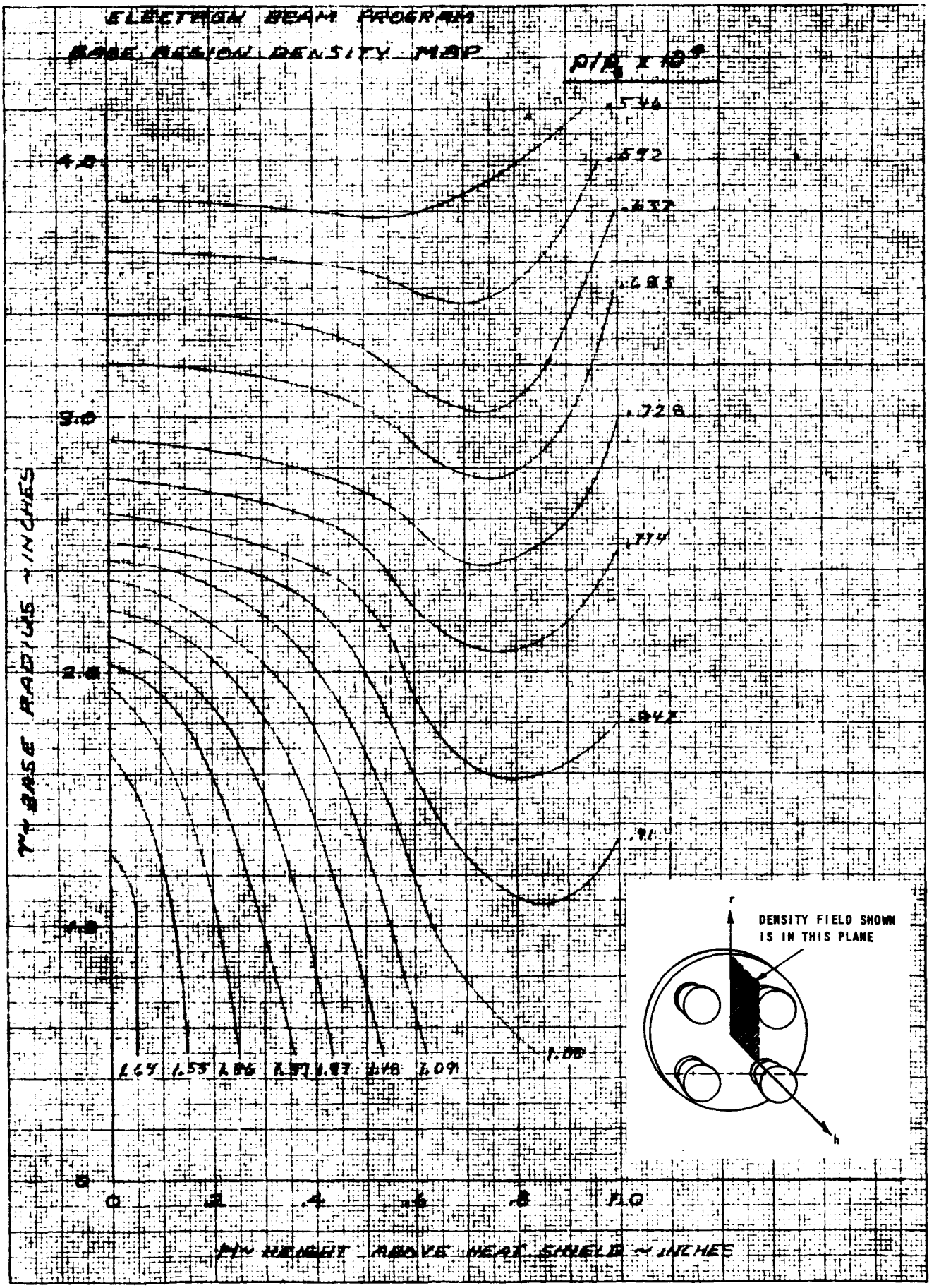
ELECTRON BEAM PROGRAM
BASE REGION DENSITY MAP
ρ/ρ₀ X 10⁴
.546
.592
.637
.683
.728
.774
.819
.911
1.00
4.0
3.0
2.0
1.0
0
TW BASE RADIUS - INCHES
1.64 1.55 1.46 1.37 1.27 1.18 1.09
0 .2 .4 .6 .8 1.0
TW HEIGHT ABOVE HEAT SHIELD - INCHES
DENSITY FIELD SHOWN
IS IN THIS PLANE
r
h

FIG. 28

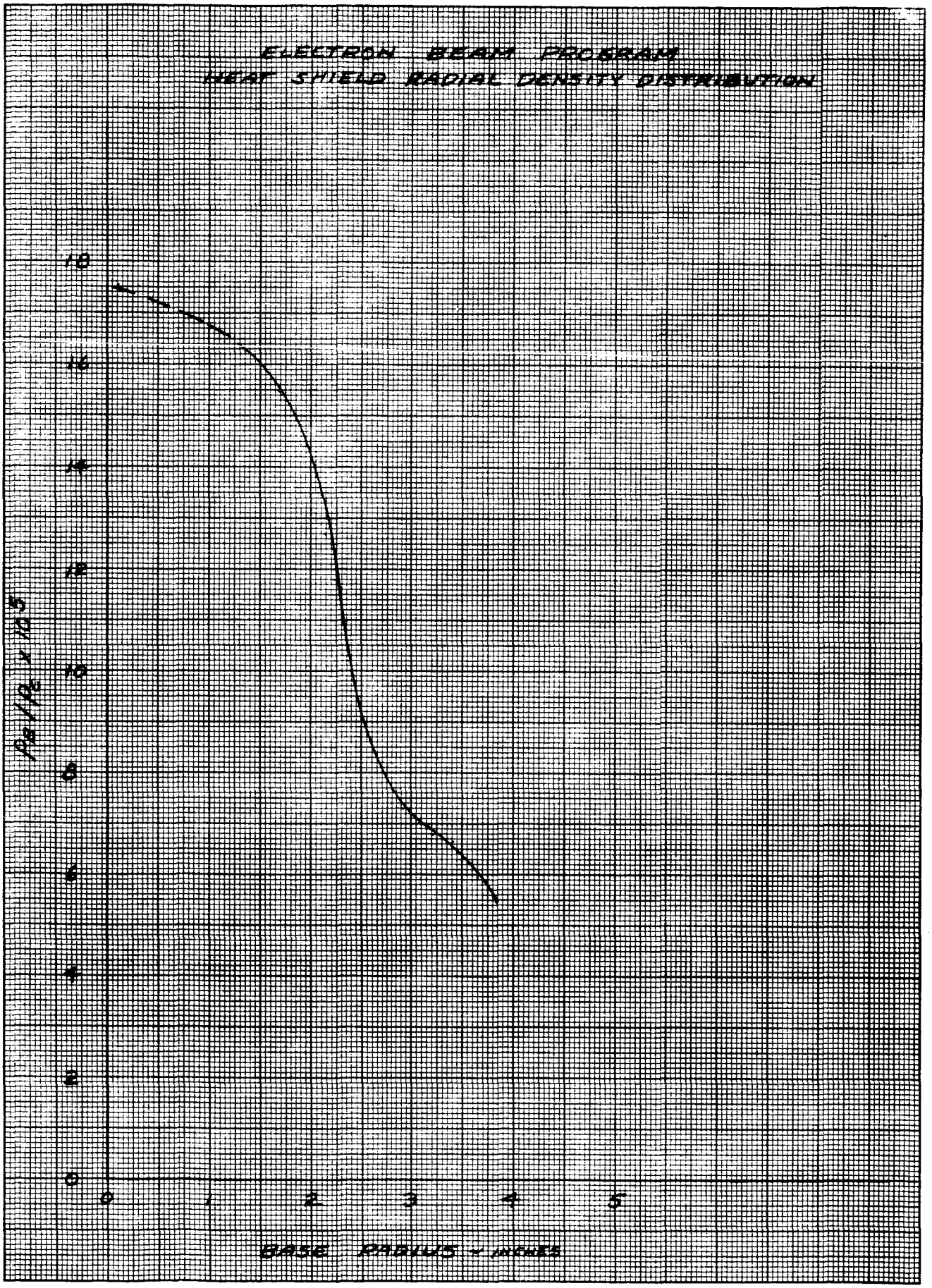
ELECTRON BEAM PROGRAM
HEAT SHIELD RADIAL DENSITY DISTRIBUTION
18
16
14
12
10
8
6
4
2
0
0
1
2
3
4
5
BASE RADIUS - INCHES

FIG. 29

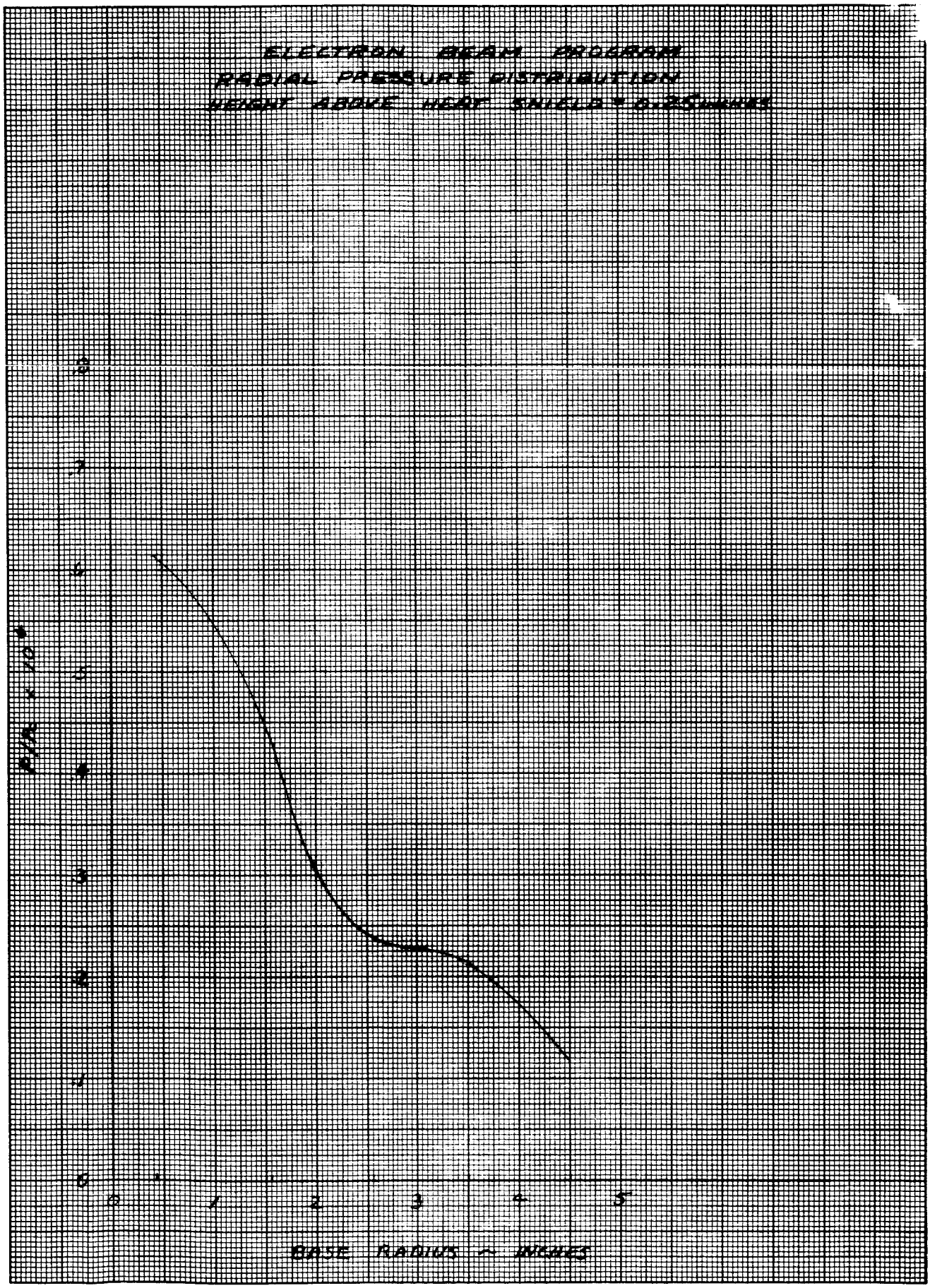

FIG. 30

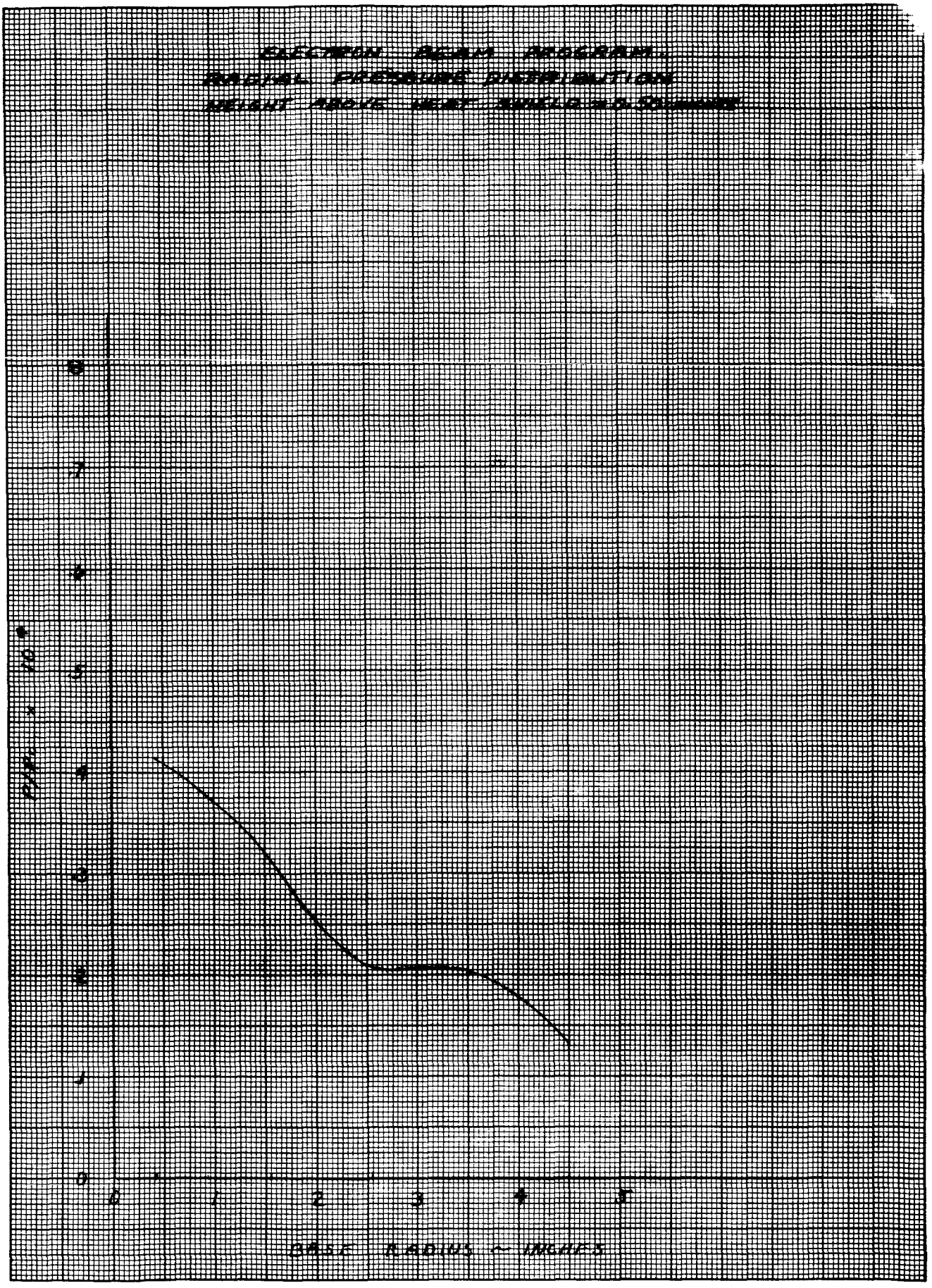

FIG. 31

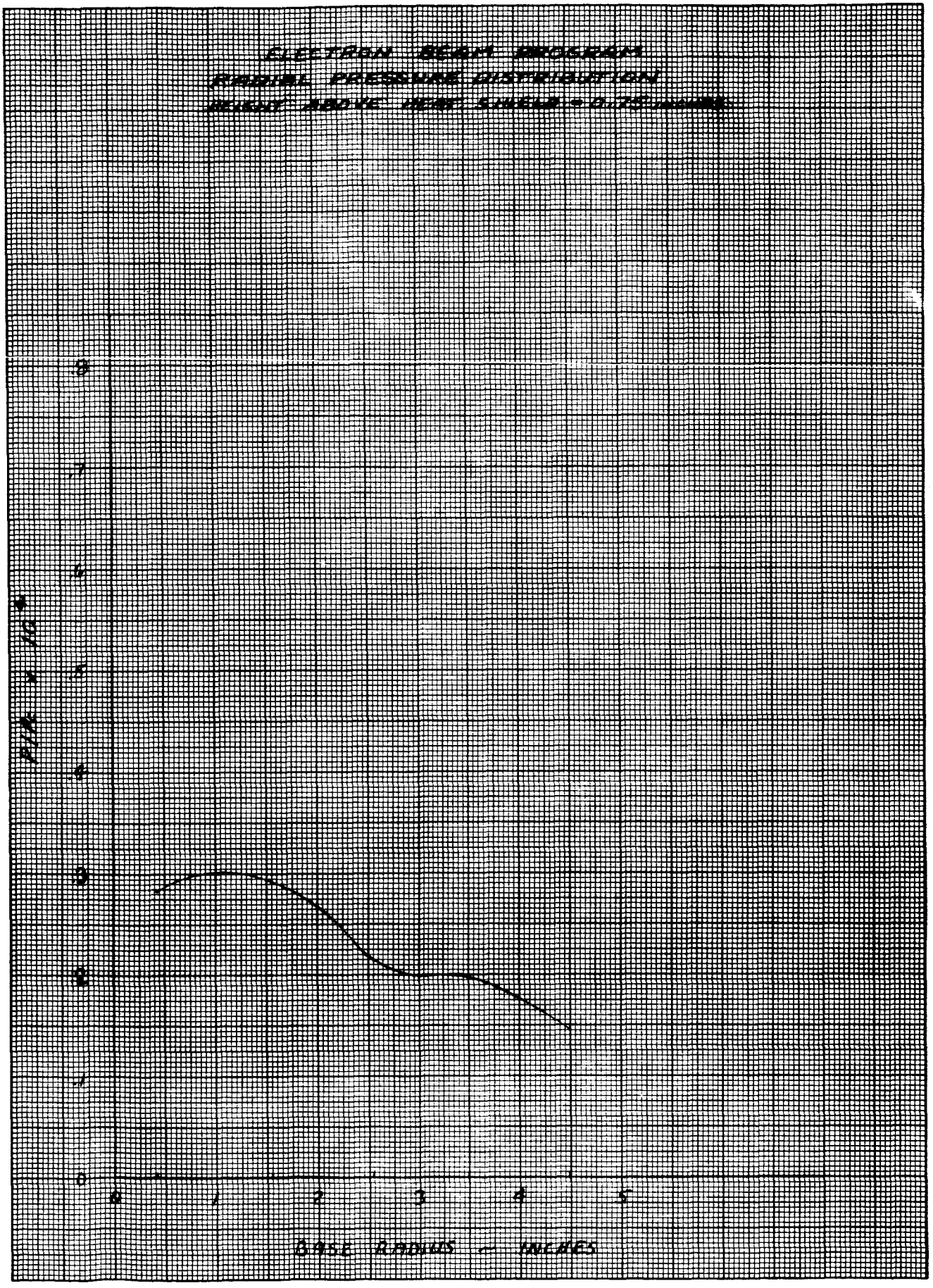

FIG. 32

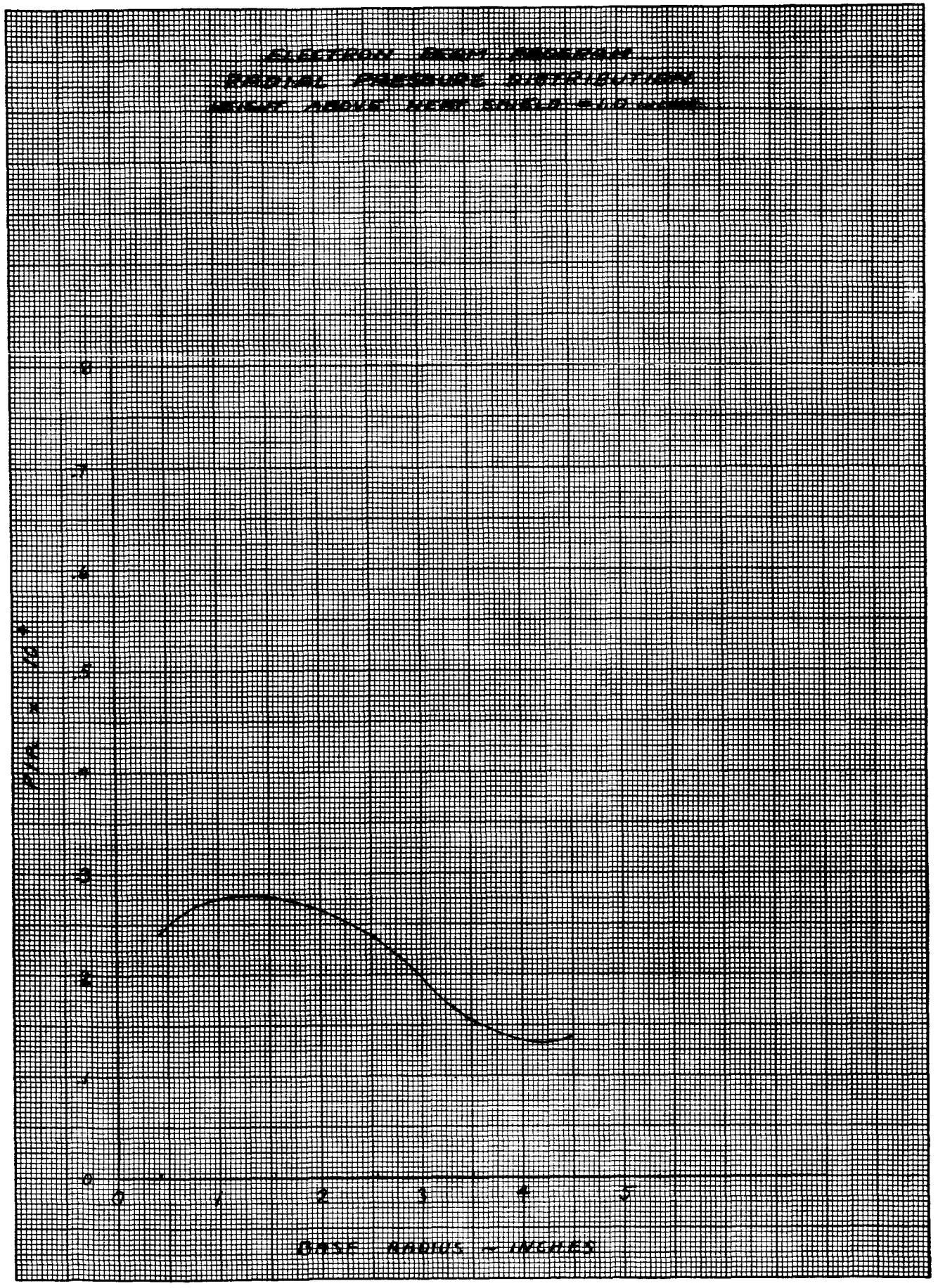

FIG. 33

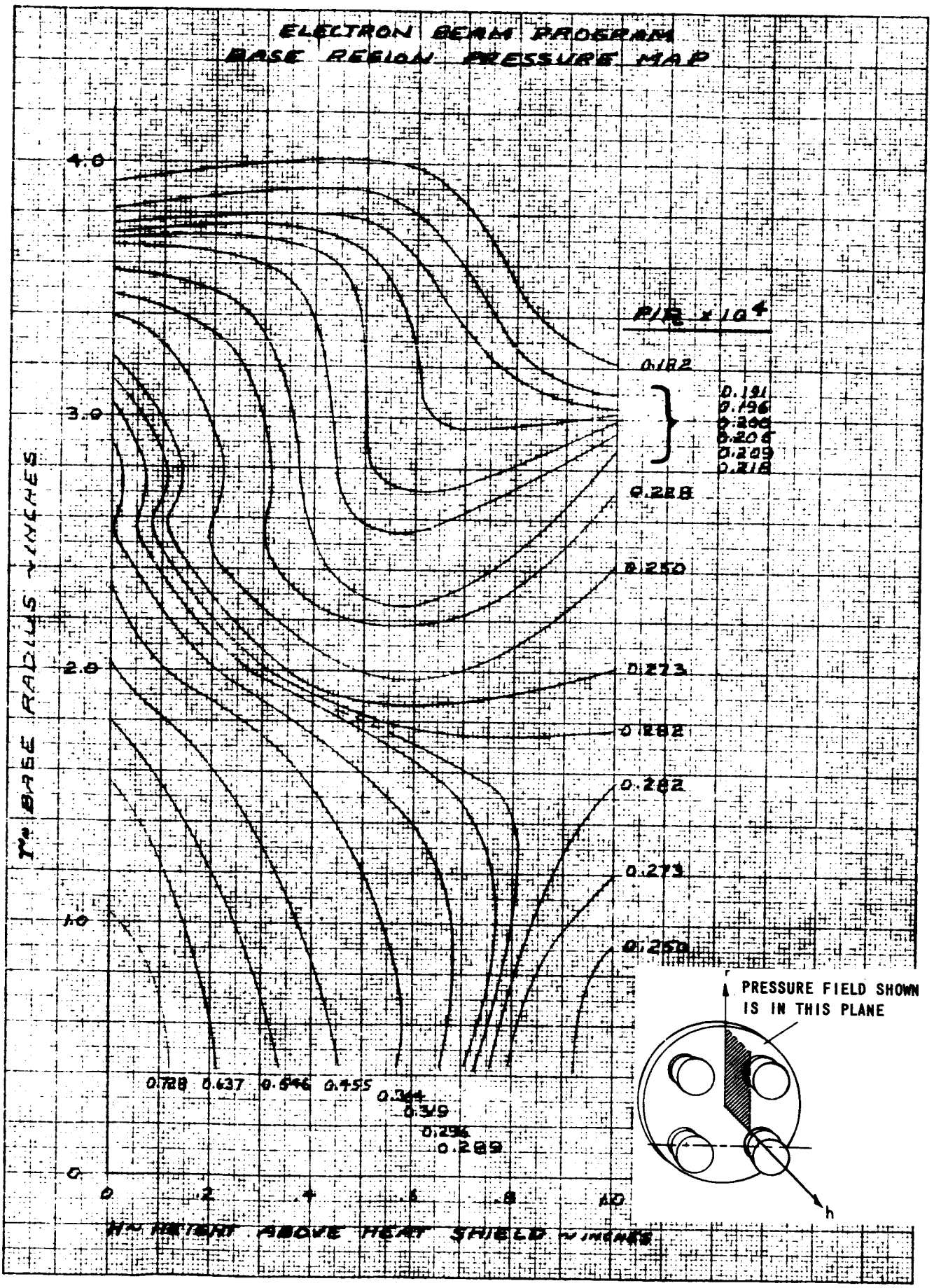
ELECTRON BEAM PROGRAM
BASE REGION PRESSURE MAP
r_w BASE RADIUS - INCHES
4.0
3.0
2.0
1.0
0
0
2
4
6
8
10
$P/P_\infty \times 10^4$
0.182
0.191
0.196
0.200
0.206
0.209
0.218
0.228
0.250
0.273
0.282
0.282
0.273
0.250
0.728
0.637
0.546
0.455
0.364
0.319
0.256
0.209
PRESSURE FIELD SHOWN IS IN THIS PLANE
r
h
h_w HEIGHT ABOVE HEAT SHIELD - INCHES

FIG. 34

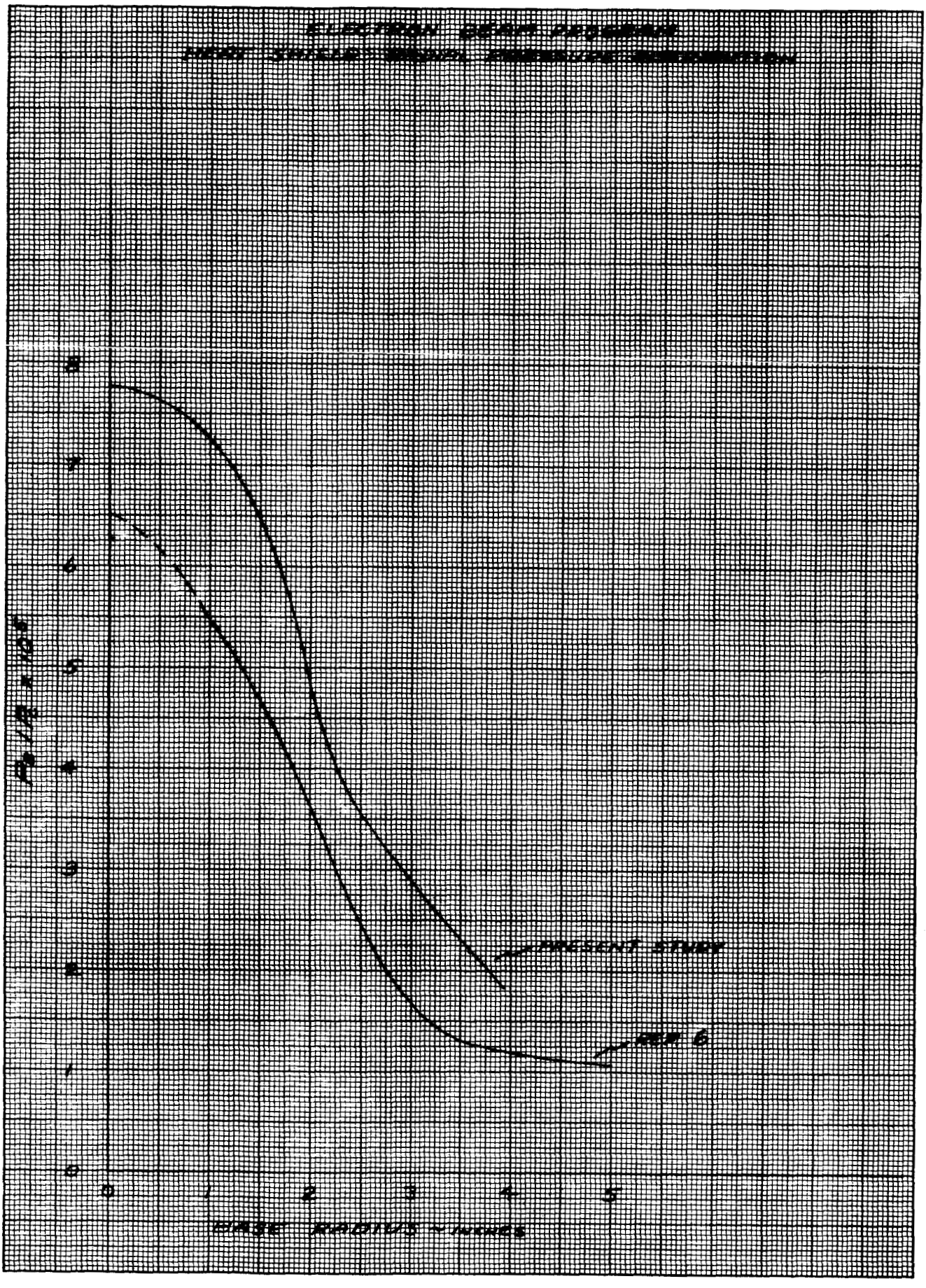

K+E 10 X 10 TO THE CENTIMETER 46 1513
10 X 25 CM. MADE IN U.S.A.
KEUFFEL & ESSER CO.

FIG. 35

K•E SEMI-LOGARITHMIC 359-64
KEUFFEL & ESSER CO.
2 CYCLES X 200 DIVISIONS

ELECTRON BEAM PROGRAM

PRESSURE DISTRIBUTION ALONG MODEL AXIAL ℄ EXTENSION (R=0)

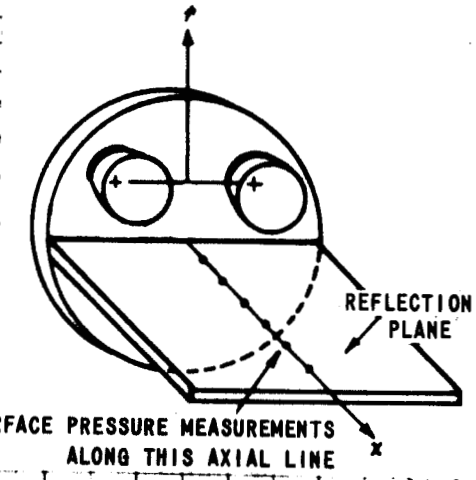

P/Pc

~ REF 6 REFLECTION PLANE DATA

~ PRESENT STUDY

NOZZLE EXIT PLANE

1.0 2.0 3.0 4.0 5.0

HEIGHT ABOVE HEAT SHIELD ~ INCHES

FIG 31

K&E SEMI-LOGARITHMIC 359-64
KEUFFEL & ESSER CO.
2 CYCLES X 200 DIVISIONS

ELECTRON BEAM PROGRAM
PRESSURE DISTRIBUTION ALONG MODEL NOZZLE ℄ EXTENSION IN PLANE BETWEEN ENGINES

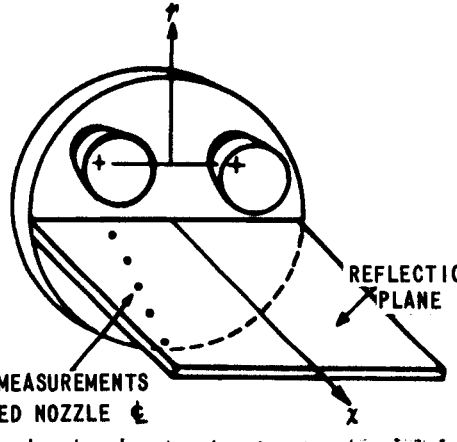

P/P$_c$

REF 6 REFLECTION PLANE DATA

PRESENT STUDY

NOZZLE EXIT PLANE

HEIGHT ABOVE HEAT SHIELD - INCHES

FIG 9A

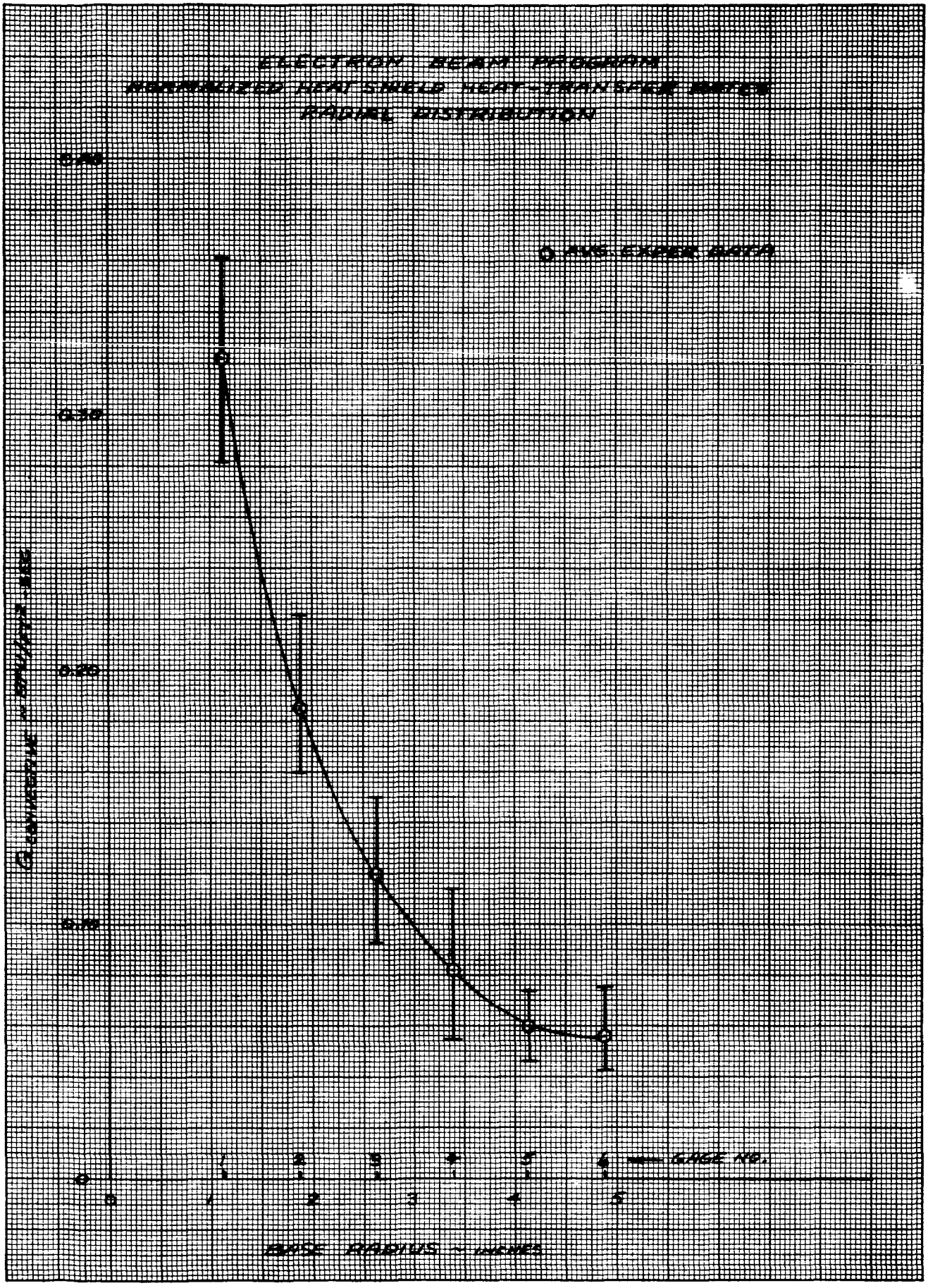

FIG. 38

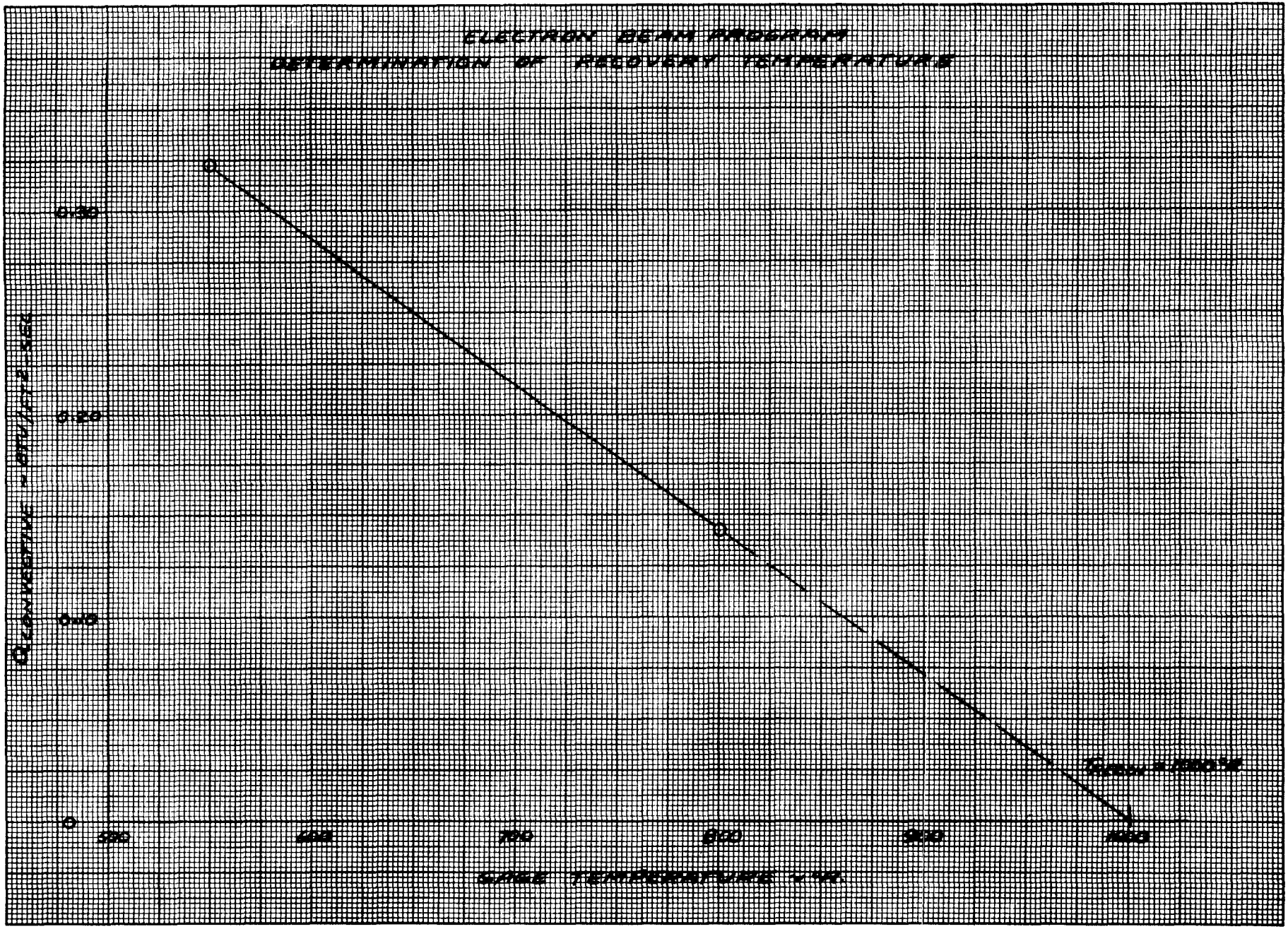

FIG. 39

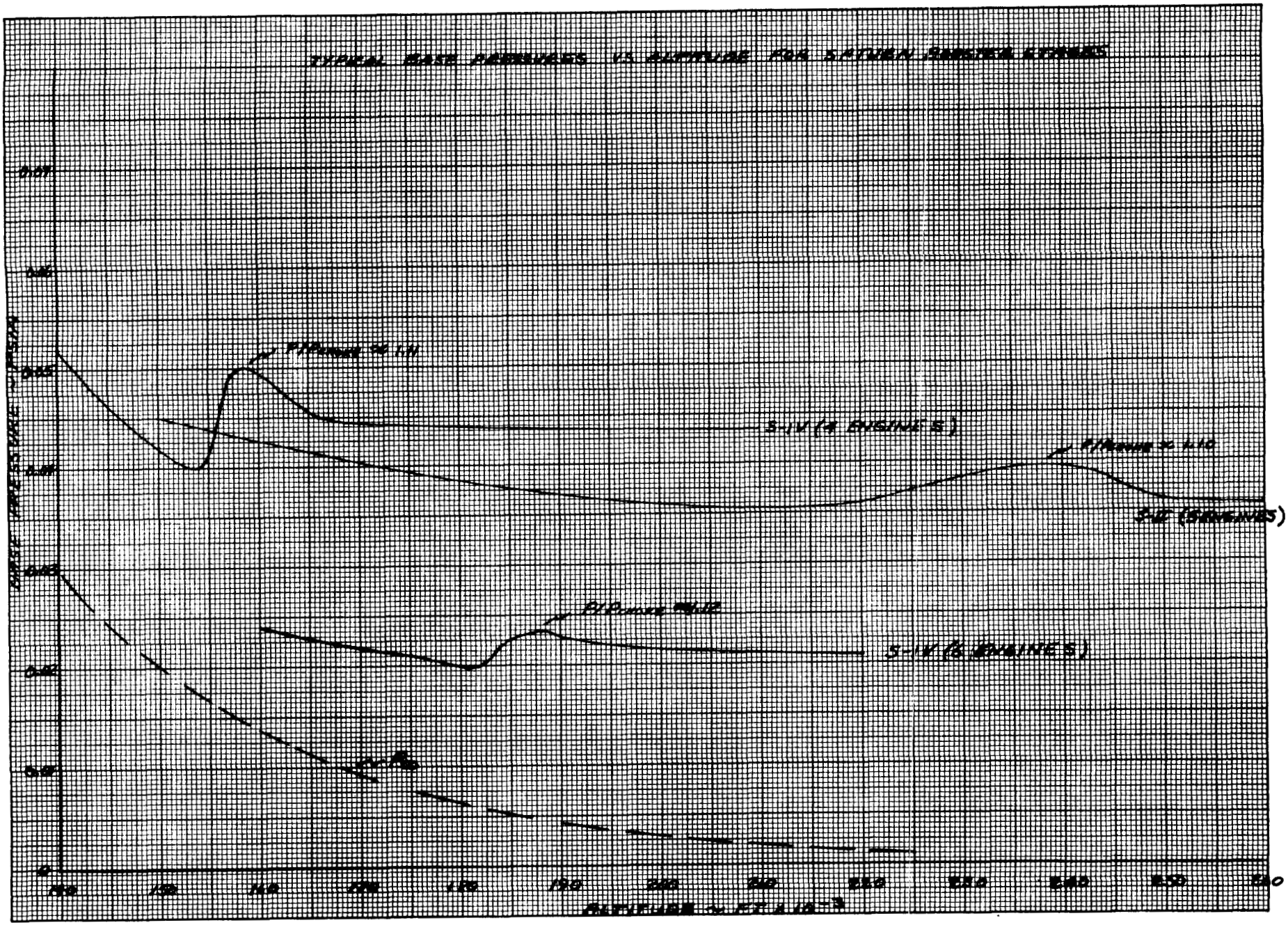

FIG. 40

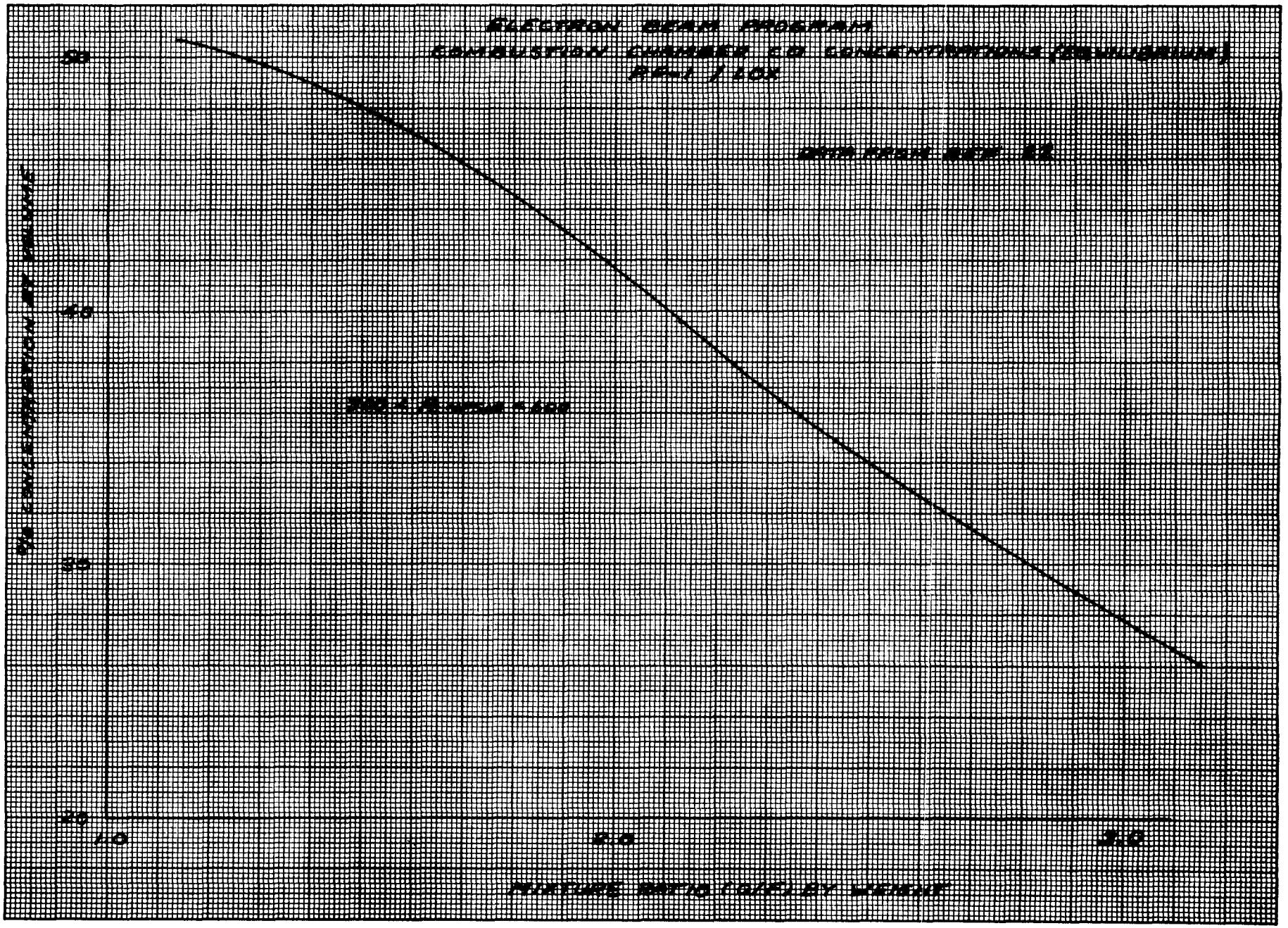

FIG. 41

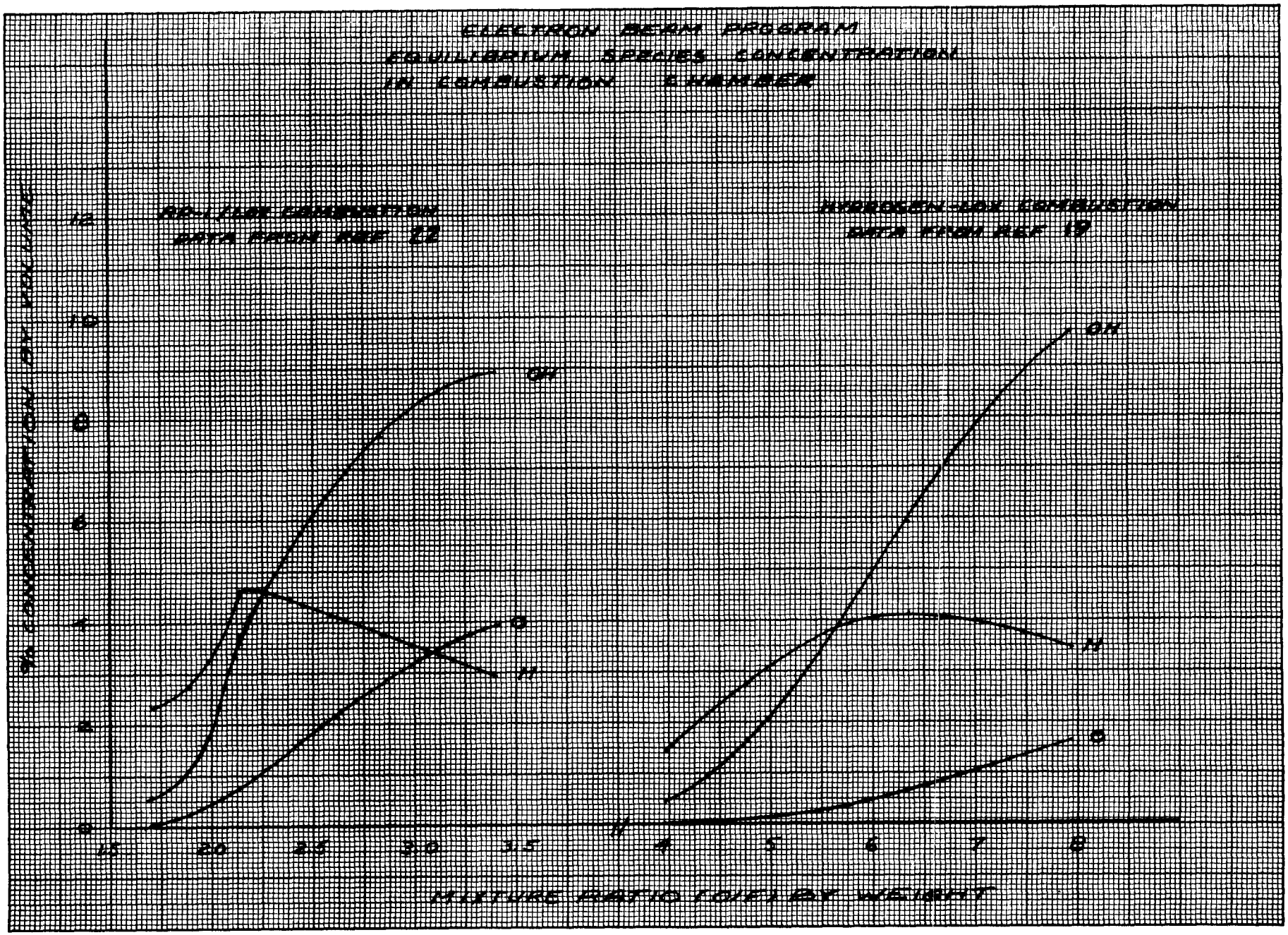

FIG. 42

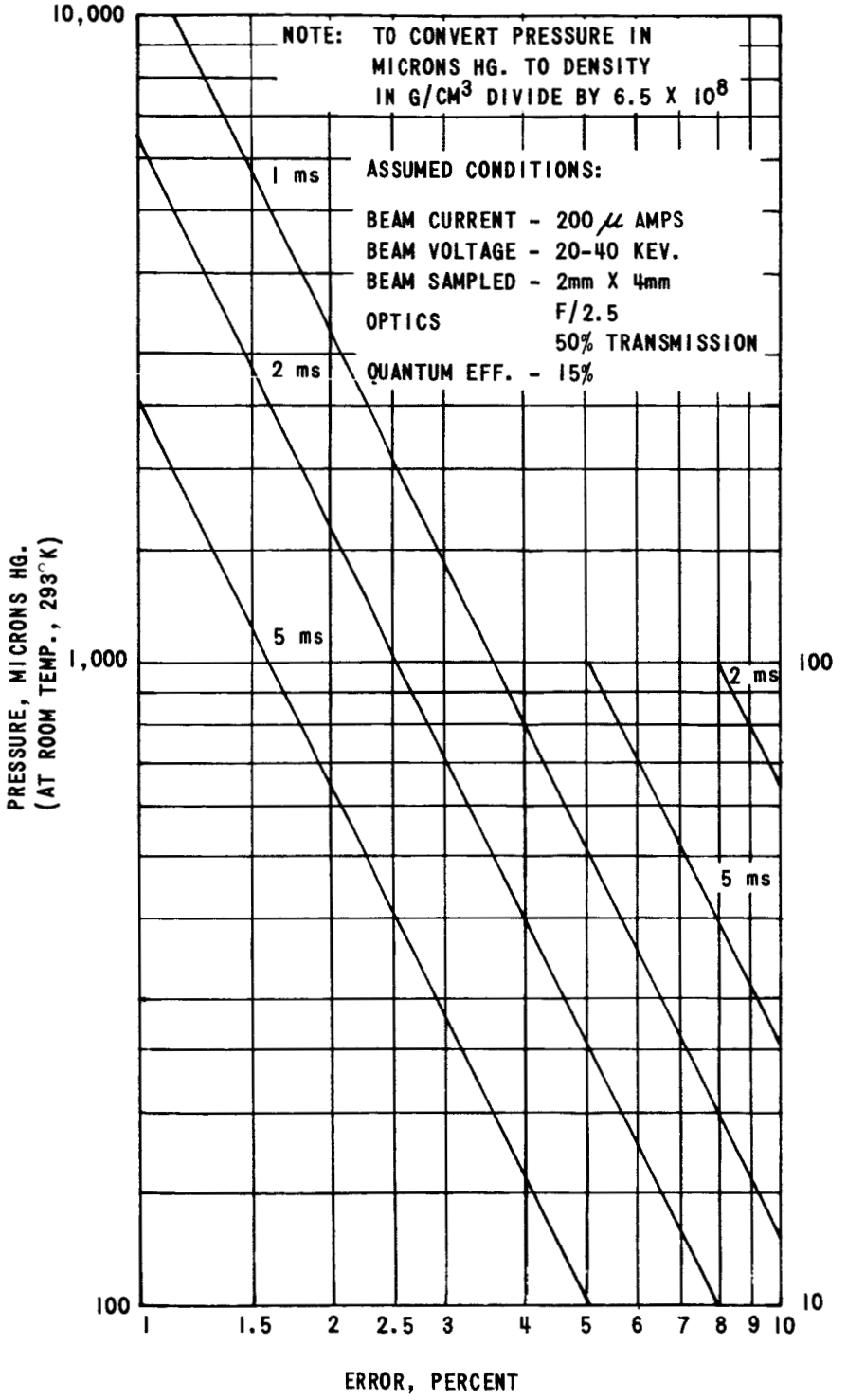

Figure 43 MINIMUM N_2 DENSITY MEASURABLE WITH ELECTRON BEAM DENSITY PROBE AS A FUNCTION OF ACCURACY AND TEST TIME

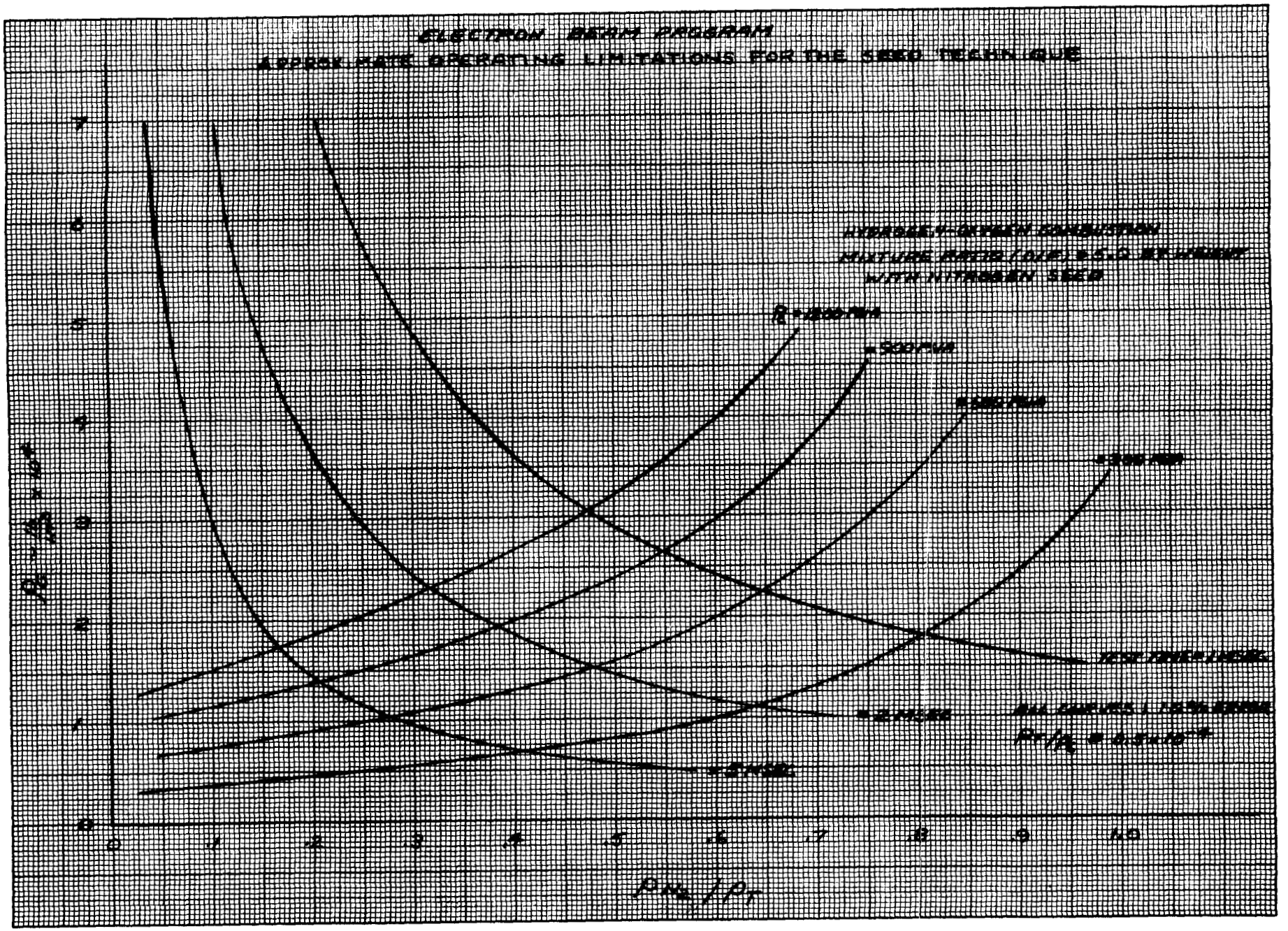

FIG. 44

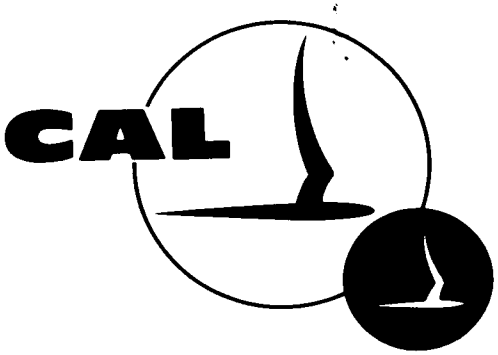
CAL